VOL.107 NO.GT8. AUG. 1981

JOURNAL OF THE GEOTECHNICAL ENGINEERING DIVISION

PROCEEDINGS OF
THE AMERICAN SOCIETY
OF CIVIL ENGINEERS

VOL.107 NO.GT8. AUG. 1981

JOURNAL OF THE GEOTECHNICAL ENGINEERING DIVISION

PROCEEDINGS OF
THE AMERICAN SOCIETY
OF CIVIL ENGINEERS

ISSN 0093-6405

William F. Marcuson III, Editor
U.S. Army Engineers

AMERICAN SOCIETY OF CIVIL ENGINEERS

CONTENTS

The Journal of the Geotechnical Engineering Division (ISSN 0093-6405) is published monthly by the American Society of Civil Engineers. Publications office is at 345 East 47th Street, New York, N.Y. 10017. Address all ASCE correspondence to the Editorial and General Offices at 345 East 47th Street, New York, N.Y. 10017. Allow six weeks for change of address to become effective. Subscription price to members is $16.00. Nonmember subscriptions available; prices obtainable on request. Second-class postage paid at New York, N.Y. and at additional mailing offices. GT.

POSTMASTER: Send address changes to American Society of Civil Engineers, 345 East 47th Street, New York, NY 10017.

The Society is not responsible for any statement made or opinion expressed in its publications.

DISCUSSION

Proc. Paper 16408

INFORMATION RETRIEVAL

The key words, abstract, and reference "cards" for each article in this Journal represent part of the ASCE participation in the EJC information retrieval plan. The retrieval data are placed herein so that each can be cut out, placed on a 3 × 5 card and given an accession number for the user's file. The accession number is then entered on key word cards so that the user can subsequently match key words to choose the articles he wishes. Details of this program were given in an August, 1962 article in CIVIL ENGINEERING, reprints of which are available on request to ASCE headquarters.

*Discussion period closed for this paper. Any other discussion received during this discussion period will be published in subsequent Journals.

16416 PRESSUREMETER TESTS AT VERY SHALLOW DEPTH

KEY WORDS: Clays; **Critical depth;** Depth factor (soils); Field tests; **Modulus of deformation; Pavement design; Pavements; Pressure measurement;** Sands; Soil mechanics

ABSTRACT: The pressuremeter shows considerable promise as a tool used in the design of pavements. The results of pressuremeter tests carried out at shallow depth can be influenced by the proximity of the ground surface. The influence is readily apparent in the case of limit pressure values, but little is known about the effect of depth on the pressuremeter modulus. However, the modulus is important for pavement design. A series of tests were run to resolve this dilemma. The pressuremeter modulus is hardly affected by the depth at which the test is run.

REFERENCE: Briaud, Jean-Louis (Asst. Prof., Civ. Engrg. Dept., Texas A & M Univ., College Station, Tex. 77843), and Shields, Donald H., "Pressuremeter Tests at Very Shallow Depth," *Journal of the Geotechnical Engineering Division,* ASCE, Vol. 107, No. GT8, **Proc. Paper 16416**, August, 1981, pp. 1023-1040

16458 SLURRY WALL SPECIFICATIONS

KEY WORDS: **Design criteria;** Objectives; Permeability; Quality control; **Slurry excavation; Slurry trenches; Specifications;** Subsurface structures

ABSTRACT: The critical design criteria and the resulting specifications for slurry trench diaphragm walls and cutoff walls are discussed. To establish diaphragm and cutoff slurry wall design criteria and specifications, the designer must clearly establish the objectives or end results that are to be obtained, and shape his specifications accordingly. There are many portions or applications of slurry wall work where truly an end-result specification may be appropriate. However, the application of end-result specifications in the present practice is a long way off until the owners and engineers gain a more thorough understanding and knowledge of the technical and construction procedures involved in slurry trench work.

REFERENCE: Millet, Richard A. (Principal, Woodward-Clyde Consultants, 3 Embarcadero Center, San Francisco, Calif. 94111), and Perez, Jean-Yves, "Current USA Practices: Slurry Wall Specifications," *Journal of the Geotechnical Engineering Division,* ASCE, Vol. 107, No. GT8, **Proc. Paper 16458**, August, 1981, pp. 1041-1056

16464 DYNAMIC FEM MODEL OF OROVILLE DAM

KEY WORDS: Acceleration; Bedrock; California; **Dams (earth); Dynamic models;** Earth dam performance; **Earth dams; Earthquakes; Finite elements;** Seismic stability; Shear modulus; Time factors

ABSTRACT: A dynamic finite element model was made of Oroville Dam. Oroville Dam is a 229 m high earth dam located in the foothills on the western slope of the Sierra Nevada in California. During August and September of 1975 the immediate area near the dam experienced seismic activity, with the main shock having a magnitude 5.7. Acceleration time histories were recorded on the crest and toe of the dam. The bedrock accelerations recorded near the dam were input into the finite element model, and the computed crest accelerations compared to the observed crest accelerations. A favorable comparison gives validity to the finite element model chosen.

REFERENCE: Vrymoed, John (Assoc. Engr., Div. of Safety Dams, Dept. of Water Resources, California), "Dynamic FEM Model of Oroville Dam," *Journal of the Geotechnical Engineering Division,* ASCE, Vol. 107, No. GT8, **Proc. Paper 16464**, August, 1981, pp. 1057-1077

16421 SETTLEMENT OF PLASTIC AND ORGANIC CLAYS

KEY WORDS: **Clays; Consolidation (soils); Creep; Deformation;** Foundations; **Settlement analysis; Shear modulus;** Shear tests; **Soil dynamics;** Soil mechanics; Soil stability; Strains; Time dependence

ABSTRACT: For most foundation loading situations, initial settlements due to undrained shear deformations are small. The common practice of computing consolidation settlements using the conventional 1-dimensional model therefore generally yields total settlement estimates of sufficient accuracy for design purposes. Initial settlements can become a predominant design consideration with highly plastic or organic foundation soils, or both, however—especially when loaded to low stability factors of safety, as illustrated by three case histories. Moreover, with slow field rates of consolidation, the occurrence of large initial settlements may also be followed by excessive undrained creep deformations. A semi-empirical method is presented for predicting the magnitude of initial settlement and the likelihood of excessive creep movements. Ways of reducing detrimental undrained shear deformations in design practice are explored.

REFERENCE: Foott, Roger (Program Mgr., Soils and Foundation Engrg., Dames and Moore, Burlington, Mass.), and Ladd, Charles C., "Undrained Settlement of Plastic and Organic Clays," *Journal of the Geotechnical Engineering Division,* ASCE, Vol. 107, No. GT8, **Proc. Paper 16421**, August, 1981, pp. 1079-1094

16424 PILES SUBJECTED TO TORSION

KEY WORDS: Analytical techniques; Foundations; **Pile loading tests;** Pile load test instrumentation; **Piles (foundations);** Shear modulus; Soil mechanics; Stiffness; **Torsion**

ABSTRACT: Analytical solutions are presented for the torsional response of piles embedded in elastic soil that is either homogeneous or where the stiffness is proportional to depth. The solutions are extended to more general variations of soil stiffness with depth and to cover behavior after peak shaft adhesion between pile and soil. Full scale torsion load tests are studied, and an analogy is suggested between the behavior of piles subjected to torsion loading and that of long compressible piles subjected to axial loading.

REFERENCE: Randolph, M. F. (Univ. Asst. Lect., Cambridge Univ., Cambridge, England CB2 1PE), "Piles Subjected to Torsion," *Journal of the Geotechnical Engineering Division,* ASCE, Vol. 107, No. GT8, **Proc. Paper 16424**, August, 1981, pp. 1095-1111

16447 EXPERIMENTAL STUDY ON FOOTINGS IN LAYERED SOIL

KEY WORDS: **Bearing capacity;** Clays; Experimental data; **Layered soils;** Model tests; Sand; **Shallow foundations; Soil mechanics**

ABSTRACT: The results are presented of an experimental study on strip and circular footings on a two-layered soil. The values of the ultimate bearing capacity obtained by the model tests are compared with those calculated according to the empirical method published recently by Satyanarayana and Garg, 1980. The extensive comparisons between the observed ultimate bearing capacity values and those predicted by the method reveal discrepancies ranging from 70 to 85 percent. Thus, the method needs more refinement and further experimental, and possibly field verifications before it can be recommended for practical applications.

REFERENCE: Hanna, Adel M. (Asst. Prof., Concordia Univ., Dept. of Civ. Engrg., 1455 de Maisonneuve Blvd. West, Montreal, Quebec, Canada, H3G 1M8), "Experimental Study on Footings in Layered Soil," *Journal of the Geotechnical Engineering Division,* ASCE, Vol. 107, No. GT8, **Proc. Paper 16447**, August, 1981, pp. 1113-1127

16474 DISPLACEMENTS DUE TO CYCLE WAVE LOADING

KEY WORDS: **Breakwaters;** Coastal engineering; Consolidation (soils); **Cyclic loads; Deformation;** Dikes; **Displacements; Finite element method;** Ocean engineering; **Offshore structures; Sands;** Soil mechanics; **Storms;** Triaxial tests; Waves (water)

ABSTRACT: The permanent deformation of soils as the result of cyclic loads is an important consideration in the design of offshore structures. Experimental studies show that the permanent strains are influenced by the porosity, the intitial shear and effective normal stresses, and the amplitude of the cyclic shear stress, as well as by the number of cycles of loading. These effects are combined into a logarithmic relation. The resulting equations have been incorporated into a finite element program that calculates permanent displacement without changes in net boundary loads or stresses. The analyses are applied to a proposed offshore barrier to show the importance of the ways in which cyclic loads combine with monotonic loads due to tides to give permanent displacements.

REFERENCE: Marr, W. Allen, Jr. (Research Assoc., Massachusetts Ínst. of Tech., Cambridge, Mass.), and Chrisitian, John T., "Permanent Displacements Due to Cyclic Wave Loading," *Journal of the Geotechnical Engineering Division,* ASCE, Vol. 107, No. GT8, **Proc. Paper 16474,** August, 1981, pp. 1129-1149

PRESSUREMETER TESTS AT VERY SHALLOW DEPTH

By Jean-Louis Briaud,[1] A. M. ASCE
and Donald H. Shields,[2] M. ASCE

INTRODUCTION

This article investigates the influence of the proximity of the ground surface on the results of pressuremeter tests. The study was part of a research program on the possible use of a special pressuremeter for pavement design (Refs. 3, 4, 5, and Fig. 1).

A pressuremeter test (1) consists of placing a cylindrical expandable probe in a borehole and inflating the probe (Fig. 2). A control unit on the ground surface is used to generate the pressure necessary to inflate the probe. The pressure against the wall of the borehole (p) and the expansion of the cavity (v) are recorded, and a p-v curve is plotted (Fig. 3). A modulus is obtained from the slope of the curve (A to B on Fig. 3), and a limit pressure is read at large strains (C on Fig. 3).

In a pressuremeter test carried out deep in the ground, the soil around the probe moves laterally, and plane strain conditions ($\epsilon_z = 0$) are closely approximated. In a shallow pressuremeter test the soil around the probe may move both laterally and upward, due to the proximity of the free boundary (the ground surface). If this hypothesis is true, there must be a depth, the critical depth, D_c, below which the surface has no significant influence on the soil deformation process. For tests above D_c, the ground surface will deform as the probe expands, whereas for tests deeper than D_c, the deformation of the ground surface during the probe expansion process must be very small or nonexistent.

Theoretically the proximity of the ground surface has an influence on pressuremeter parameters, or on any other soil parameter measured at depth; this is true because normally the at-rest stresses increase with depth. For example, one would expect that since the at rest state of stress has an influence on the modulus of deformation of a soil such as sand (7), the modulus will increase with depth along with the increase in at-rest stress. A clear distinction, then, must be made between the variation of a parameter with depth due to increasing at rest or other stresses, and the variation due to the critical depth phenomenon.

[1]Asst. Prof., Civ. Engrg. Dept., Texas A&M Univ., College Station, Tex. 77843.
[2]Head, Civ. Engrg. Dept., Univ. of Manitoba, Winnipeg, Canada, R3T 2N2.

Note.—Discussion open until January 1, 1982. To extend the closing date one month, a written request must be filed with the Manager of Technical and Professional Publications, ASCE. Manuscript was submitted for review for possible publication on September 24, 1980. This paper is part of the Journal of the Geotechnical Division, Proceedings of the American Society of Civil Engineers, ©ASCE, Vol. 107, No. GT8, August, 1981. ISSN 0093-6405/81/0008-1023/$01.00.

Because the two variations are superposed, the distinction is sometimes difficult to make when reading a profile of test results.

The depth of influence of a wheel load is shallow, and if a pressuremeter were to be used for pavement design, the pressuremeter tests would have to be performed within that shallow depth (300 mm–2,000 mm or 1 ft–6 ft). Since the deformation characteristics of the pavement structure were required, a detailed study of the critical depth problem was obligatory, at least with respect to measured modulus values since limit pressures are of little interest to the pavement

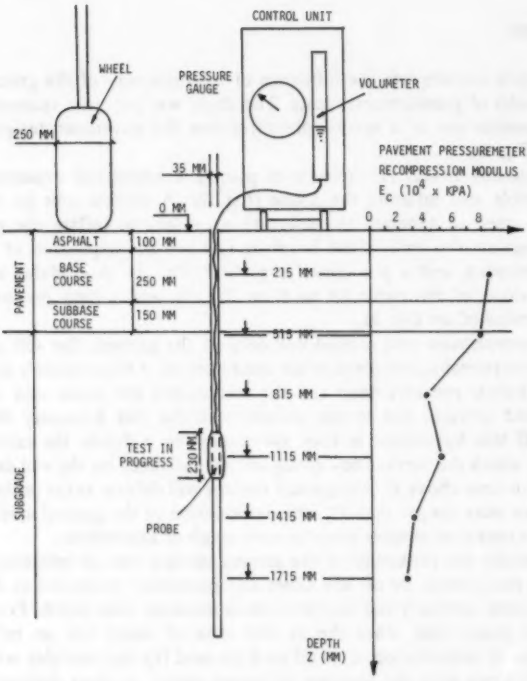

FIG. 1.—Pavement Pressuremeter Test (1 in. = 25.4 mm; 1 kPa = 20.885 psf)

engineer. There was concern that if the critical depth, D_c, occurred within the depth of testing, two different interpretation techniques would have to be used with the pressuremeter test results: (1) One technique above D_c; and (2) one below D_c.

The study involved:

1. Pressuremeter tests at various depths in a large, 2-m (6.6-ft) deep container filled with sand at a variety of densities.

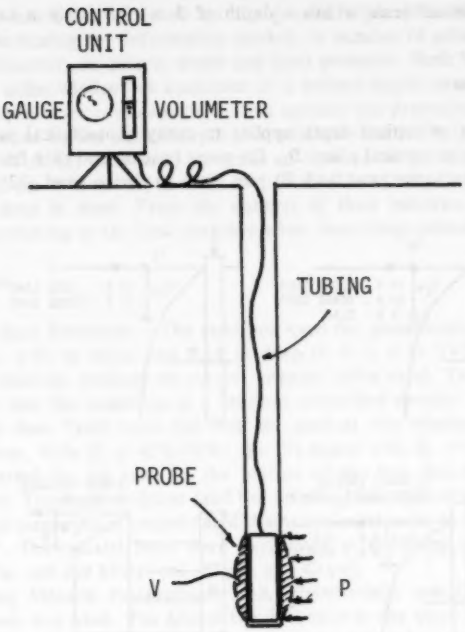

FIG. 2.—Pressuremeter Test

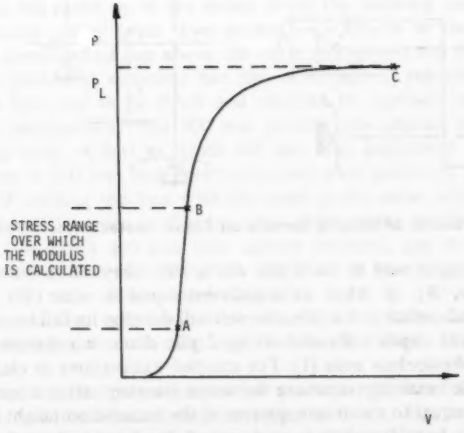

FIG. 3.—Typical Pressuremeter Curve

2. Pressuremeter tests within a depth of 3 m (9.8 ft) in a natural deposit of clay.

Literature Survey

The concept of critical depth applies to many geotechnical problems (Fig. 4). In the case of vertical piles, D_c, for point bearing and skin friction is about 10 pile diam in loose sand and 20 pile diam in dense sand (12); in clay, D_c

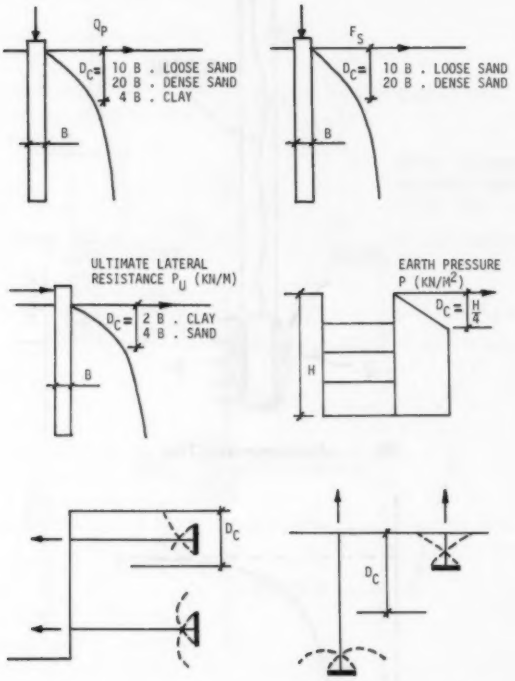

FIG. 4.—Influence of Ground Surface on Some Geotechnical Problems

for point bearing is said to be 4 pile diam, since beyond 4 diam the bearing capacity factor, N_c, is taken as a constant equal to nine (10). In the case of the horizontal capacity of a pile, the soil will develop its full lateral resistance beyond a critical depth estimated to be 2 pile diam in cohesive soils and 4 pile diam in cohesionless soils (1). For strutted excavations in clays, the earth pressure on the retaining structure becomes constant after a certain critical depth which is equal to about one quarter of the excavation height (11). Anchor plates also have been found to have a critical depth, and D_c probably depends on the orientation of the plate.

Very little has been published on the precise topic of critical depth and pressuremeter testing for deformation moduli. A number of articles have been published, however, on critical depth and limit pressure. Both Ménard (9) and Jezequel (8) acknowledge the existence of a critical depth in a limit pressure profile. Jezequel does comment that in his opinion the pressuremeter modulus is less influenced by the critical depth phenomenon than is the limit pressure.

Baguelin, et al. (1) state that, as a rule of thumb, the pressuremeter seems to be below the critical depth if it is at least 1 m (3 ft) deep in clay and 2 m (6 ft) deep in sand. From the context of their remarks, these authors seem to be referring to the limit pressure when describing critical depth.

Tests in Sand

Sand and Sand Container.—The sand box used for pressuremeter testing was 1.85 m long, 1.85 m wide, and 2.14 m deep (6 ft × 6 ft × 7 ft). The sand was a dry, uniform, medium to coarse, angular, silica sand. Ten tons of sand were rained into the container at a uniform controlled density throughout the depth of the box. Tests were run with the sand at two relative densities: (1) Medium dense, with D_r = 65%–70%; and (2) dense with D_r = 90%–95%. The pressure exerted by the sand on the bottom of the box was in the order of 34 kPa (5 psi). The medium dense sand had an effective angle of internal friction, ϕ', of 37° as measured in consolidated drained triaxial tests; in the dense state, ϕ' was 41°. The triaxial tests were performed at confining pressures of 34 kPa, 135 kPa, and 269 kPa (5 psi, 20 psi, and 40 psi).

Tests using Ménard Pressuremeter.—A commercially available, Model GA pressuremeter was used. The Model GA is similar to the more widely available GC model (1) and was equipped with a BX probe which has an effective length of 420 mm (16.5 in.) and an OD of 58 mm (2.28 in.). The probe was secured at the proper depth in the middle of the empty box, and then the sand was rained around the probe up to the proper level; the resulting tests are referred to as the 'buried probe' tests. Two probes were placed in the box for each filling. They were located one above the other and spaced 900 mm (3 ft) apart. Burying two probes at one time had the advantage of reducing the number of times the box had to be filled and emptied by one-half as compared to single probe installations. This 900 mm spacing was chosen on the basis of the following tests. A test at depth 600 mm was performed after a test at depth 600 mm + 900 mm had been performed (two probes in the box). After emptying and refilling the box with the sand at the same relative density, a test at depth 600 mm was performed (one probe in the box). The curves of the two tests at depth 600 mm were almost identical, and it was concluded that the spacing of 900 mm (3 ft) was sufficient to prevent any influence of one test on the other. Furthermore Baguelin, et al. (p. 113 of Ref. 1) state that when the vertical spacing between two tests is 1.20 probe lengths, the zones of influence do not overlap significantly; the length of the probe used was 420 mm.

The standard Menard pressuremeter test procedure (1) was followed precisely for all tests, and the Menard pressuremeter modulus, E_M, and the net limit pressure (p_l^*) were calculated for each test. The modulus, E_m, is obtained from the slope of the pressuremeter curve at small deformations (Fig. 3 and

Ref. 1). The net limit pressure, p_l^*, represents the resistance of the soil; it is computed from p_l measured at large deformations on the pressuremeter curve, minus the estimated at-rest total lateral pressure of the soil at the depth of the probe (Fig. 3 and Ref. 1). Nine tests were performed with the sand in a dense state (D_r = 90%–95%), and an E_M and a p_l^* profile were obtained (Figs. 5 and 6). Eleven tests were performed with the sand in a medium dense state (D_r = 65%–70%), and an E_M and a p_l^* profile were obtained (Figs. 5 and 6). The lines in Figs. 5 and 6 will be referred to later.

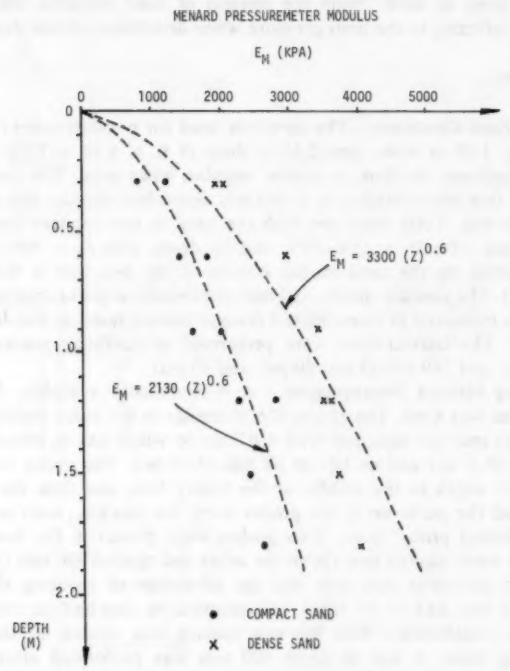

FIG. 5.—Menard Pressuremeter Tests: Modulus Profile in Sand (1 m = 3.281 ft; 1 kPa = 20.885 psf)

For four of the tests in the medium dense sand, surface movements were measured. Square aluminum plates (30 mm × 30 mm, 1.2 in. × 1.2 in.) were placed at 150 mm (5.9 in.) intervals across the box over the sand surface. A graduated pointer which travelled across the box on a graduated rail was lowered into contact with a mark made on each aluminum plate (Fig. 7). The exact location of each plate was measured before the probe was inflated (zero reading) and at the maximum inflation of the probe (close to p_l). The absolute error on the measurements was 0.5 mm (0.2 in.) and the surface contours at full inflation (p_l^*) are shown on Fig. 8.

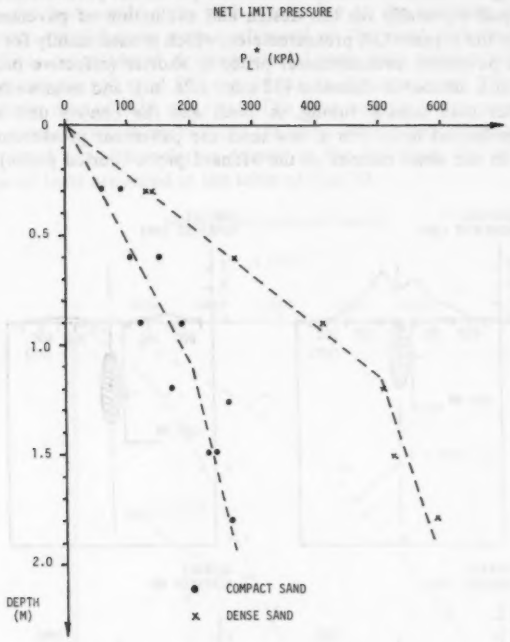

FIG. 6.—Menard Pressuremeter Tests: Limit Pressure Profile in Sand (1 m = 3.281 ft; 1 kPa = 20.885 psf)

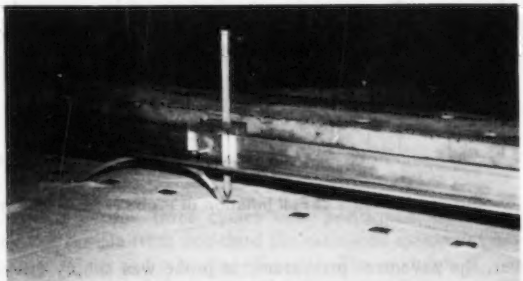

FIG. 7.—Set up for Measuring Surface Movements

Tests using Pavement Pressuremeter.—The pavement pressuremeter (Fig. 1) was developed especially for the design and evaluation of pavements (3,4,5). Compared to the Menard GA pressuremeter, which is used mainly for foundation studies, the pavement pressuremeter probe is shorter (effective probe length: 230 mm, 9 in.), smaller in diameter (32 mm, 1.26 in.), and monocellular. Single tubing, rather than coaxial tubing, is used, and the control unit is designed for strain controlled tests. For a few tests the pavement pressuremeter probe was placed in the same manner as the Menard probe (buried probe). For most

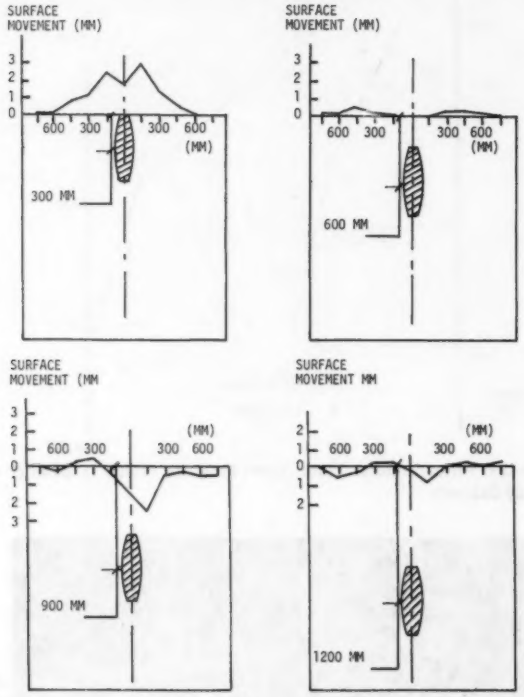

FIG. 8.—Surface Contours at Full Inflation of Probe (1 in. = 25.4 mm)

tests, however, the pavement pressuremeter probe was simply driven into the sand, and tests were performed every 300 mm (1 ft) of depth, working from top to bottom of the box. Only a deformation modulus (E) can be measured with the pavement pressuremeter (4); profiles of E in medium dense and dense sand are shown on Fig. 9. Due to the difficulty of making the density of the compact sand uniform close to the bottom of the sand box, some profiles show a large scatter of results between 1.8 m–2.1 m (6 ft–7 ft) depth (Fig. 9).

Triaxial Tests.—In an effort to predict how the modulus of deformation of the sand in the box would vary with depth due to the increase in confining pressure alone, triaxial tests were performed on the sand at a variety of cell pressures. Four consolidated drained triaxial tests with unload/reload cycles were run on samples of sand 100 mm (4 in.) in diameter, and 200 mm (8 in.) high, at a strain rate of 0.38 mm/min. The four samples were prepared using a miniature spreader which reproduced the same raining procedure as was used in the large sand box. The relative density of the dry sand, the cell pressure, and the type of tests are listed in the table of Fig. 10.

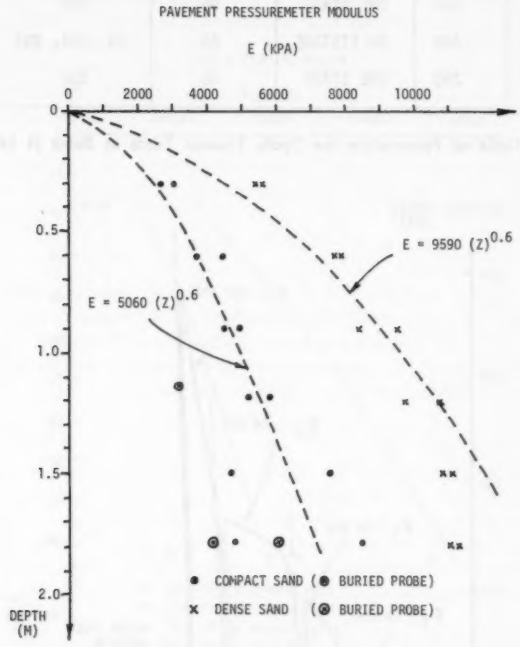

FIG. 9.—Pavement Pressuremeter Tests: Modulus Profile in Sand (1 mm = 3.281 ft; 1 kPa = 20.885 psf)

For each cell pressure, three cycles were performed; each cycle consisted of unloading the sample from one-third the estimated maximum deviator stress to zero deviator stress and reloading (Fig. 11). The modulus, E_T, is the secant modulus from the start of the test to the first unloading point (Fig. 11). The modulus, E_{Tc}, is calculated from the slope of the third loading cycle (Fig. 11).

Most triaxial tests were multistage tests (Fig. 11). The cell pressure was set at a first value, and a cyclic test performed; then the cell pressure was increased to a second value and another test performed; finally the process was repeated

TEST NO.	TYPE OF TEST	RELATIVE DENSITY D_R(%)	CELL PRESSURE σ_3 (KPA)
247	MULTISTAGE	95	34, 104, 207
248	ONE STAGE	95	207
249	MULTISTAGE	65	34, 104, 207
250	ONE STAGE	65	207

FIG. 10.—Table of Parameters for Cyclic Triaxial Tests in Sand (1 kPa = 20.885 psf)

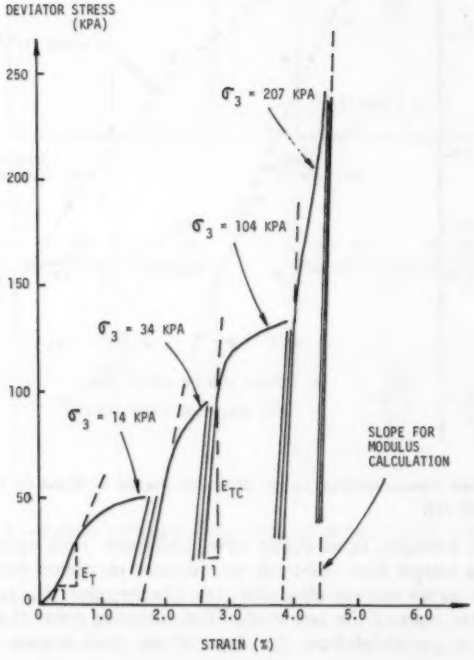

FIG. 11.—Cyclic Triaxial Test (1 kPa = 20.885 psf)

for a third value of the cell pressure. Some tests were only one stage tests, and only one cell pressure was used. Fig. 12 shows the influence of the magnitude of the cell pressure on the moduli, E_T and E_{Tc}.

Analysis of Results—Critical Depth at Full Expansion of Probe.—The p_l^* profiles from the Menard pressuremeter tests (Fig. 6) have two important characteristics: (1) One is that a break occurs in the profile; and (2) the second is that a straight line extension of the profile goes through the origin. These two characteristics are more obvious in the case of the tests in the dense sand than in the medium dense sand. The break in the profile occurs around 1.2 m (4 ft).

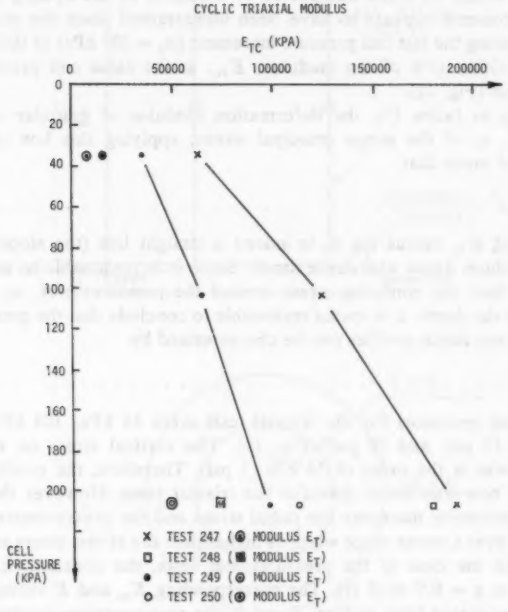

FIG. 12.—Triaxial Modulus Versus Cell Pressure in Sand (1 kPa = 20.885 psf)

The surface movement measurements (Fig. 8) seem to indicate that when the probe is below 0.9 m (3 ft) depth, even when the probe is fully inflated the surface is not involved significantly in the deformation process. These observations, on the shape of the p_l^* profile and on the surface movements, lead to the conclusion that there is a critical depth (D_C), at least at full expansion of the probe. For the Menard GA-BX probe in medium dense to dense sand, D_C is about 1.2 m (4 ft). In this case, the ratio of the critical depth (D_C) to the probe diameter (ϕ_p) is

$$\frac{D_C}{\phi_p} = \frac{120}{5.8} = 20 \qquad (1)$$

Interestingly, this ratio of 20 is the ratio of depth to pile diameter, which is said to be the critical depth ratio for pile design in dense sand (12).

Analysis of Results—Critical Depth at Partial Expansion of Probe.—The shape of the pressuremeter modulus profiles is very similar to the shape of the triaxial moduli versus cell pressure curve (Fig. 12). In the case of the triaxial tests no critical depth phenomenon can be involved. There was some concern, however, that the triaxial modulus versus confining (cell) pressure curves were influenced by the method of testing. It was thought that possibly in multistage testing the sample would be either compacted or loosened by the cycling of the first load. This concern appears to have been unwarranted since the moduli, E_{T_c}, measured during the last cell pressure increment (σ_3 = 207 kPa) of the multistage tests were within 10% of the modulus, E_{Tc}, at the same cell pressure in the one stage test (Fig. 12).

According to Janbu (7), the deformation modulus of granular soils varies as a power, n, of the minor principal stress; applying this law of behavior to E_{Tc} would mean that

$$E_{Tc} = K(\sigma_3)^n \qquad (2)$$

A plot of log E_{Tc} versus log σ_3 is indeed a straight line (the slope, n, is 0.6 for both medium dense and dense sand). Since it is reasonable to assume that in the sand box the confining stress around the pressuremeter, σ_3, increases linearly with the depth, z, it seems reasonable to conclude that the pressuremeter modulus versus depth profiles can be characterized by

$$E = k(z)^{0.6} \qquad (3)$$

The confining pressures for the triaxial tests were 34 kPa, 104 kPa, and 207 kPa (5 psi, 15 psi, and 30 psi) (Fig. 12). The vertical stress on the bottom of the box was in the order of 34 kPa (5 psi). Therefore, the confining stress level in the box was lower than for the triaxial tests. However the inflation of the pressuremeter increases the radial stress and the pressuremeter modulus is measured over a stress range which is higher than the at-rest stress as indicated on Fig. 3. In the case of the pressuremeter tests, the constant, k, has been determined at z = 0.9 m (3 ft). The corresponding E_M and E versus z curves are plotted as dotted lines in Figs. 5 and 9; the pressuremeter modulus profiles are well described by the "power law" curves.

Because the curvature in the E_M and E versus z plots can be explained as being due to the increase in confining stress with depth (based on both the triaxial tests and Janbu's law), it seems reasonable to conclude that a critical depth effect on the modulus of deformation in this sand deposit is not apparent from the tests.

Tests in Clay

Site Conditions.—The natural deposit of clay is part of a clay plane of overconsolidated marine deposit. A brown desiccated silty clay extends to a

depth of 2.4 m underlain by a grey silty clay to 3.1 m. On the average, the natural water content of this sensitive clay is 35%, the plastic limit is 17%, and the liquid limit is 34%. The natural unit weight is 18 kN/m^3 (115 pcf), and the clay is made up of 39% clay sizes, 50% silt sizes, and 11% sand sizes. The ground-water table was at the ground surface at the time of testing.

A circular silo was built at the site. According to Gloetzl cells measurements, the circular raft foundation for the silo (Fig. 13) exerted an average bearing pressure on the clay of 34 kPa (0.34 tsf) when the silo was empty. Several

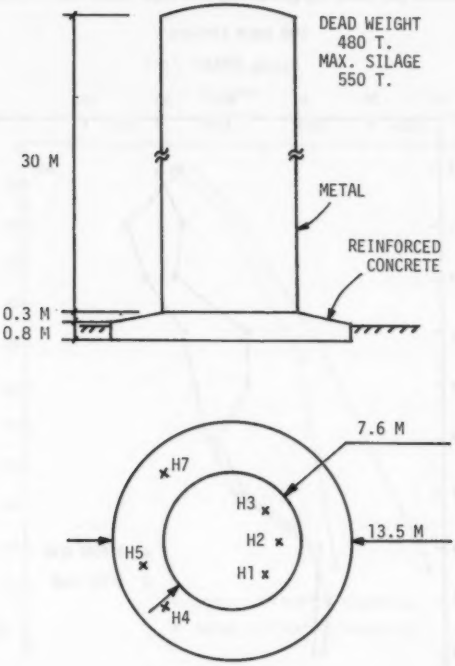

FIG. 13.—Clay Site: Silo and Slab Foundation (1 m = 3.281 ft)

tests including pressuremeter tests were run before the silo was built and then 2 weeks after the silo was built through the slab of the silo. The pressure exerted by the silo was equivalent to 2 m of clay; if a critical depth existed, the before construction and after construction pressuremeter modulus profiles would show different critical depths.

Vane Tests.—In order to determine the uniformity of the clay with depth, vane shear tests were run 2 weeks before and 2 weeks after the silo was constructed. The vane was 67 mm (2.65 in.) wide, 149 mm (5.87 in.) high (vertical

edge), and had 45° tapered ends. The test procedure followed the American Society for Testing and Materials (ASTM) D2574. Two holes were tested with the vane down to 3,000 mm (10 ft) depth; Hole H3 was tested before the silo was constructed, and Hole H4 was tested 2 weeks after construction. The vane shear strength profiles are shown on Fig. 14. The sensitivity of the soil, as determined by the vane, averaged four between 0 mm and 2,000 mm (0 ft and 6.7 ft) depth, and eight between 2,000 mm and 3,000 mm (6.7 ft and 10 ft) depth.

Triaxial Tests.—In Hole H5 (Fig. 13), undisturbed samples of the clay were taken with 63 mm (2.5 in.) diam Shelby tubes at 1,000 mm (3.3 ft) and 1,800

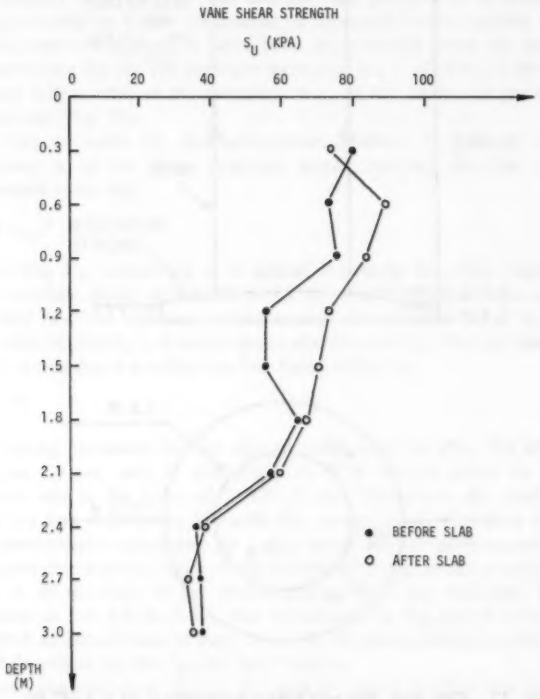

FIG. 14.—Vane Test Profiles: Clay Site (1 m = 3.281 ft; 1 kPa = 20.885 psf)

mm (6 ft) depth. Hole 5 was drilled 2 weeks after the silo had been constructed. The triaxial specimens were 38 mm (1.5 in.) in diam and 76 mm (3 in.) high; they were placed in the triaxial cell and reconsolidated to the in situ vertical effective stress.

The procedure used for the triaxial tests was the same as that used for the tests on sand, except that drainage was prevented during the tests on the clay. The method for determining E_T and E_{Tc} was identical to the method used

for the triaxial tests on sand. The clay moduli versus cell pressure (σ_3) profiles are shown on Fig. 15. The increase in undrained modulus with cell pressure could be due to the fact that the clay deposit is overconsolidated or partially saturated.

Pavement Pressuremeter Tests.—Two weeks before construction of the silo, two bore holes H1 and H2 were tested with the pavement pressuremeter (Fig. 13). The holes were bored with a 32-mm (1.26-in.) hand auger down to 2,100 mm (7 ft); the pressuremeter was inserted in each hole to 2,100 mm (7 ft), and then pushed to 3,000 mm (10 ft). Tests were done at 300 mm (1 ft) intervals from the bottom of the hole up. The resulting profiles of moduli are shown on Fig. 16.

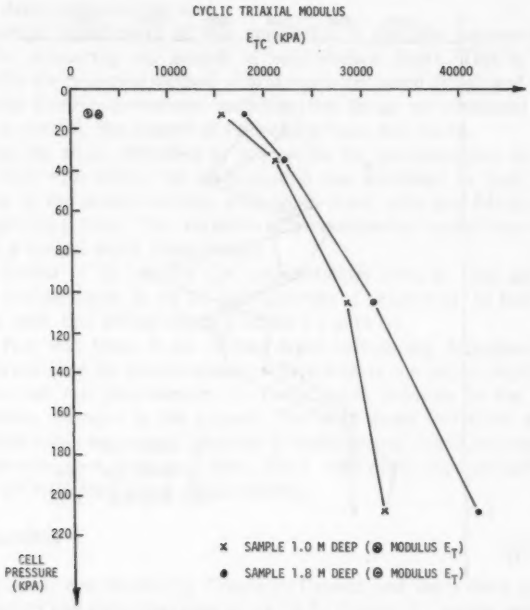

FIG. 15.—Triaxial Modulus Versus Cell Pressure in Clay (1 kPa = 20.885 psf)

Sleeves were installed in the formwork before the concrete foundation slab of the silo was poured in order to allow tests to be carried out through the slab after the silo had been built.

Two weeks after construction, while the silo was still empty, one hole (H7) was tested with the pavement pressuremeter. Hole H7 was prepared and tested in the same way as Holes H1 and H2. The modulus profile is shown on Fig. 16.

Analysis of Results.—As can be seen from the vane profile (Fig. 14), the deposit is stronger in the dessicated crust from 0 m–2 m depth than it is from

2 m–3 m depth. From 0 m–2 m, the field vane shear strength averaged 70 kPa, and the undrained laboratory shear strength, as estimated from the two multistage triaxial tests (Tests No. 255 and 256), averaged 100 kPa. From 2 m–3 m, the field vane shear strength is less and averages 35 kPa. The pavement pressuremeter modulus profiles (Fig. 16) show the same overall strong-soft variation with depth.

The pressuremeter modulus profiles, before the concrete slab was poured (Holes H1 and H2, Fig. 13), show a slight increase in modulus with increase in depth from 0 m–2 m, but there is no clear break in the curves. Pressuremeter

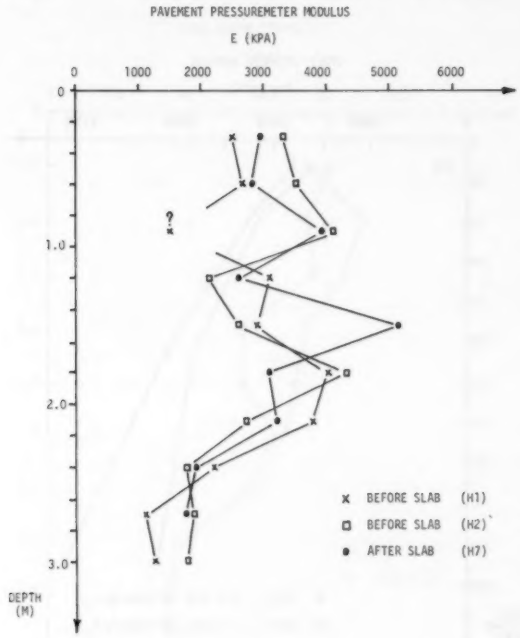

FIG. 16.—Pavement Pressuremeter Tests: Modulus Profile in Clay (1 m = 3.281 ft; 1 kPa = 20.885 psf)

tests through the raft foundation of the silo were carried out in Hole H7 at the same levels as were the tests in H1 and H2. If there had been a critical depth, it would have moved up as the slab was built, since the slab and the silo applied a pressure of 34 kPa to the ground surface—equivalent to about 2 m of clay. Comparison of the E profiles of H1 and H2 with the profile of H7 (Fig. 16) shows no obvious difference. It can be concluded, therefore, that there is no clear evidence of a critical depth in the pavement pressuremeter modulus profiles—at least to the equivalent depth of 5 m which was investigated. The slight increase in modulus values with depth may be due to the increase

in confining stress around the pressuremeter with depth. This increase in modulus values is much less pronounced for the clay than for the sand.

Conclusions

1. The results of 66 presuremeter tests in an artificially deposited sand, and the results of the 38 pressuremeter tests in a natural clay deposit, seem to indicate that the proximity of the ground surface has no significant influence on the small strain deformation of the soil around the pressuremeter probe.

A corrollary to this first conclusion is that cylindrical expansion of the borehole is as valid an assumption at shallow depth as it is at large depth, and that the same mathematical technique can be used to obtain E from a shallow test as from a deep pressuremeter test.

The practical significance of this conclusion is that the pressuremeter can be used for measuring soil moduli at very shallow depth. This is extremely important for the proposed method of pressuremeter based design and evaluation of rigid and flexible pavements including the design of pavement overlays, compaction control, the control of foundation beds, and so on.

2. During the study described in this paper, the pressuremeter moduli were found to vary with depth; this phenomenon was attributed to such factors as an increase in the at-rest stresses with depth (sand tests and variations in the soil strength (clay tests). The variation in pressuremeter moduli was seemingly not due to a critical depth phenomenon.

3. The results of 20 Menard GA pressuremeter tests in sand indicate that there is a critical depth as far as limit pressure is concerned. In both compact and dense sand, this critical depth is about 1.2 m (4 ft).

4. The fact that there is no critical depth influencing deformation moduli measurements using the pressuremeter, whereas there is a critical depth affecting p_f^*, shows that the phenomenon of critical depth depends on the magnitude of the volume changes in the ground. This may mean that there may be no critical depth influence on pile capacity at working load (small deformation)—at least for cast-in-place (prebored) piles. The critical depth phenomenon may only appear at ultimate load (large displacement).

Acknowledgments

This research was funded by Transport Canada and the writers are grateful for the support and encouragement given by L. Hunter, G. Argue, and J. Bertok of Transport Canada throughout the project. The National Research Council of Canada provided a scholarship to the first writer which enabled him to carry out the work as part of a Ph.D. Program at the University of Ottawa where the second writer was a Professor of Civil Engineering.

Appendix.—References

1. Baguelin, F., Jezequel, J.-F., and Shields, D. H., *The Pressuremeter and Foundation Engineering*, Trans Tech Publications, Rockport, Mass., 1978.
2. Bowes, W. H., and Russel, L. T., *Stress Analysis by the Finite Element Method for Practicing Engineers*, Lexington Books, Lexington, Mass., 1975.
3. Briaud, J.-L., "The Pressuremeter: Application to Pavement Design," thesis presented

to the University of Ottawa, at Ottawa, Canada, in 1979, in partial fulfillment of the requirements for the degree of Doctor of Philosophy.

4. Briaud, J.-L., and Shields, D. H., "A Special Pressuremeter and Pressuremeter Test for Pavement Evaluation and Design," *Geotechnical Testing Journal*, Vol. 2, No. 3, 1979, pp. 143–151.
5. Briaud, J.-L., and Shields, D. H., "Use of a Pressuremeter Test to Predict the Modulus and Strength of Pavement Layers," presented at the 1981 Annual Meeting of the Transportation Research Board, held at Washington, D.C., to be published in the *Transportation Research Record*, 1981.
6. Hartman, J. P., "Finite Element Parametric Study of Vertical Strain Influence Factors and the Pressuremeter Test to Estimate the Settlement of Footings in Sand," thesis presented to the University of Florida, at Gainesville, Fla., in 1974, in partial fulfillment of the requirements for the degree of Doctor of Philosophy.
7. Janbu, N., "Soil Compressibility as Determined by Oedometer Test and Triaxial Tests," *Proceedings of the European Conference on Soil Mechanics and Foundation Engineering*, Vol. 1, 1963, p. 19.
8. Jezequel, J.-F., Lemasson, H., Touze, J., "Le Pressiometre Menard: Quelques Probelmes de Mise en Oeuvre et leur Influence sur les Valeurs Pressiometriques," *Bulletin de Liaison des Laboratoires des Pont et Chaussees No. 32*, Paris, France, 1968, pp. 97–120.
9. Menard, L., "Calcul de la Force Portante des Fondations sur la Base des Resultats des Essais Pressiometriques," *Sos-Soils*, Longjumeau, France, Vol. 2, No. 5 et 6, 1963, p. 10.
10. Skempton, A. W., "The Bearing Capacity of Clays," *Proceedings British Building Research Congress*, Vol. 1, 1951, pp. 180–189.
11. Terzaghi, K., and Peck, R. B., *Soil Mechanics in Engineering Practice*, John Wiley and Sons, Inc., New York, N.Y., 1967.
12. Vesic, A. S., "Tests on Instrumented Piles, Ogcechee River Site," *Journal of the Soil Mechanics and Foundations Division*, ASCE, Vol. 96, No. SM2, Proc. Paper 7170, 1970, pp. 561–584.

CURRENT USA PRACTICE: SLURRY WALL SPECIFICATIONS

By Richard A. Millet[1] and Jean-Yves Perez,[2] Members, ASCE

INTRODUCTION

To establish diaphragm and cutoff slurry wall design criteria and, thus, specifications, the designer must clearly establish the objectives or end results that are to be obtained. This paper considers the critical design criteria and the resulting specifications for both slurry trench diaphragm walls and cutoff walls.

Diaphragm and cutoff walls are initiated with a common process. This process is the excavation of a narrow trench without the use of significant lateral support other than that provided by a bentonite-water slurry which is pumped into the trench so that the slurry level is maintained at or near the top of the trench throughout the excavation process.

In the diaphragm wall process, after completion of a segment of excavated trench, either cast-in-place concrete (tremie process) or precast panels are used to displace the stabilizing mud and construct a load-bearing wall (vertical and lateral).

There are two types of slurry cutoff walls: (1) Soil-bentonite; and (2) cement-bentonite. In the soil-bentonite cutoff process, the bentonite slurry is displaced by a soil-bentonite mixture similar in consistency to high slump concrete. The soil backfill forms a low permeability highly plastic cutoff wall. In the cement-bentonite cutoff process, cement is added to a fully hydrated bentonite-water slurry. The cement-bentonite-water slurry is then used to both stabilize the slurry wall during excavation, and upon setting of the cement, for the permanent cutoff wall itself.

The critical design criteria for the two types of slurry walls are

1. Diaphragm walls: (1) Structural strength and integrity; (2) permanence; and (3) permeability.

[1]Principal, Woodward-Clyde Consultants, 3 Embarcadero Center, Suite 700, San Francisco, Calif. 94111.

[2]Assoc., Woodward-Clyde Consultants, 11 East Adams Street, Suite 1500, Chicago, Ill. 60603.

Note.—Discussion open until January 1, 1982. To extend the closing date one month, a written request must be filed with the Manager of Technical and Professional Publications, ASCE. Manuscript was submitted for review for possible publication on June 26, 1980. This paper is part of the Journal of the Geotechnical Engineering Division, Proceedings of the American Society of Civil Engineers, ©ASCE, Vol. 107, No. GT8, August, 1981. ISSN 0093-6405/81/0008-1041/$01.00.

2. Cutoff walls: (1) Permeability; (2) deformability; and (3) permanence.

These critical criteria can be subdivided and the corresponding building blocks of a specification developed. It is important to realize that specifications should be no more restrictive than is necessary to achieve the desired end product. To make specifications more complex and restrictive than necessary only results in raising the bid prices, delaying the progress of the work, and increasing the potential of contract litigation. Restrictive specifications may also tend to stunt the specialty contractor from trying new ideas in difficult situations in this still developing field.

End-result (performance-guaranteed) specifications are acceptable if (and this is an important if) the owner, engineer, and contractor truly understand and can agree on what end results are to be obtained. Until owners and engineers become more familiar with slurry trench techniques, applications, and limitations, some method specification will be continued to be used. However, these specifications should be tailored to the true needs of the owner. With this philosophy, we shall examine in more detail the basic criteria for slurry wall construction.

Diaphragm Wall

Structural Strength and Integrity.—Eight main criterion are recommended for consideration: (1) Continuity and stability of excavation; (2) steel reinforcement or precast panel placement, or both; (3) concrete placement (tremie process); (4) concrete fluidity (slump test); (5) concrete strength (water-cement ratio); (6) panel connections; (7) support systems (struts, rakers, tiebacks, etc); and (8) internal excavation procedures (control of soil and ground-water pressures).

Continuity and Stability of Excavation

Critical Excavation Tolerances.—Specifications normally will indicate the minimum width and depth of the wall. In addition, it is normal to specify a maximum deviation from plumbness for the wall. With respect to depth and width, these criteria are usually established by the structural requirements of the diaphragm wall, the excavating equipment thought most appropriate for the site conditions, and with regard to depth, the geologic formations into which the diaphragm wall is to be founded. In general, the excavation tolerances, and particularly, the alignment of the diaphragm wall, can be better controlled when adequate guide walls are constructed ahead of the trenching operations.

With regard to plumbness, structural or potential architectural considerations are important. The state of the art is such that walls have been built to depths of over 400 ft (122 m) with less than 6 in. (152 mm) deviation from the vertical, i.e., 1:800. However, one should specify such severe limitations on verticality only in cases where this is deemed to be a necessary requirement for the intended purpose of the wall. On most projects, tolerances of 1:80–1:100 have been used and found to be satisfactory.

Slurry Properties.—The properties of the trench stabilizing slurry are important in that they control to a great extent the stability of the trench, the removal of excavated material, and the adequacy of concrete placement. Primary slurry

properties thought to be important and typically specified are viscosity, density, unit weight or specific gravity, filtrate loss, and pH.

In slurry trench practice, viscosity is generally measured with a Marsh funnel. Viscosity is a measure of the ability of a fluid to resist shearing; a minimum viscosity of approximately forty Marsh seconds is appropriate for slurry wall construction. This value of viscosity has been found to give consistently reasonable results in ensuring the satisfactory excavation, stability, and concreting of the trench.

Minimum density of slurry has typically been set slightly over that of ground water. Some specifications have set minimum densities so high that, if prepared with bentonite alone, the mixture would not even flow. Such high densities can only be obtained if fine sands or other excavated material are mixed in with the slurry. Because it is important in a diaphragm wall to minimize the sand content of the slurry so that the eventual tremie concreting operations are not impeded, it is important that a minimum density for a diaphragm wall should not be made a severe limitation (actually, it is probably more appropriate to rely on control of the viscosity). Specified maximum unit weight typically is on the order of 65 lb/ft (29 kg/m^3)–75 lb/ft (34 kg/m^3), and is limited to ensure the tremie processes are not impeded.

Another factor considered in slurry trench specifications is the maximum allowable sand content prior to concrete placement. This parameter can be measured directly by screen tests or, more commonly, indirectly by the density of the slurry. Prior to tremie concreting of the diaphragm wall, it is typically specified that the sand content should not exceed 5%.

Filtrate loss for a bentonite slurry is determined by a standard filter press test [American Petroleum Institute (API) Test PP131B]. The filter press test is used to simulate the formation of filter cake that is built up on the excavated surfaces by the electrokinetic forces and seepage forces pushing the slurry through the sides of the trench. Filtrate loss and corresponding cake thickness are indicative of how much slurry loss will occur during excavation of the trench, and how fast the cake will form or reform on the sides of the trench when damaged, e.g., by the excavating tool.

Filtrate loss is indeed a measurement of the stability of the slurry. A polluted slurry, be it by cement or by other chemicals such as salts or acids, will have a high filtrate loss.

To ensure a slurry of adequate quality, the engineer should specify a reasonable upper limit for the standard filtrate loss. Normal range of filtrate loss for bentonite slurries for slurry wall construction is from 15 cm^3–30 cm^3.

Usual range of filtrate loss for cement-bentonite slurries is much higher, in general from 100 cm^3–180 cm^3. Actually, in this application, it is preferred to measure the filtrate loss of the fully-hydrated bentonite slurry before the addition of cement. That filtrate loss should be maintained below 30 cm^3.

The last important control item on slurry properties is pH, especially in an area where the chemistry of the soil excavated or of the groundwater could dramatically change the pH of the bentonite slurry mixture. The most desirable range for the slurry pH is in the order of 6.5–10. If the pH becomes greater than 10.5, the slurry should be watched very closely for it will tend to floculate and settle out. At this point it may be necessary to require the addition of a defloculating agent to ensure continued effectiveness of the slurry.

Groundwater Conditions.—It is extremely important that ground-water conditions in the area of the trench and excavation be thoroughly understood. This will include a sound understanding of the seasonal variations, as well as the potential for dramatic changes in ground-water levels due to anomalous weather conditions. Conditions such as artesian pressures and other geologic anomalies, such as springs and man-made sources of water (such as broken sewers) also should be thoroughly understood in order to avoid difficulties with the stability of the trench excavation. Once ground-water conditions are defined, specifications should require that the slurry in the excavation be kept a minimum of 3 ft (1 m)–5 ft (1.5 m) above the maximum ground-water level. The ability to set the minimum distance that the slurry should be above highest ground-water level is directly related to the ability one has in establishing that ground-water level, i.e., the less certainty, the greater the distance one should stay above the estimated ground-water table.

Subsurface Conditions.—As with ground water, it is important to thoroughly understand the subsurface soil or bedrock conditions in the area of the proposed excavation, or both. Areas of problem excavation, such as boulders, cemented layers, broken rock, extremely pervious horizons, impervious layer boundaries, foundation levels, etc., must be thoroughly understood and presented to the contractor if the diaphragm wall is to be properly excavated and constructed.

Steel Reinforcement Placement

The steel reinforcement requirements for a concrete diaphragm wall follow standard America Iron and Steel specifications or other appropriate steel specifications. In addition to these basic reinforcing specifications, it is important to recognize that the steel should be such that tremie concrete can be easily and thoroughly placed around the steel without honeycombs and slurry-filled voids. Consequently, it is important that steel reinforcement not be so dense and tightly placed as to present problems in concreting. Spacers on the external reinforcing bars on the reinforcing cage must be installed to ensure proper placement of the reinforcing cage in the slurry wall and ensure proper concrete coverage of the steel on the external faces of the wall. To facilitate future construction, sleeves and trumpets for future tiebacks, bearing plates for future struts and structural members, knockout panels, and shear keys can be included in the reinforcing cage. It is important to remember that because the reinforcing cage is placed in sections panel by panel, it must be checked to ensure the integrity of the cage while and prior to its placement into the excavation. Techniques to connect reinforcing cages across panel joints are available.

The adherence of slurry to the reinforcing bars does affect the concrete-to-steel bond, but not sufficiently to control design. Reduction factors of 0.8–0.6 have been used.

Placement of precast panels into a cement-bentonite slurry trench is a relatively new advancement of diaphragm walls. As with any diaphragm wall, the most difficult part of the precast panel operation is to ensure panel connections are intact and properly aligned. Proper spacers must again be used and vertical and horizontal alignment of the panels must be monitored, during and after installation. Existing proprietary precast panel techniques usually include a special surface treatment of the excavation side of the panels to facilitate removal of the hardened cement-bentonite slurry.

Concrete Placement (Tremie Process)

The standard tremie concreting processes are applicable in the placement of concrete in bentonite slurry diaphragm wall construction. The tremie pipe(s) should remain embedded in the fresh concrete for at least 5 ft (1.5 m) at all times. When concreting wide panels, e.g., panels wider than 30 ft (9.2 m), it is recommended that more than one tremie pipe be specified. A rule of thumb is to use one tremie per 15 ft (4.6 m) of panel. The design of the concrete mix must ensure that the maximum size of aggregate is appropriate to the tremie process as regards the spacing of steel reinforcement. The tremie process also is affected by the slurry viscosity, density, and consequently, sand content. It is important that in the tremie process, sufficient concrete be on hand to adequately backfill a panel section without interruption so as not to cause a formation of horizontal cold joints and, thus, slurry seams during the concreting process.

Concrete Fluidity (Slump Test)

It is normally considered good practice to specify concrete fluidity (as measured by the standard concrete slump test) in the range of 7 in.–9 in. (180 mm–230 mm). This will ensure adequate flow of the concrete in the tremie system and the displacement of the slurry in the wall panels. Stiffer mixes usually lead to voids and open honeycombs in the panels, particularly where the reinforcing cage is dense.

Concrete Strength (Water-Cement Ratio)

The strength of the concrete in the backfilled diaphragm wall is directly related to the water-cement ratio of the concrete mix. Consequently, normal American Concrete Institute (ACI) specifications and practice can be followed in specifying the required structural strength of the concrete.

Panel Connections

There are various positive panel construction connection techniques that can be specified to ensure that there is a structural tie between adjacent panel sections and that these sections have adequate strength and integrity to support the design loads imposed upon them. Some of these connections are proprietary, others have become standard practice. In many cases, this is a good place to require an end-result specification, i.e., require that the strength, integrity, and continuity of the joints is maintained and allow the contractor to use his ingenuity to develop an appropriate scheme.

Support Systems (Struts, Rakers, Tiebacks, Etc.)

The support system needed to provide the temporary or permanent support for concrete diaphragm walls after excavation inside the wall enclosure is very similar to that for any retaining wall. Consequently, struts, rakers, and earth and rock tiebacks are appropriate and have been used successfully with diaphragm walls.

In addition, cantilever design by internal stiffening with vertical still members, and by post-tensioning, are recent developments.

Internal Excavation Procedures (Control of Soil and Ground-Water Pressures)

Many times, structural support of diaphragm walls has been determined by the design engineer only in a final excavated condition, whereas internal support systems described previously and ground water and soil conditions inside the excavation area, are left totally up to the contractor. This can cause difficulties in that there may be certain combinations of construction conditions, i.e., ground water, excavated soil and rock conditions, and installation procedure of retention system, which can lead to higher stresses during excavation than considered for the permanent conditions.

If the engineer feels this may be the case, it may be necessary to either work out a compatible system with the eventual contractor or place limits in the specification on the procedures that must be followed in installing the support system for the concrete diaphragm wall, and on the sequence of excavation.

A simple example of a possible problem would be permitting total dewatering of the interior of the excavation and removal of a large lift thickness of excavated material without the placement of the first interior support, e.g., tieback, raker, etc. These conditions must be examined in close detail on a job-by-job basis and then the engineer must decide what are the maximum limits he can permit the contractor to develop, and where he must specify control to ensure the structural strength and integrity of the wall.

Permanence.—Permanence of a concrete diaphragm wall is of eminent importance. In most cases, the concrete diaphragm wall has become a permanent part of the structure and, thus, must endure for the life of the structure. There are four areas of general concern and interest: (1) Active role in foundation; (2) reinforced concrete permanence; (3) tieback permanence; and (4) architectural considerations.

Active Role in Foundation

As previously identified, many typical concrete diaphragm walls become an integral part of the foundation of the proposed structure, either as a permanent retaining wall or vertical load-bearing member, or both. In this regard, all considerations that are involved in any permanent foundation unit must be reviewed and evaluated in controlling and specifying the desired end result.

Reinforced Concrete Permanence

As for any other subsurface structures, time-dependent corrosion must be taken into account for diaphragm slurry walls. The quality of the concrete may be altered with time by aggressive ground water. In some cases, sulfate resistant cement may have to be specified. In other cases, the concrete may have to be designed to withstand the long-term corrosive action of saline or acidic waters. Because the concrete in a diaphragm slurry wall is actually cured under rather ideal humidity and temperature conditions, shrinkage cracks are not usually of concern.

Tieback Permanence

A recent practice that has been developed in Europe concerns the use of permanent earth tiebacks to support permanent concrete diaphragm walls. This practice consists of providing access to the jacking head of earth anchors; this permits the rejacking of the anchors over the life of the structure.

Corrosion is also a concern for permanent stressed tiebacks. The designer should be aware of the corrosion potential of the soil and rock mass surrounding the tiebacks. The specifications should include measures, such as protective coatings and grouting, cathodic protection, etc.

Architectural Considerations

In many applications, the interior portions of concrete diaphragm walls can be left exposed, i.e., subway excavations, basements of parking garages in buildings, etc. Where this is the case, certain limitations on concrete projections into the excavation may be appropriate. There have been many case histories where the interior of the diaphragm walls, when exposed upon excavation, have been found to be quite satisfactory for use without any additional cosmetic applications.

Permeability.—With regard to the permeability of the concrete diaphragm wall, it is typical to specify that there be no free-water leakage through the wall, but depending upon the architectural and social use of the interior part of the exposed slurry wall, dampness of the wall may be permitted. It is of course possible that in certain applications even dampness needs to be limited. If this is the case, the engineer will have to recognize that the more restrictive the specifications, the greater the likely bid costs.

For permeability, five primary criteria are recommended for consideration: (1) Continuity and stability of excavation; (2) concrete placement; (3) concrete fluidity (slump); (4) panel connections; and (5) sleeves and other wall inserts.

Continuity and Stability of Excavation

Considerations are identical to those listed under structural strength and integrity of diaphragm walls, i.e., critical excavation techniques, slurry properties, groundwater conditions, and subsurface conditions. If the wall is not continuous and stable, then excess seepage, leakage, or dampness is certain. Of particular concern are two items: (1) The contact conditions at the bottom of the wall ensuring a watertight cutoff; and (2) the tolerances in the wall to ensure that corners and panels are closed.

Concrete Placement

Again, the same consideration consistent with structural strength and integrity applies; the tremie process must follow the same good practices as required for any tremie process.

Concrete Fluidity (Slump)

To ensure low permeability of the wall, a fluid concrete mix is needed to prevent bad concrete joints and honeycombs.

Panel Connections

There are proprietary and generally sound practices available in the profession to handle panel connections. However, most leakage through diaphragm walls occurs at the panel joints. An end-result specification may be applicable and thus permit the contractor to use his ingenuity in avoidance of leakage or dampness problems at these panel connection joints.

Sleeves and Other Wall Inserts

As mentioned previously, for future construction ease, various sleeves and inserts, e.g., for tiebacks, can be installed in the reinforcing cage prior to concreting. Often these inserts constitute a preferential seepage path for outside ground water. To avoid unacceptable water inflow, grouting behind the sleeves and inserts may have to be specified.

Cutoff Wall

The use of concrete diaphragm walls has had much exposure in the technical and construction literature; however, the use of the so-called plastic slurry cutoff

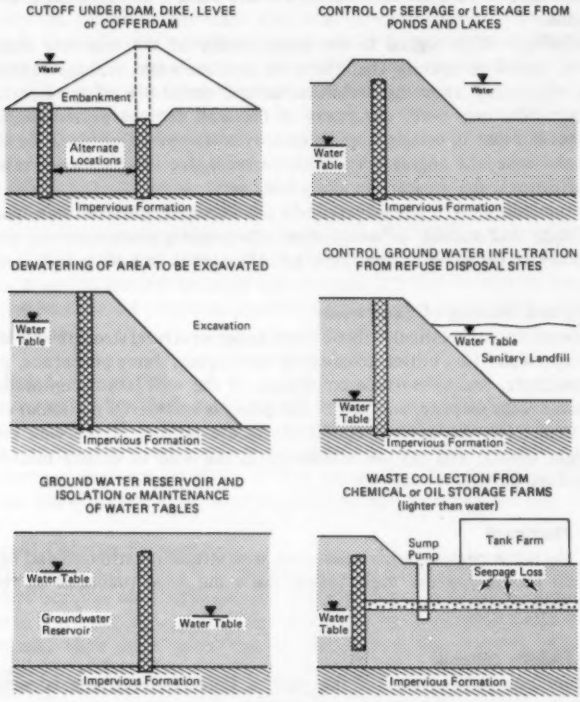

FIG. 1.—Typical Applications of Slurry Trench Cutoff Wall

wall has not had such wide-spread exposure. Fig. 1 presents typical applications of the cutoff wall as constructed with the slurry method. As can be seen from Fig. 1, applications can range from forming an impervious cutoff for a dam or dike empoundment to the containment of subsurface oil and chemical pollutants.

At the present state of the practice, two types of plastic cutoff walls are

used: (1) Walls excavated with a bentonite-water slurry and backfilled with a soil-bentonite mixture; and (2) walls excavated with a cement-bentonite-water slurry which does not need to be backfilled as cement causes the slurry to harden to strengths comparable to that of a stiff clay. With the aforementioned applications and types of cutoff walls in mind, there are three prinicpal design criteria which we believe to be important considerations in the preparation specifications for construction of plastic cutoff walls. These criteria are permeability, deformability, and permanence.

Permeability.—Permeability is, of course, the most important characteristic of the cutoff wall in that the major reason this type of slurry trench/wall is constructed is to minimize the passage of fluid. Cutoffs can prevent infiltration into an excavation, retain water in a reservoir, or prevent a leakage of polluted chemicals, oils, gasoline, etc., out of a containment area. The following five factors are important to the eventual permeability of a slurry trench cutoff wall: (1) Continuity and integrity; (2) thickness of wall (hydrostatic head); (3) cutoff backfill properties; (4) backfill placement for soil-bentonite cutoff; and (5) connection detail with surface structures.

Continuity and Integrity

It is quite important that the slurry trench excavation be continuous so as not to permit seepage zones or zones of pervious material to breach the cutoff. In this regard, the following factors must be considered.

Critical Excavation Tolerances (Width, Depth, and Vertical Inclination).—The same factors considered in the diaphragm wall section are applicable here. The depth will be controlled in many cases by the subsurface conditions, i.e., the depth to an aquiclude and the type of containment or permeability barrier that is to be constructed. The width will be dependent upon the required permeability of the cutoff wall, the materials that make up the wall, the waterhead across the wall, and the size of available excavation equipment. These latter items will be considered subsequently. The inclination and deviation from verticality will only be important as they affect the continuity and integrity of the wall and should be specified accordingly.

Slurry Properties.—The slurry properties important to ensuring stability of the wall during excavation and backfilling are identical to those specified for diaphragm walls, i.e., viscosity, density, filtrate loss, pH, and to a lesser extent for the cement-bentonite slurry sand content.

Ground-water Conditions.—Ground-water conditions must be thoroughly understood along the entire length of the cutoff wall in order to prevent difficulties with regard to caving of the trench due to high hydrostatic pressures encountered during the excavation. As was considered for diaphragm walls, it is important that a minimum of 3 ft–5 ft (1 m–1.5 m) of slurry head be maintained in the excavation above the level of the maximum anticipated ground-water conditions. Seasonal fluctuation of ground-water levels must be established in this regard.

Subsurface Conditions.—Potential anomalous subsurface conditions that will impede either the continuity of the cutoff wall as it is being excavated or the tie-in with the subsurface aquiclude must be understood. Solutions for closures of windows in the walls must be evaluated. The minimum penetration into an aquiclude at the base of the wall must be thoroughly examined before it is specified. If the aquiclude is a competent impervious bedrock, a very minor

penetration may be satisfactory. A considerable cost penalty would be imposed on the project by requiring a 2-ft (0.6-m) penetration into a competent bedrock if it is not truly required. If, however, the excavation is to be carried into a clay aquiclude, then it might be reasonable to specify a 2-ft or 3-ft (0.5 m or 1 m) penetration into the aquiclude. Such penetration may avoid problems with regard to cleaning the bottom of the excavation, as essentially a sump has now been provided in which soil which has settled out of the slurry may collect without causing a seepage path through the wall.

Thickness of Wall (Hydrostatic Head)

In setting minimum thickness of the cutoff wall, hydrostatic head and permeability of the backfill materials must be evaluated. A typical relationship that has been developed for the use of soil-bentonite backfill slurry walls is that the wall should have a thickness of 5 ft–7.5 ft (1.5 m–2.3 m).

For a cement-bentonite slurry trench cutoff wall, the increased shear strength of the backfilled wall has typically permitted the wall thickness to be set at a minimum physical excavation thickness, i.e., somewhere between 24 in. and 36 in. (610 mm–910 mm). This width is satisfactory up to a depth of at least 100 ft (30 m) of hydrostatic head. Beyond that point, more detailed and sophisticated engineering evaluations should be carried out to evaluate the ability of cement-bentonite cutoff walls to resist hydrofracturing.

Cutoff Backfill Properties

Soil-Bentonite Backfill.—In many cases, specifications have established a gradation of soil-bentonite backfill that compares to that of a glacial clay till, i.e., a wide range of particle sizes from coarse to fine with the resultant bentonite content somewhere in the range of 2%–4% by weight and on the order of 10%–20% fines (soil particles finer than the openings of a No. 200 standard U.S. sieve). Permeabilities of such mixtures have been measured to be on the order of 10^{-6} mm/s. It must be pointed out that other gradations have been used satisfactorily for soil-bentonite backfill, including fine sands and clays.

The second factor with respect to specification of the backfill concerns its consistency. Typically, the consistency of soil-bentonite backfill is controlled by a concrete slump test. To control the slope of the backfill and to ensure that liquid slurry is not trapped in the backfill, it has been found that a slump in the range of 4 in.–6 in. (100 m–150 mm) is appropriate. If the slump is greater than this, then a very flat backfill slope is obtained which can pose problems with regard to efficiency of excavation. If the slump is less, honeycombs, voids, and entrapment of pervious materials may result which can cause breaches in the cutoff wall.

Cement-Bentonite (Self-Hardening Slurry).—The principal factors affecting the permeability of the cement-bentonite slurry (which is also the slurry used during the excavation process) are cement-water ratio, bentonite-water ratio, and, of course, mechanical procedure in making eventual panel connections between the fresh cement-bentonite slurry and the set cement-bentonite. It is important to recognize that the cutoff wall is formed by the cement-bentonite mixture which is the same material that is used to stabilize the trench during excavation. Typical permeability of cement-bentonite slurry cutoff wall is also on the order of 10^{-6} mm/s.

It is important to specify in the cement-bentonite process that the bentonite be fully hydrated with water prior to the addition of any cement. When this procedure is followed, the cement-water ratio typically will be the controlling factor in the eventual strength, deformability, and permeability of the backfill.

It is important, when panel connections are made between two excavation units, that a thorough overlapping is obtained to ensure that no windows or cold joints are created. Experience has indicated that connections may be made as long as one week later into set cement-bentonite and adequate continuity has been obtained. In some cases, retarder can be added to the cement-bentonite slurry to prevent flash set and cracking and, therefore, permit plastic contact between adjacent panel units. In many cases, the cement-bentonite slurry trench process has been used in a continuous fashion, with connections made along the wall on a daily basis.

Backfill Placement for Soil-Bentonite Cutoff

The initial backfilling procedure for a soil-bentonite cutoff wall requires that the soil-bentonite mixture be placed by a tremie process in the slurry-stabilized cutoff trench. The initial process continues until sufficient material has been placed in the excavation to permit the backfill material to become exposed at the top of the trench. Standard practices with regard to tremie should be maintained. Backfill also has been successfully tremied with a clamshell bucket.

After exposure of the backfill material at the top of the trench, the remainder of the backfill is pushed with a dozer onto the exposed backfill at the top of the slurry wall. Free fall through slurry is not permitted. Pushing the backfill forces the material to slide down into the trench under its own weight. This process is continued until the entire excavation has been backfilled. Typical slopes of the backfill surface during the backfilling process range from 5:1–10:1; the slope depends upon the slump of the backfill material and the gradation of the material involved. The higher the slump and the more uniform the gradation, the greater or flatter the slope of the backfill surface will be. A low slump and a coarse grade of material reversely will have the steepest slopes. Of course, the steeper the slope and the lower the slump, the greater the possibility of trapping sediment, partially excavated material, or fluid slurry in the cutoff wall.

Connection Detail with Surface Structures

Fig. 2 demonstrates the application of a soil-bentonite cutoff wall beneath a dam or dike embankment. It is important to recognize in the engineering application of cutoff walls that there will be some settlement and consolidation of a soil-bentonite cutoff wall. Fig. 2(*a*) presents a typical application of a slurry wall in such a circumstance. Note that if proper connection details are not carried out, there is potential for a seepage path to develop, due to consolidation of the backfill material, at the top of the soil-bentonite cutoff wall. However, a simple construction detail of forming an impervious dike, which probably would be needed to provide a working platform for the construction of the slurry wall anyway [see Fig. 2(*b*)], reduces the potential risk for such a seepage path to develop. Considerations such as this connection detail are a fundamental part of proper application of slurry wall cutoffs.

Deformability.—It is important to recognize that under major dam embankments

up to 10% foundation strain may occur and that slurry cutoff walls must be capable of sustaining such high levels of deformation without cracking or failing. This is significantly different than conditions typically faced by diaphragm walls. A major factor which controls the deformability of the cutoff wall is the cutoff material properties. The following consideration is thus separated into the two types of basic material, i.e., soil-bentonite and cement-bentonite.

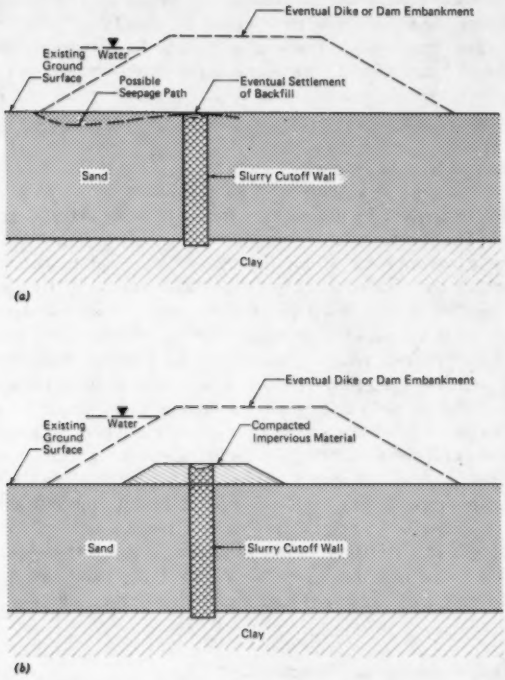

FIG. 2.—Connection Detail for Soil-Bentonite Slurry Trench Cutoff Under Embankment

Soil-Bentonite.—As considered briefly with regard to backfill slope and permeability, backfill strength is effected by gradation and slump of the backfill material. The coarser the gradation of the backfill, the more rigid and firm the eventual performance of the wall. Conversely, the greater the slump, the more flexible the wall will be with respect to potential deformations. With regard to soil-bentonite walls, however, it is suggested that when specifying a reasonable gradation of coarse to fine material and a slump of 4 in.–6 in. (100 mm–150 mm), there is little problem with deformation or cracking. Consequently, in general, it can be said that soil-bentonite walls are quite deformable and typically do not have problems with regard to cracking.

Cement-Bentonite.—The factors which effect the deformability of cement-bentonite slurry trench cutoff walls are the cement-water ratio and the bentonite-water ratio. Significant laboratory testing has been carried out to relate the cement-water ratio and, to a lesser degree, bentonite-water ratio to the deformability (without cracking) of various cement-bentonite mixtures. It has been determined that the higher the strength, i.e., the higher the cement-water ratio, the stiffer, more

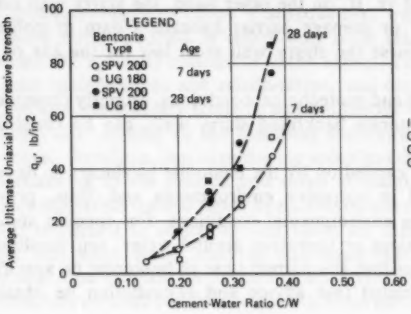

INFLUENCE OF TYPE OF BENTONITE ON ULTIMATE UNIAXIAL COMPRESSIVE STRENGTH OF CEMENT-BENTONITE SLURRIES

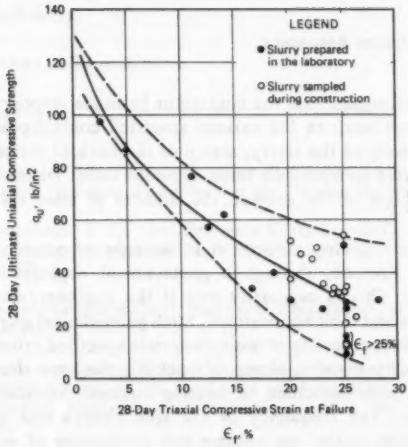

RELATION BETWEEN ULTIMATE UNIAXIAL COMPRESSIVE STRENGTH AND TRIAXIAL STRAIN AT FAILURE

FIG. 3.—Typical Strength Deformability Tests for Cement-Bentonite Slurries

rigid, and thus, less deformable, the eventual cement-bentonite wall. Correspondingly, investigation of the bentonite-water ratio indicates that the higher the bentonite-water ratio, the more flexible, the more deformable the wall may be. Fig. 3 presents a summary of typical test results for a particular application of a cement-bentonite wall. It can be seen from this plot that the cement-water ratio has a dramatic effect on deformability of the cement-bentonite backfill.

In this particular case, a 10% deformation was required. Because of the more complex relationships that must be evaluated in the application of a cement-bentonite slurry trench cutoff wall, more sophisticated testing may be required on a specific project basis to ensure the desired end result will be obtained.

Permanence.—The use of slurry trench cutoff walls may or may not have a permanent application. If a slurry cutoff wall is used around an excavation to provide a temporary dewatering expedient, then the life of the wall may be only on the order of 1 yr–2 yr. If, on the other hand, the slurry wall cutoff has been applied as a cutoff or seepage barrier beneath a dam or pollutant containment pond, then of course the slurry wall must last for the life of the structure.

Under normal environmental and geotechnical conditions, properly constructed soil-bentonite and cement-bentonite backfilled slurry walls can be considered permanent structures.

Continued research is being carried on by the bentonite producers to develop bentonites that may be used in corrosive environments and, thus, provide permanence even under severe environmental conditions. For specific applications of bentonites for anomalous or corrosive ground water, soil conditions, or containments, it is important that the correct type of bentonite be specified. In this regard, it is recommended that advice and consultation be obtained from bentonite producers.

Construction Quality Control / Quality Assurance

It is often required, in specifications, that the contractor be made responsible for running basic quality control tests on the various specified control points, i.e., viscosity of the slurry, density of the slurry, slump of the backfill material, etc. This testing is usually reported on a periodic basis, typically daily. Depending upon the size, volume, and scope of the project, the number of tests should be delineated.

In addition to the contractor's quality control, it is strongly recommended that the owner and engineer provide, through a geotechnical organization, construction quality assurance. This is especially true if the engineer/owner are not familiar with slurry walls and their applications. Such geotechnical quality assurance services would include spot testing of the appropriate specified criteria, i.e., again, slurry viscosity, slurry density, slump of backfill, concrete slump, depth of trench, proper tie-in with aquiclude or bearing stratum, verticality, cleaning of trench bottom, etc. The frequency of the spot checks and spot testing would be dependent upon, again, the volume and production of work and the discrepancy, if any, between spot checks and the contractor's quality-control testing. Such an independent quality assurance organization provides the owner with the necessary controls over the desired products and criteria that had been established in the specifications. It should be emphasized that there should not be items in the specifications that require quality control if these items are not, in fact, important to the end results or desired objective of the construction. In other words, quality control and quality assurance should be specified only for those items that truly have an effect on the desired end product.

Conclusions

There are many and varied applications for the use of slurry diaphragm and slurry cutoff walls. Their full application and exposure has not yet been developed in the United States. Because of this fact, the specialty contractors who have engaged in slurry wall construction efforts overseas and to a limited extent in the United States have developed a degree of expertise above that of owners and architect/engineer firms. Consequently, owners and architect/engineers are faced with a process in which they must establish specifications for work in which the specialty contractor is the expert. This can lead to rather awkward contract specifications and relationships, and can often result in specifications that require unnecessary controls and limitations which only generate additional cost and add nothing to the technical superiority of the wall or cutoff. It is important, therefore, that in preparing specifications for a slurry wall, a thorough understanding of the desired end result is maintained and only those specific criteria that effect the end result be addressed and controlled by the specifications.

It is important to recognize that there are many portions or applications of slurry wall work where truly an end-result specification may be appropriate. However, the application of end-result specifications in the present practice is a long way off until the owners and engineers gain a more thorough understanding and knowledge of the technical and construction procedures involved in slurry trench work.

Appendix.—Bibliography

Boyes, R. G. H., *Structural and Cut-Off Diaphragm Walls,* Halsted Press, New York, N.Y., 1975.

Caron, C., "Un Nouveau Style de Perforation La Boue Autodurcissable," *Annales de l'Institut Technique du Batiment et des Travaux Publics,* No. 311, Montereau, 1973.

D'Appolonia, D. J., "Soil-Bentonite Slurry Trench Cutoffs," *Journal of the Geotechnical Engineering Division,* ASCE, Vol. 106, No. GT4, Proc. Paper 15372, Apr., 1980, pp. 399–417.

"Cement-Bentonite Slurry Wall Saves Time, Money, as Tailings Dam Cutoff," *Engineering News Record,* Dec. 2, 1976, p. 20.

Grouts and Drilling Muds in Engineering Practice, Symposium organized by the British National Society of Soil Mechanics and Foundation Engineering at the Institute of Civil Engineers, Institution of Civil Engineers, May, 1963, Butterworths, London, England, 1963.

Diaphragm Walls & Anchorages, Proceedings, Conference organized by the Institution of Civil Engineers London, Institution of Civil Engineers, Sept. 18–20, 1974, London, England, 1975.

A Review of Diaphragm Walls, Proceedings, Institution of Civil Engineers, London, England, 1977.

"New Horizons for Construction Materials," *International Construction,* Oct., 1975, pp. 304–308.

"Cast in Situ Diaphragm Walls," *Proceedings,* VII International Conference—Specialty

Sessions 14 and 15, International Society of Soils Mechanics and Foundation Engineering, Mexico, 1969, Paris, France, 1970.

"Principals of Drilling Mud Control," Petroleum Extension Service, The University of Texas, Division of Extension, Austin, Tex.

Rogers, W. F., *Composition and Properties of Oil Well Drilling Fluids*, 3rd ed., Gulf, Houston, Tex., 1963.

Ryan, C. R., "Slurry Cutoff Walls—Design and Construction," Resource Management Products Slurry Wall Technical Course, Chicago, Ill., 1976.

Schneebeli, G., *"Les Parois Moulees dans le Sol,"* 2nd ed., Eyrolles, Paris, France, 1972.

Sherard, et al., *Earth and Earth-Rock Dams: Engineering Problems of Design and Construction*, John Wiley and Sons, Inc., New York, N.Y., pp. 304–308.

Winter, C. D., "Slurry Trench Construction," *The Military Engineer*, Vol. 68, No. 446, Nov., 1976.

Xanthakos, P., "Underground Construction in Fluid Trenches," Presented at the 1974, National Education Seminar, held at the University of Illinois, Chicago Circle, N.I.C.E., Inc., Palos Park, Ill.

Xanthakos, P., *Slurry Walls*, McGraw-Hill, Book Co., Inc., New York, N.Y., 1979.

DYNAMIC FEM MODEL OF OROVILLE DAM

By John Vrymoed,[1] M. ASCE

INTRODUCTION

Oroville Dam and Lake, keystones of the California State Water Project, are situated in the foothills on the western slope of the Sierra Nevada. The site is located 5 miles east of the City of Oroville and approximately 85 miles north of Sacramento. The dam, on the Feather River, is the highest earthfill dam in the United States. It rises 770 ft above stream-bed excavation and spans 5,600 ft between abutments at its crest. Two small embankments, Bidwell Canyon and Parish Camp Saddle Dams, complement Oroville Dam in containing the 3,537,577 acre-ft Lake Oroville. The dam and lake, along with their appurtenant structures, comprise a multiple-purpose project involving water conservation, power generation, flood control, recreation, and fish and wildlife enhancement.

The dam is zoned, rolled earthfill with impervious core, gravel shells, and appropriate transition zones. The shell materials were obtained from the vast fields of tailings produced many years ago by dredgers working over the flood plane of the Feather River for gold.

Seismic activity occurred during the months of August and September of 1975 within close proximity to Oroville Dam. During this time bedrock and dam crest acceleration time histories were recorded. The recorded bedrock motion of the August 1, 1975 main shock, and September 27, 1975 aftershock, having magnitudes of 5.7 and 4.6, respectively, were input into a two-dimensional finite element model of the dam and the computed crest motion compared to the recorded crest motions.

DESCRIPTION OF EMBANKMENT MATERIALS AND DYNAMIC INSTRUMENTATION SYSTEM

Embankment Materials.—Materials comprising the various zones of the dam considered in the analyses, shown in Fig. 1, are described as follows.

Zone 1.—Impervious core consisting of a well-graded mixture of clays, silts, sands, gravels, and cobbles to 3-in. (76-mm) maximum size. Compaction was in 10-in. (254-mm) lifts by 100-ton (90,700-kg) pneumatic rollers. Average in-place dry density achieved was 140 pcf (2,240 kg/m^3) at 8.0% moisture (average

[1] Assoc. Engr., Div. of Safety of Dams, Dept. of Water Resources, Calif.

Note.—Discussion open until January 1, 1982. To extend the closing date one month, a written request must be filed with the Manager of Technical and Professional Publications, ASCE. Manuscript was submitted for review for possible publication on June 24, 1980. This paper is part of the Journal of the Geotechnical Engineering Division, Proceedings of the American Society of Civil Engineers, ©ASCE, Vol. 107, No. GT8, August, 1981. ISSN 0093-6405/81/0008-1057/$01.00.

100% relative compaction, DWR Standard 20,000 ft-lb/cu ft (98,600 m-kg/m^3).

Zone 2.—Transition zones consisting of a well-graded mixture of silts, sands, gravels, cobbles, and boulders to 15-in. (380-mm) maximum size (6% limit on minus No. 200 U.S. Standard sieve material). Compaction was in 15-in. (380-mm) lifts by smooth-drum vibratory rollers. Average in-place dry density achieved was 151 pcf (2,400 kg/m^3) at 3.9% moisture (average 99% relative compaction).

Zone 3.—Shell zone of predominately sands, gravels, cobbles, and boulders to 24-in. (610-mm) maximum size; up to 25% minus No. 4 U.S. Standard sieve sizes permitted. Compaction was in 24-in. (610 mm) lifts by smooth-drum vibratory rollers. Average in-place dry density achieved was 147 pcf (2,350 kg/m^3) at 3.1% moisture (average 99% relative compaction).

Zone 4.—Buffer zone designed to compress contains between 15% and 45% passing No. 200 (0.074 mm) U.S. Standard sieve with 8-in. (200-mm) maximum size. Compaction was in 15-in. (380-mm) lifts by a smooth-drum vibratory roller.

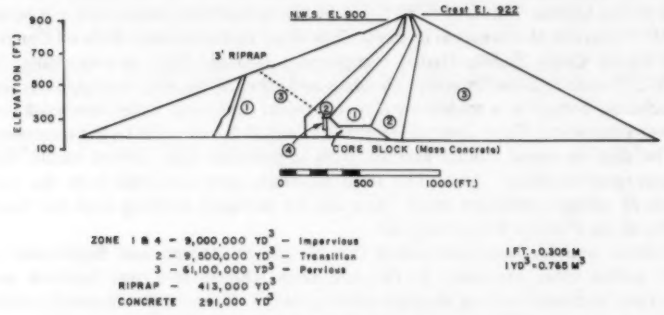

FIG. 1.—Oroville Dam Maximum Section

Dynamic Instrumentation.—Four force-balance type accelerometers were installed in the dam at the maximum section, Station 53 + 05 by the Department of Water Resources (DWR); the locations shown on Fig. 2 are as follows.

1. No. 1: Beneath the crest at Elevation 680.
2. No. 2: Beneath the crest at Elevation 801.
3. No. 3: Downstream toe, on rock Elevation 150.
4. No. 4: On the crest at downstream edge Elevation 922.

These instruments measure accelerations in the vertical and downstream direction, N46° E and along the axis 90° to this direction. In cooperation with the U.S. Geologic Survey, (USGS), three additional instruments were placed at the site. One was located at the crest along side the DWR accelerometer, one in the core block gallery, and one on rock at Elevation 1120 about 1 mile northwest of the dam (Seismograph Station). The core block and crest instruments were oriented the same as previously described; one axis of the seismograph station instrument was oriented N37° E. With the exception of the core block unit, all strong motion instruments were operable during the period of activity.

Six dynamic pore-pressure cells were installed in the upstream shell and transition zones as shown on Fig. 2. Each cell showed a response during one event or another of the August–September 1975 earthquake series. Five groups of stress cells were located in the downstream shell (Fig. 2). Each cell group measures stresses vertically and on angles of 45° in the up and downstream directions. Each cell has two transducers; one measures both static and dynamic stresses (CEC), and the other measures static stress only (MAIHAK). Cell

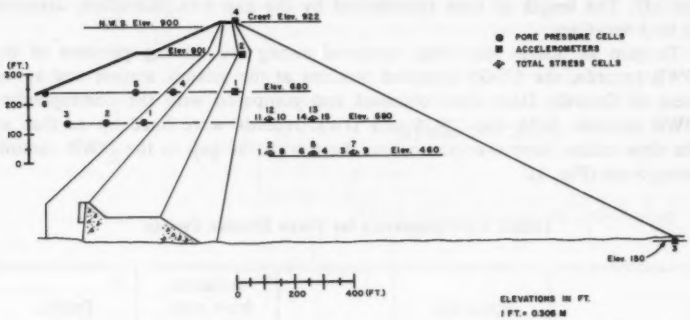

FIG. 2.—Oroville Dam Embankment: Dynamic Instrumentation

Numbers 1, 2, 5, 6, 7, 10, 11, 12, and 14 were operable during the earthquake activity.

Recorded Events

Three of the recorded events were of significance for analyzing the response of Oroville Dam. The main event of August 1, Magnitude 5.7; an aftershock of Magnitude 4.7 on August 5; and an aftershock of Magnitude 4.6 on September 27. Many other foreshocks and aftershocks were recorded but were not used in these analyses. Parameters of interest for the three events are listed in Table 1. The original accelerometer traces of these events are shown in Ref. 1.

August 1, 1975.—The DWR accelerometers were triggered by a minor foreshock and were still recording when the main shock occurred. With the arrival of the large accelerations of the main shock, other instruments (pore pressure and stress cells) were triggered resulting in an overload and a temporary loss of power. This loss of power caused all of the instruments to stop recording for most of the duration of the strong motion. After several seconds, the back-up power source had been activated and all of the instruments started to record again resulting in a gap in all the records.

The length of time represented by the gap was determined by examination of aftershock records. The records show the space between a previous and subsequent event to be of the same length as the gap in the August 1 record. After August 8, the recording speed of the recorders was increased by a factor of 2.5 in./sec–1.0 in./sec (25 mm/s). The resulting increased angular momentum

of the drum increased the space between two events to approximately 1 in. It was therefore determined that the gap in the August 1 records represented the distance the accelerometer drum rolled after power had been cut off.

The power failure was reenacted so that some insight might be given to the amount of time which elapsed between main power cutoff and the back-up power source being activated. It was determined that the generator, which is the source for the back-up power supply, needed a minimum of 5 sec–6 sec to start and supply power to the recorders once the main power supply was cut off. The length of time represented by the gap was, therefore, assumed to be 5 sec–6 sec.

To gain an insight into what occurred during the missing portions of the DWR records, the USGS recorded motions at the seismic station and at the crest of Oroville Dam were obtained and compared with the corresponding DWR records. Both the USGS and DWR records were lined up so that all the time traces have a common time base with the gap in the DWR records being 6 sec (Fig. 3).

TABLE 1.—Parameters for Three Seismic Events

Seismic event (1)	Epicenter latitude and longitude (2)	Magnitude (3)	Distance from dam, in miles (kilometers) (4)	Depth, in miles (kilometers) (5)
August 1	39° 26′–33′ 121° 31′–71′	5.7	6.9 (11.1)	5.5 (8.8)
August 5	39° 28′–73′ 121° 31′–46′	4.7	4.2 (6.8)	5.5 (8.9)
September 27	39° 30′–65′ 121° 32′–69′	4.6	2.2 (3.5)	3.5 (5.6)

The motions recorded by the DWR and USGS instruments located on the crest are identical (starting from the second part of the DWR recorded crest motion) and any differences are due to low and high pass filtering and instrument correction performed on the USGS recorded crest motion. The DWR records were not corrected for instrument response, as they would not be used in any subsequent analyses. It was noted in Ref. 2 that the first few seconds of the USGS recorded crest motion were lost. The lined up DWR and USGS crest motions as shown on Fig. 3(*b*) indicate that approximately 2.5 sec of initial crest motion is missing from the USGS record.

The USGS recorded base motion at the seismic station was positioned so that the beginning of this record lines up with the start of the strong motion recorded on DWR accelerometer 3, Fig. 3(*d*). This positioning of the USGS recorded base motion shows that the strong motion had essentially ceased by the start of the USGS recorded crest motion.

The positioning of the DWR and USGS records as shown on Fig. 3 is the best estimate of the sequence of events describing the motions experienced by the dam during the earthquake on August 1, 1975.

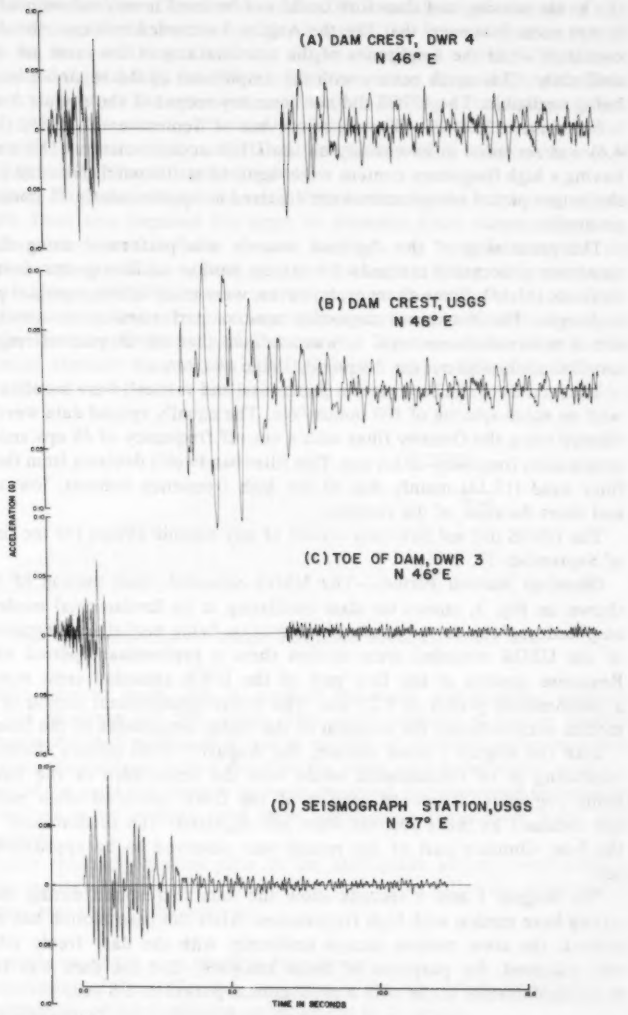

FIG. 3.—Oroville Dam Acceleration Records August 1, 1975: Upstream-Downstream Component of Motion

August 5, 1975.—The DWR recorded motions again have a major part of the event missing and therefore could not be used in any subsequent analysis. It was seen, however, that like the August 1 recorded motions, the dam freely oscillates while the amplitudes of the accelerations of the crest are decreasing uniformly. This again occurs with the amplitudes of the recorded base motion being negligible. The USGS did not have any record of the August 5 event.

September 27, 1975.—The seismic event of September 27, 1975, (Magnitude 4.6) was recorded in its entirety on the DWR accelerometers. The components having a high frequency content were digitized at 100 points/in.–150 points/in.; the longer period components were digitized at approximately 75 points/in.–100 points/in.

The processing of the digitized records was performed using the routine computer processing methods for strong motion accelerograms developed by Trifunac (13,14). Some changes, however, were made in this standard processing technique. The instrument correction was not performed as the accelerometers are of a force-balance type. It was assumed that the instrument response was unaffected throughout the frequency range of interest.

The records of the base motion (horizontal and vertical) were baseline corrected with an equal spacing of 100 points/sec. The equally spaced data were low-pass filtered using the Ormsby filter with a cut-off frequency of 48 cps and a roll-off termination frequency of 1.0 cps. This filter bandwidth deviates from the standard filter used (13,14) mainly due to the high frequency content, low amplitude, and short duration of the records.

The USGS did not have any record of any seismic events for the time period of September 27, 1975.

Observed Natural Period.—The USGS recorded crest motion of August 1, shown on Fig. 3, shows the dam oscillating in its fundamental mode with the amplitudes of the corresponding base motion being negligible. Response spectra of the USGS recorded crest motion show a predominant period of 0.8 sec. Response spectra of the first part of the DWR recorded crest motion show a predominant period of 0.25 sec. This lower predominant period of the crest motion occurs during the duration of the higher amplitudes of the base motion.

Like the August 1 crest motion, the August 5 crest motion shows the dam oscillating in its fundamental mode with the amplitudes of the base motion being negligible. Response spectra of the DWR recorded crest motion were not obtained as these records were not digitized. The predominant period of the free vibration part of the record was observed to be approximately 0.75 sec.

The August 1 and 5 records show the dam to respond during the time of strong base motion with high frequencies. After the base motion has essentially ceased, the crest motion decays uniformly with the dam freely vibrating. It was assumed, for purposes of these analyses, that the dam was responding in its fundamental mode with a predominant period of 0.8 sec.

Determination of Shear Modulus for Embankment Shell Material

General.—The August Oroville earthquake afforded an excellent opportunity for back figuring the value of the dynamic shear modulus at low strain levels since acceleration records were obtained for base rock and dam crest. The

aftershock of September 27 of which good crest and toe records were obtained was used in the analyses. The break in the DWR acceleration records of the August 1 event rendered them unusable. Instead, the Seismic Station record was used for base-rock input and the output compared to the USGS crest instrument record. Although the Seismic Station is some distance from the base of the dam, its records do represent rock motions having a frequency content similar to that of the records obtained at the dam toe. It was, therefore, felt that a reliable estimate of dynamic shear modulus would result with use of both the September 27 and August 1 events.

Static Stress Analysis.—The static stress distribution for the maximum section of Oroville Dam was required for input to dynamic finite element analysis. The nonlinear incremental finite element method was used to simulate the construction sequence of the embankment and subsequent filling of the reservoir.

Computer program ISBILD was used to carry out the static stress analysis. This program is very similar to the computer program used in the earlier analysis of Oroville Dam by Kulhawy and Duncan (4). The use of an incompatible isoparametric element by program ISBILD is the major difference between the program used in the earlier analysis which uses a two linear strain triangular element.

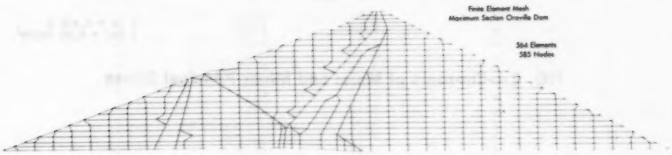

FIG. 4.—Finite Element Mesh: Maximum Section Oroville Dam

The finite element mesh, Fig. 4, used in the static and dynamic analyses contains 564 elements and 585 nodes. This mesh contains a greater number of elements in the shell zones and a smaller number of elements in the transition zone between the shell and core zones than the mesh used in the earlier analysis. As a result of the good comparison between observed and computed settlements in the previous static analysis, the same stress-strain parameters were used in this analysis.

Piezometer readings obtained prior to the earthquake activity were used to obtain the seepage force distribution in the core. The following sequence of construction was used in the analysis.

1. Construction of the core block in four layers.
2. Construction of the cofferdam, upstream of the core block, in 14 layers.
3. Construction of the remaining embankment in 27 layers.
4. Application of water load in four stages, simulating filling of the reservoir.

The results of this analysis correspond to those obtained in the previous analysis. Contours of major and minor principal stress and the orientation of these stresses is shown in Figs. 5 and 6, respectively.

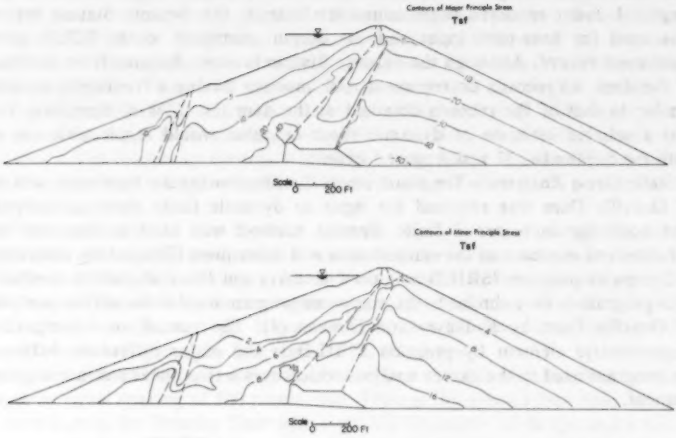

FIG. 5.—Contours of Major and Minor Principal Stress

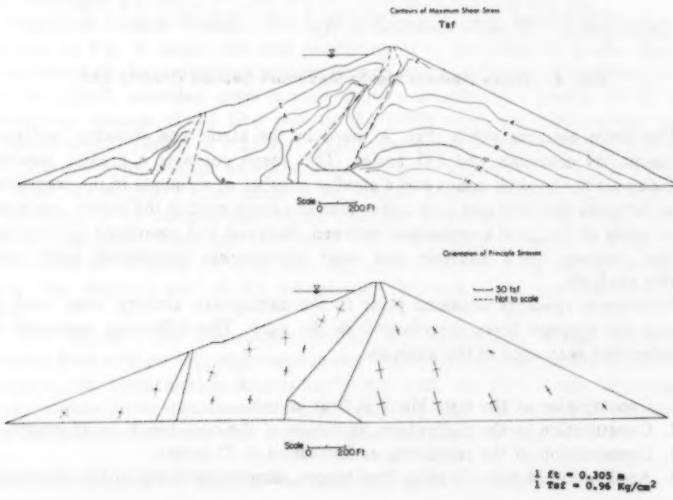

FIG. 6.—Contours of Maximum Shear Stress and Orientation of Principle Stresses

Static stresses are measured periodically at the locations shown in Fig. 2. All but three of the static stress cells were functioning at the time of the earthquakes. Over the years, static stress values have remained relatively constant. The comparison between measured and calculated static stress values is presented in Table 2. Inspection of Table 2 shows good agreement between measured and calculated vertical stresses. Inclined stresses and compression toward the downstream toe also show good agreement.

The operable cells measuring comparison toward the upstream toe yield more erratic results when compared to the calculated values. The disagreement between the calculated and measured values for the inclined cells is understandable considering the difficulty of their placement and compaction of the adjacent embankment material.

Three-Dimensional Effect.—The recorded crest motion represents the response of a three-dimensional (3-D) system. Present computer capabilities only allow for a two-dimensional (2-D) analysis of a dam the size of Oroville. A 2-D analysis

TABLE 2.—Static Stress Comparison

Cell No.	Stress Tsf		Direction of Stress
	Maihak Cell	FEM Analysis	
1	13.8	16.6	b
2	29.5	28.2	a
3	14.4	11.1	b
4	-	23.0	c
5	30.9	25.6	a
6	15.1	14.2	b
7	22.3	21.0	a
8	11.0	24.5	c
9	-	20.8	c
10	7.9	18.9	c
11	11.5	12.1	b
12	25.4	20.2	a
13	18.0	17.0	a
14	10.0	9.1	b
15	-	17.1	c

1 Tsf = 95.7 KPa

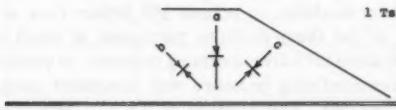

overestimates the natural period because the greater stiffness of the system resulting from the abutments is disregarded. Studies by Makdisi (6) compare the computed natural period of embankments by 2-D analyses with the natural period computed by 3-D analyses. The difference between the two computed natural periods depends greatly upon the ratio of maximum height to crest length of the dam. Results show that for the maximum height to crest length ratio of Oroville Dam, the ratio of computed natural periods by 2-D and 3-D analyses is 1.25. Thus, to obtain the actual dynamic material properties for Oroville Dam, the computed natural period for the maximum section should be greater than the observed natural period by a factor of 1.25. As the crest acceleration records exhibited a natural period of 0.8 sec, the value sought by the 2-D analysis would be 1.0 sec.

Method of Response Computation.—The dynamic FEM analyses were carried out with computer program LUSH (5). The details of the solution technique

and the formulation of the system matrices are readily available in Ref. 5. Basically, the program solves the equation of motion for undamped systems as follows:

$$[M]\{\ddot{u}\} + [K]\{u\} = -\{m\}\,\ddot{y}(t) \quad \ldots\ldots\ldots\ldots\ldots\ldots\ldots\ldots\ldots\ldots (1)$$

in which $\{u\}$ and $\{\ddot{u}\}$ = the nodal point displacement and acceleration vectors, respectively; $[M]$ and $[K]$ = the mass and stiffness matrices; and $\ddot{y}(t)$ = the given input acceleration time history. Viscous damping is incorporated in the formulation of the complex shear modulus expression. The program solves Eq. 1 in the frequency domain. The linear equivalent method is used to model the variation of damping and shear modulus with shear strain by successive iterations.

The calculation of natural period was made with solution of the eigenvalue problem

$$[K] = w^2\{M\} \quad \ldots\ldots\ldots\ldots\ldots\ldots\ldots\ldots\ldots\ldots\ldots\ldots\ldots\ldots\ldots\ldots (2)$$

in which $[K]$, $\{M\}$ and w represent stiffness matrix, mass vector, and natural circular frequency, respectively. The formulation of the stiffness matrix is based upon shear moduli which correspond to the average shear strain experienced during the duration of base motion.

Shear moduli values for the core material were determined by the use of the undrained strength and shear modulus relationship for clays as outlined in Ref. 12. The zones of core material in the maximum section constitute only 10% of the total cross-sectional area and were found to have a negligible influence in the response analyses.

The shear modulus for the shell material was computed by the following relationship:

$$G_{max} = K_{2max}\,1000\,(\sigma m')^{1/2} \quad \ldots\ldots\ldots\ldots\ldots\ldots\ldots\ldots\ldots\ldots\ldots (3)$$

in which G_{max} = the shear modulus, in pounds per square foot, at small shear strains (10^{-4}%); K_{2max} = the shear modulus parameter at small shear strains (10^{-4}%); and $\sigma m'$ = the mean effective confining pressure, in pounds per square foot. The mean effective confining pressure was computed using the results from the static FEM analysis. The average K_2/K_{2max} reduction curve for cohesionless soils reported in Ref. 12 was used in the analyses. The parameter K_{2max} was the value sought.

K_{2max}.—The maximum horizontal displacement obtained from the August 1 USGS crest displacement time history, is 0.6 in. (15 mm). Using 750 ft (230 m) as the height of the maximum section of the dam, a maximum shear strain of 6.7×10^{-3}% is computed. An effective shear strain of 4.3×10^{-3}% is obtained by using 0.65 as an averaging factor. Assuming that this is the effective shear strain that would be computed by the dynamic FEM analysis, a value for K_2/K_{2max} of 0.8 is found using the average reduction curve. With this ratio for K_2/K_{2max} a value of 320 for K_{2max} was found to correspond to a natural period of 0.8 sec by solution of the eigenvalue problem.

As the natural period sought was 1.0 sec due to three-dimensional effect, a K_{2max} value of 205 was computed, by inverse proportion. This value for K_{2max} is representative of the Oroville Dam shell material.

This value is slightly higher than the value of 190 reported by Seed (12).

Results by Wong (17) from strain controlled cyclic triaxial tests conducted on a model gradation of Oroville shell material indicated a K_{2max} of 140. The model gradation limited the maximum particle size to 2 in. (50 mm).

In view of the available data reported in the literature, shown in Fig. 7, a K_{2max} value of 205 appears to be a reasonable value for the Oroville shell material.

It is important to keep in mind the limitations on the use of the two values of K_{2max}. A K_{2max} of 205 is representative of the shell material in Oroville Dam. The K_{2max} value of 320 is only useful for analyses of the maximum section of Oroville Dam by two-dimensional techniques to simulate the actual

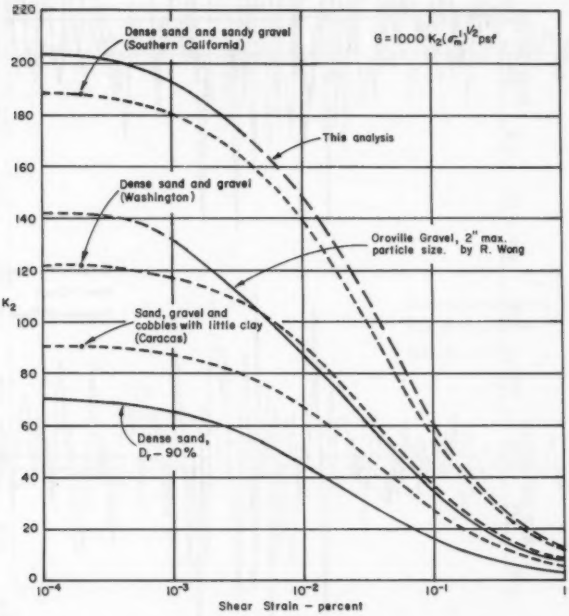

FIG. 7.—Moduli Determinations for Gravelly Soils

three-dimensional behavior. The use of a K_{2max} value of 320 in a two-dimensional analysis will simulate the actual three-dimensional accelerations and displacements by artificially stiffening the material. Stiffening the material in this manner results in stresses which are too high, because the strengthening effect of the third dimension is not modeled in the analysis. So that for a proper stress analysis the value of 205 for K_{2max} is appropriate.

The validity of the parameters determined by the methods described was determined by check analyses using the acceleration records of the September 27 and August 1 events.

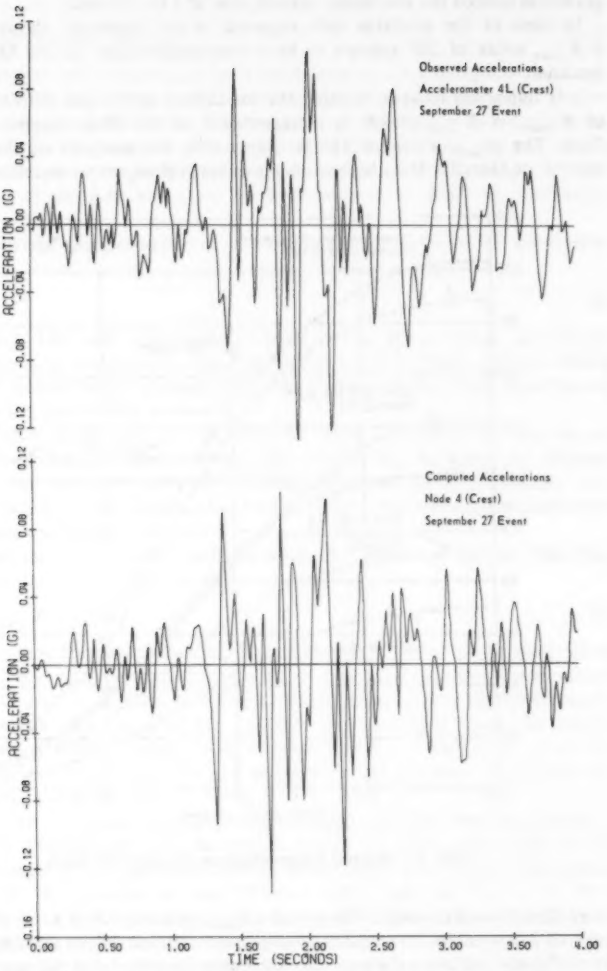

1 G = 9.8 m/sec^2

FIG. 8.—Observed and Computed Acceleration Time Histories, September 27, 1975: Crest of Oroville Dam

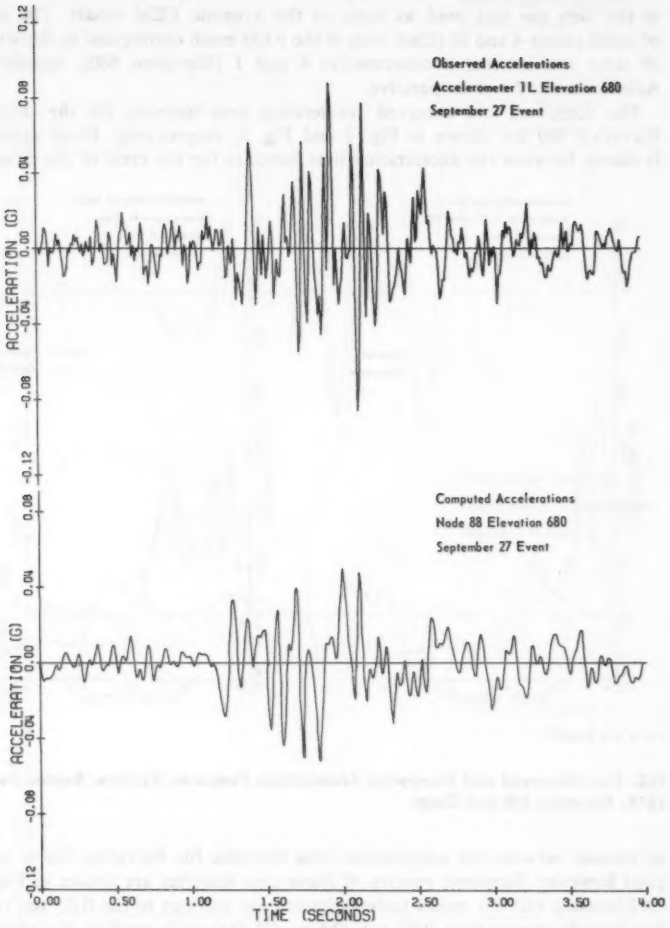

1 G = 9.8 m/sec^2

FIG. 9.—Observed and Computed Acceleration Time Histories, September 27, 1975: Elevation 680

Comparison of Observed and Computed Motions

September 27 Event.—The bedrock motion of the September 27 event recorded at the dam toe was used as input to the dynamic FEM model. The output of nodal points 4 and 88 (Elev. 680) in the FEM mesh correspond to the location of crest and internal accelerometers 4 and 1 (Elevation 680), respectively. Accelerometer 2 was inoperative.

The computed and observed acceleration time histories for the crest and Elevation 680 are shown in Fig. 8 and Fig. 9, respectively. Good agreement is shown between the acceleration time histories for the crest of the dam. The

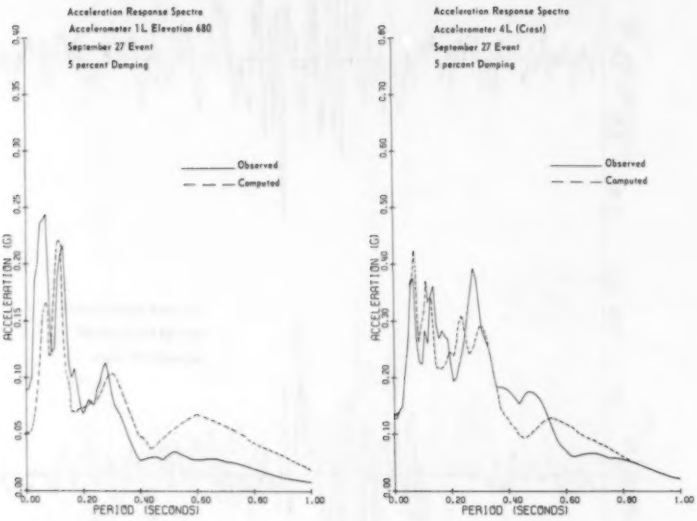

1 G = 9.8 m/sec^2

FIG. 10.—Observed and Computed Acceleration Response Spectra, September, 27, 1975: Elevation 680 and Crest

agreement between the acceleration time histories for Elevation 680 is not as good however. Response spectra of these time histories are shown in Fig. 10. At Elevation 680 the model underestimates the motions in the 0.05 sec range. For periods greater than 0.05 sec, the model favorably predicts the observed response spectra. For the crest of the dam, favorable agreement is shown between observed and computed response spectra particularly in the 0.05 sec range. Deviations between response spectra for both the crest and Elevation 680 occur for periods in excess of 0.4 sec. These deviations are primarily due to the September 27 event lacking significant motions with periods in excess of 0.4 sec. The acceleration time histories were integrated to obtain displacement time histories as shown in Fig. 11. The maximum displacement of the observed

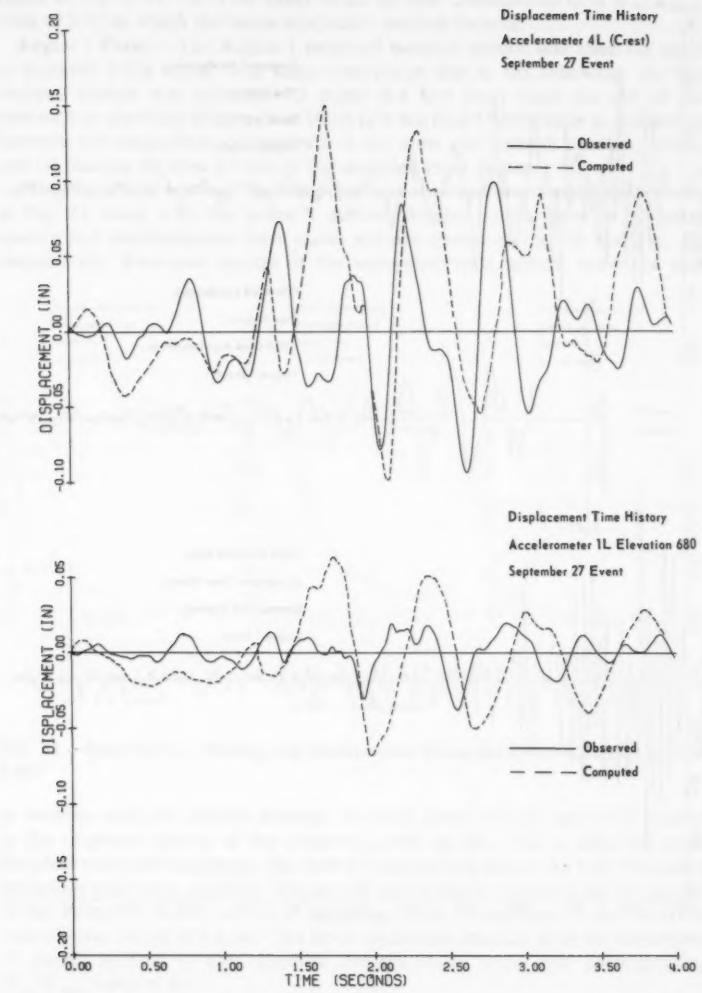

1 inch = 2.54 cm

FIG. 11.—Observed and Computed Displacement Time History, September 27, 1975: Elevation 680 and Crest

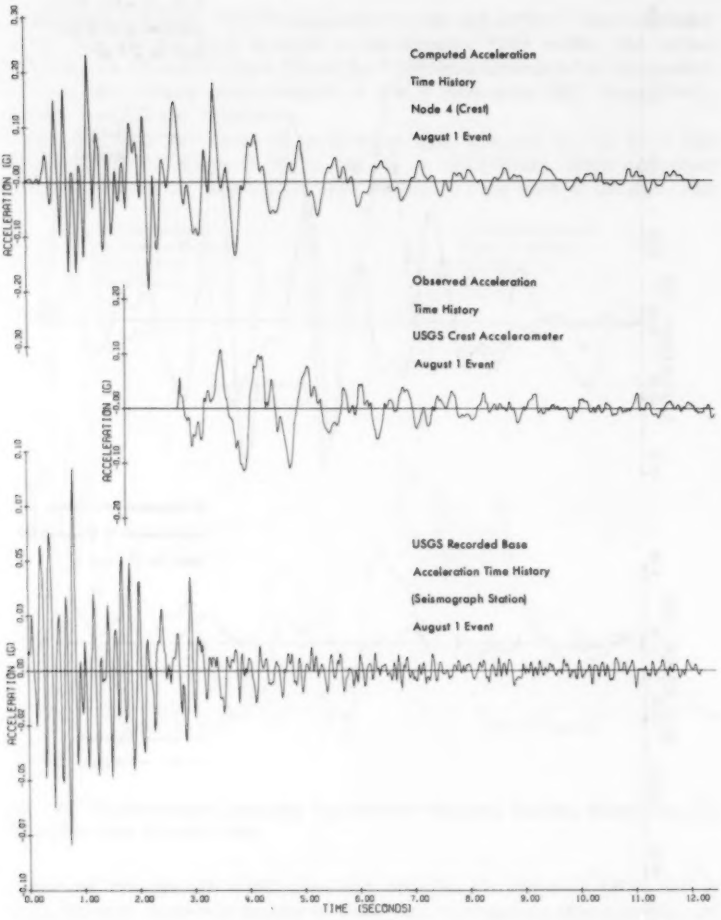

1 G = 9.8 m/sec^2

FIG. 12.—Observed and Computed Crest and Bedrock Acceleration Time History: August 1, 1975

crest motion is 0.1 in. (2.5 mm) which corresponds to an average induced shear strain of $7.2 \times 10^{-4}\%$. This shear strain in turn corresponds to a K_2/K_{2max} ratio of 0.92 to which the linear equivalent method iterated.

August 1 Event.—The August 1 recorded bedrock motion was used for input to dynamic FEM model with some reservation due to the following: (1) The bedrock motion was recorded 1.5 miles (2.4 km) away from the toe of the dam with an elevation difference of 900 ft (275 m); (2) a 9° difference in orientation between the longitudinal components of the crest and bedrock accelerometers; and (3) missing the first 2.5 sec of the recorded crest motion.

The comparison between the computed and observed crest response is shown in Fig. 12 along with the bedrock motion. Similar comparisons of response spectra and displacements were made and are shown in Fig. 13 and Fig. 14, respectively. Response spectra of the computed crest motion show the dam

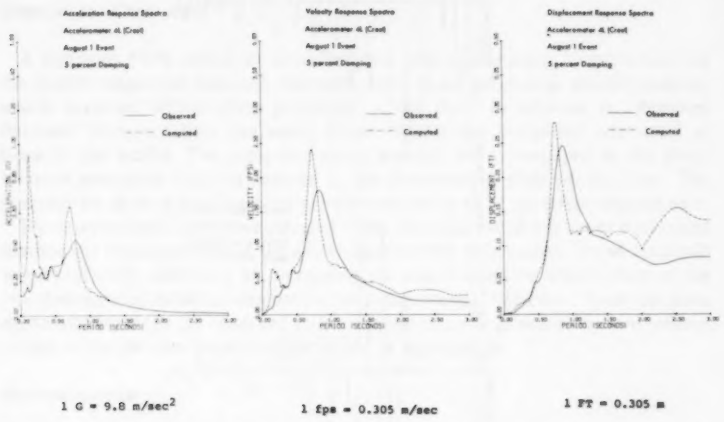

FIG. 13.—Acceleration, Velocity and Displacement Response Spectra, August 1, 1975: Crest

to oscillate with two distinct periods. The first period of 0.15 sec is not evident in the response spectra of the observed crest motion. This is expected since the observed crest motion has the first 2.5 sec missing where the high frequency motions would have occurred. The second period shown on the response spectra of the observed motion occurs at 0.75 sec which corresponds to the observed predominant period of 0.8 sec. The linear equivalent method, as in the September 27 event, iterated to the observed average shear strain and corresponding K_2/K_{2max} ratio of 0.8.

The favorable comparisons between the computed and observed acceleration time histories response spectra and induced average shear strains gives validity to the FEM model chosen.

Recordings of stress for the August 1 event were also marred by a gap due to the power loss. Before the gap, a peak dynamic stress of 23 psi (190 kPa) was recorded by cell No. 5, the other stress cells showed very minor fluctuations.

During the September 27 event a maximum stress of 9 psi (60 kPa) was recorded by cell No. 5. The recorded stresses were too small for any meaningfull comparisons with computed stresses. The computed stresses for the September 27 event were on the order of 6 psi (40 kPa)–9 psi (60 kPa).

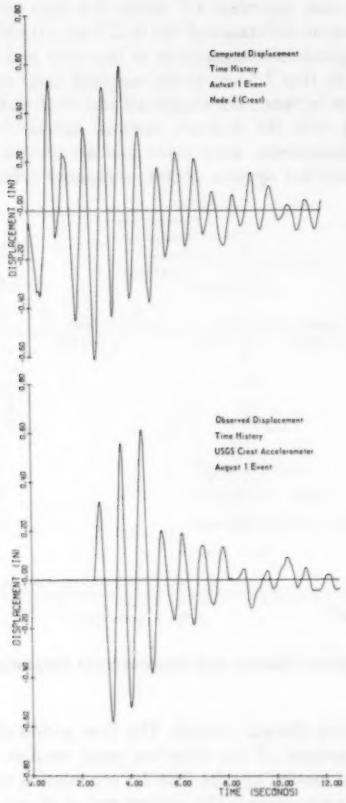

1 inch = 2.54 cm

FIG. 14.—Observed and Computed Displacement Time History, August 1, 1975: Crest

Pore-pressure cell No. 1 registered a maximum pressure increase of 13 psi (90 kPa) which was dissipated during the 6-sec gap. Pore-pressure cells 4, 5, and 6 also showed a minor fluctuation on the order of 2 psi (15 kPa)–5 psi (35 kPa).

Fortuitously, the crest monuments were surveyed a couple of weeks prior

to the August 1 earthquake. The monuments were again surveyed immediately after the event. Measurements indicated that the crest at the maximum section had settled 0.4 in. (10 mm). An attempt was made to duplicate this settlement with the FEM model. Two static "gravity turn-on" FEM analyses were made using the computed modulus at small shear strains (10^{-4}%) and the elastic modulus at the average induced shear strain caused by the August 1 earthquake. The difference between the two analyses in displacement of the crest was taken as the settlement induced by the earthquake. A permanent displacement of 0.5 in. (15 mm) was determined in this manner which compares favorably with the measured settlement of 0.4 in. (10 mm). This method of computing permanent settlement assumes that the settlement is due to gravity loads of the structure acting upon a reduced elastic modulus. This reduction of elastic modulus is a result of the induced strain caused by the earthquake.

Summary and Conclusion

A dynamic FEM model of Oroville Dam was constructed. Construction of the model employed dynamic characteristics observed during seismic activity which occurred within close proximity to the dam. In addition to observed dynamic characteristics, the static stress distribution computed was used as input to the model. The computed static stresses were compared to the static stresses measured by cells located in the downstream shell of the dam. The comparison showed good agreement between mostly all of the stress components.

By observation of the natural period of the dam and use of the linear equivalent method the shear modulus of the shell materials was determined. These materials were artificially stiffened by increasing the shear modulus which allowed the two-dimensional model to simulate a three-dimensional behavior. From the good agreement between the observed and computed motions produced by two seismic events it can be concluded that the model is appropriate.

Acknowledgment

The writer wishes to acknowledge the support during the course of this study of his good friends and colleagues William J. Bennett, Rashid Ahmad, Emil Calzascia, and E. W. Stroppini, who gave the writer the time and freedom to develop the capability to conduct these types of studies.

Appendix I.—References

1. "The August 1, 1975, Oroville Earthquake Investigations," *Bulletin 203-78*, California Department of Water Resources, pp. 192–220.
2. "Oroville, California Earthquake, 1 August, 1975," *Special Report 125*, California Division of Mines and Geology.
3. Castro, G., "Liquefaction and Cyclic Mobility of Saturated Sands," *Journal of the Geotechnical Engineering Division*, ASCE, Vol. 101, No. GT6, Proc. Paper 11388, June, 1975, pp. 551–569.
4. Kulhawy, F. H., Duncan, J. M., "Nonlinear Finite Element Analysis of Stresses and Movements in Oroville Dam," *Report No. TE-70-2*, Department of Civil Engineering, Institute of Transportation and Traffic Engineering, University of California, Berkeley, Calif., Jan., 1970.
5. Lysmer, J., Udaka, T., Seed, H. B., Hwang, R., "LUSH a Computer Program for

Complex Response Analysis of Soil-Structure Systems," *Report No. EERC 74-4*, Earthquake Engineering Research Center, University of California, Berkeley, Calif., Apr., 1974.
6. Makdisi, F., "Performance and Analyses of Earth Dams During Strong Earthquakes," Thesis presented to the University of California at Berkeley, in 1976, in partial fulfillment of the requirements for the degree of Doctor of Philosophy.
7. Mori, K., Seed, H. B., Chan, C. K., "Influence of Sample Disturbance on Sand Response to Cyclic Loading," *Journal of the Geotechnical Engineering Division*, ASCE, Vol. 104, No. GT3, Proc. Paper 13594, Mar., 1978, pp. 323–339.
8. Nobari, E. S., and Duncan, J. M., "Effect of Reservoir Filling on Stresses and Movements in Earth and Rockfill Dams," *Report No. TE-72-1*, Department of Civil Engineering, Institute of Transportation and Traffic Engineering, University of California, Berkeley, Calif., Jan., 1972.
9. Ozawa, Y., and Duncan, J. M., "Isbild: A Computer Program for Analysis of Static Stresses and Movements in Embankments," *Report No. TE-73-4*, Department of Civil Engineering, Institute of Transportation and Traffic Engineering, University of California, Berkeley, Calif., Dec., 1973.
10. Seed, H. B., Lee, K. L., Idriss, I. M., Makdisi, F., "Analysis of the Slides in the San Fernando Dams During the Earthquake of February 9, 1971," *Report No. EERC 73-2*, Earthquake Engineering Research Center, University of California, Berkeley, Calif., June, 1973.
11. Seed, H. B., Idriss, I. M., Makdisi, F., Banergee, N., "Representation of Irregular Stress Time Histories by Equivalent Uniform Stress Series in Liquefaction Analyses," *Report No. EERC 75-29*, Earthquake Engineering Research Center, University of California, Berkeley, Calif., Oct., 1975.
12. Seed, H. B., and Idriss, I. M., "Soil Moduli and Damping Factors for Dynamic Response Analyses," *Report No. EERC 70-10*, Earthquake Engineering Research Center, University of California, Berkeley, Calif., Dec., 1970.
13. Trifunac, M. D., "Low Frequency Digitization Errors and a New Method for Zero Baseline Correction of Strong-Motion Accelerograms," Earthquake Engineering Research Laboratory, *EERL 71-07*, California Institute of Technology, Pasadena, Calif., 1970.
15. Vrymoed, J., and Calzascia, E., "Simplified Determination of Dynamic Stresses in Earth Dams," *Proceedings of the ASCE Geotechnical Engineering Division Specialty Conference*, Vol. II, Earthquake Engineering and Soil Dynamics, June 19–21, 1978, Pasadena, Calif.
16. Wong, K. S., and Duncan, J. M., "Hyperbolic Stress-Strain Parameters for Nonlinear Finite Element Analyses of Stresses and Movements in Soil Masses," *Report No. TE-74-3*, Department of Civil Engineering, Institute of Transportation and Traffic Engineering, University of California, Berkeley, Calif., July, 1974.
17. Wong, R. T., "Deformation Characteristics of Gravels and Gravelly Soils Under Cyclic Loading Conditions," Thesis presented to the University of California at Berkeley, Calif., in 1974, in partial fullfillment of the requirements for the degree of Doctor of Philosophy.

Appendix II.—Notation

The following symbols are used in this paper:

c = cohesion;
d = parameter;
F = parameter;
G = Poisson's ratio, parameter;
G_{max} = shear modulus at small strains;
K = modulus number;
$\mathbf{K}$ = stiffness matrix;
K_2 = shear modulus parameter;

K_{2max} = shear modulus parameter at small strains;
M = mass matrix;
n = modulus exponent;
R_f = failure ratio;
u = node point displacement;
$\ddot{u}$ = node point acceleration;
w = natural circular frequency;
$y(t)$ = input acceleration time history;
γ = unit weight;
σ'_m = mean effective confining pressure;
σ_1 = major principle stress;
σ_3 = minor principle stress; and
ϕ = friction angle.

UNDRAINED SETTLEMENT OF PLASTIC AND ORGANIC CLAYS

By Roger Foott,[1] M. ASCE, and Charles C. Ladd,[2] F. ASCE

INTRODUCTION

When a load is rapidly applied over a limited area above a clay layer, undrained shear deformations occur, giving rise to *initial* undrained settlements. Techniques for predicting initial settlements based on elastic theory are available. However, these settlements are frequently small compared to consolidation movements, so explicit prediction of initial settlement is often not performed during design. Subsequent undrained creep movements under constant load can cause additional undrained settlement; but routine predictive techniques for these movements are not readily available, and creep settlements are only rarely considered in design practice.

This paper presents performance data on three plastic, organic clays where initial settlements or continuing undrained creep movements, or both, resulted in substantial settlement in addition to that due to consolidation. With these types of soil, such settlements can represent a major design consideration. The paper recommends on approximate method for estimating initial settlement and discusses ways in which the potential for large, undrained initial and creep settlements can be recognized and accounted for in design practice.

UNDRAINED SETTLEMENTS

When a load is rapidly applied over a limited area above a clay soil deposit, the shear stresses induced in the clay cause lateral deformation of the soil resulting in settlement. This settlement is commonly considered an instantaneous response to the applied loading, therefore, occurring under undrained conditions and known as initial settlement, ρ_i.

Prediction of initial settlement is generally performed using a model derived from elastic theory and having the form

[1]Program Mgr., Soils and Foundation Engrg., Dames and Moore, Burlington, Mass.
[2]Prof. of Civ. Engrg., Massachusetts Inst. of Tech., Cambridge, Mass.

Note.—Discussion open until January 1, 1982. To extend the closing date one month, a written request must be filed with the Manager of Technical and Professional Publications, ASCE. Manuscript was submitted for review for possible publication on September 4, 1980. This paper is part of the Journal of the Geotechnical Engineering Division, Proceedings of the American Society of Civil Engineers, ©ASCE, Vol. 107, No. GT8, August, 1981. ISSN 0093-6405/81/0008-1079/$01.00.

$$\rho_i = \frac{q\,B\,I_\rho}{E_u} \qquad (1)$$

in which q = the stress applied to the foundation soil; B = the width of the loaded area; I_ρ is an influence factor which depends on the geometry of the problem; and E_u = the undrained Young's modulus for the soil. This relationship assumes that the soil is linearly elastic and of infinite strength. When the clay is saturated, Poisson's ratio for undrained loading is 0.5, and this value is often included in the value of I_ρ.

Application of Eq. 1 requires an evaluation of E_u for the clay. Direct measurement of E_u via laboratory tests is extremely difficult since this parameter is very sensitive to such factors as: the shear stress level and the strain rate; the degree of sample disturbance, especially with unconsolidated-undrained tests; and the consolidation stress and the effects of aging when consolidated-undrained tests are used [e.g., Ladd (11)]. The alternative procedure of selecting values based on empirical correlations is, therefore, widely used, generally in the form of the normalized parameter E_u/c_u, in which c_u = the undrained shear strength of the clay. Bjerrum (1), for example, suggested that E_u/c_u values in the range of 500–1,500 were appropriate, with the lower value applying to very plastic clays subjected to large load increments and the higher limit applying to lean clays with small load increments.

D'Appolonia, et al. (4) presented an improvement in the estimation of ρ_i by including an explicit correction for the effects of local overstressing within the clay deposit. In essence, the *elastic* component computed via Eq. 1 is increased to account for the additional settlement caused by contained plastic flow, wherein a portion of the foundation soil becomes overstressed, resulting in increased lateral stress increments adjacent to the overstressed zone. D'Appolonia, et al. also evaluated field values of E_u/c_u based on 10 case studies: seven yielded E_u/c_u of 1,000–2,500 and the remaining three gave values of 800, 400, and 80–160. Based on these data they concluded that E_u/c_u of 1,000–1,500 was appropriate for "lean inorganic clays of moderate to high sensitivity," but that "considerably lower" values apply to "highly plastic clays and for organic clays." This latter comment is one of the earliest indications that ρ_i may be much more significant with plastic and organic clays than with other cohesive deposits, which have much higher values of E_u/c_u.

The values of ρ_i obtained using the above prediction method tend to be small in comparison to the consolidation settlement ρ_c, at least for *soft ground* conditions wherein the clay is loaded into the virgin compression range. This is particularly so when the loaded width, B, is several times larger than the clay layer thickness, H, for which the values of I_ρ become very small (Fig. 6).

Also, when a ρ_i estimate is made, the conventional one-dimensional ρ_c computation should logically be modified to incorporate a correction as described by Skempton and Bjerrum (19). This correction accounts for the fact that, because of the shear deformations which cause ρ_i, the pore pressure increment immediately after loading, Δu_i, is not equal to the vertical stress increment, $\Delta\sigma_v$, as assumed in the conventional one-dimensional ρ_c computation. In all cases, except perhaps for a very sensitive soft clay loaded to low factors of safety, this correction will result in values of Δu_i that are less than $\Delta\sigma_v$, with a corresponding reduction in ρ_c (1). This reduction in ρ_c can compensate for

most, if not all, of the estimated ρ_f, especially for cases involving highly overconsolidated clay foundations. Indeed, Seed (17) reported that the estimation of ρ_c using the conventional one-dimensional procedure "appeared to give a reasonably correct assessment of the ultimate settlement."

Thus, in many practical situations, there appears to be little merit in extending a settlement prediction beyond evaluation of ρ_c using the conventional one-dimensional model. This conclusion is reinforced by the frequent uncertainties in the computation of ρ_c. These include the distribution of stress increment with depth, idealization of the actual soil profile, evaluation of the amount of prestress (overconsolidation) in the clay, the selection of compressibility parameters, and the applicability of the assumed one-diemsnional consolidation strains under two- or three-dimensional loading conditions. In most cases the range of the ρ_c estimate does not justify modifying the settlement prediction to include the small values of ρ_f typically predicted.

Moreover, Tavenas and Leroueil (21) conclude that the response of most clay foundations is not truly undrained during typical field loading situations, as implied above. They suggest that significant pore pressure dissipation usually occurs during initial loading with all overconsolidated foundation clays, which then rapidly reach a normally consolidated state during continued subsequent loading. In the normally consolidated state, pore pressure dissipation is much slower. Thus, according to these authors, a truly undrained response develops only in those portions of the foundation clay which have become normally consolidated during the latter stages of construction.

In addition to the *instantaneous* undrained settlements, ρ_f, which occur essentially during loading (and perhaps accompanied by some consolidation settlement as per above), settlement can also occur due to undrained creep of the clay, ρ_{cr}. As with ρ_f, ρ_{cr} is due to lateral deformation of the clay resulting from the applied shear stresses in the early stages of consolidation, but it can continue long after the load is applied.

Time-dependent undrained shear deformations have been the subject of considerable research [e.g., Singh and Mitchell (18) and Mitchell (15)], and computer models have been developed [e.g., Edgers et al. (5)] to predict the creep behavior of foundations. Determination of appropriate parameter values for use in these models is extremely difficult, however, and they remain primarily a research tool. As a practical matter, settlement due to undrained creep is rarely evaluated, is probably usually small, and might typically be interpreted as being part of the consolidation settlement. In any case, prediction of settlement due to undrained creep is not part of conventional geotechnical design practice.

Three Field Studies

Having reviewed the general approach used in design regarding undrained settlement, pertinent aspects of the observed field behavior at three sites will not be presented. All three field studies involved loading organic or highly plastic clays, or both, into the virgin compression range.

Atchafalaya Levees.—In 1965 the U.S. Army Corps of Engineers (New Orleans District) constructed three levee test sections in the Atchafalaya Basin to evaluate alternative levee designs. The test sections were built over existing levees on approximately 120 ft (37 m) of soft to medium highly plastic CH clay (plasticity

index, I_p, typically 50%–80%). The undrained shear strength, c_u, profile through the clay foundation soils evaluated using the SHANSEP procedure [Ladd and Foott (13)] is shown in Fig. 1, discontinuities in the strength contours at El.

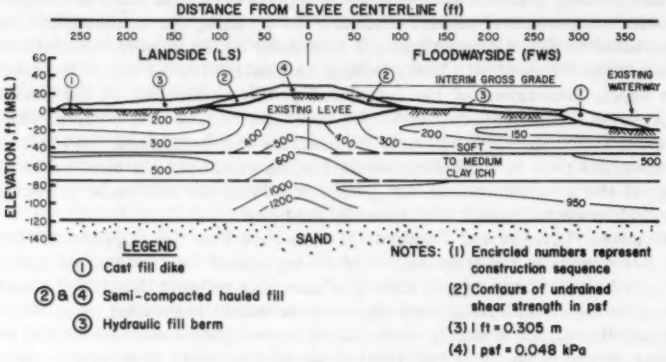

FIG. 1.—Atchafalaya Test Section III: Plan for Raising Levee Grade [after (8,10)]

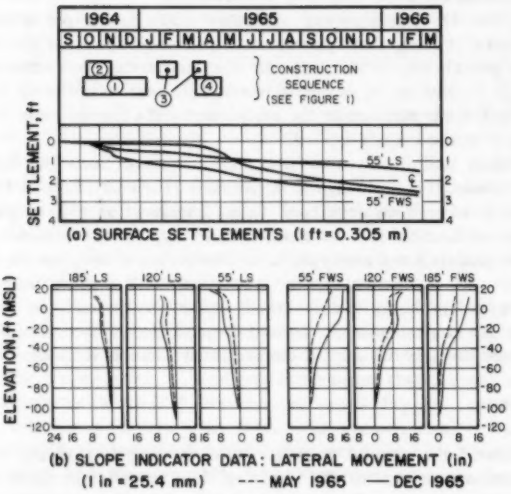

FIG. 2.—Atchafalaya Test Section III: Typical Settlement and Lateral Movement Data [after (10)]

−45 and −75 representing the top of overconsolidated clay layers [Foott and Ladd (7)]. The test section performance has been described and investigated

by Kaufman and Weaver (10), Edgers et al. (5), Fuleihan and Ladd (9), and Foott and Ladd (7,8). Of present interest is the performance of Test Sections II and III, which experienced large initial settlements and ongoing lateral creep movements associated with relatively little dissipation of excess pore pressure.

Fig. 1 shows Test Section III and the sequence used to construct it to an interim gross grade of El. 27. The levee had a nominal design factor of safety of 1.3 and an actual value probably closer to 1.15 [Foott and Ladd, (7)]. Test Section III was extensively instrumented and selected surface settlement and lateral movement data obtained during and for one year after construction are presented in Fig. 2.

The surface settlement data in Fig. 2(*a*) show that substantial settlements occurred at all locations during the construction period and the subsequent year of observation, these settlements ranging up to almost 3 ft (0.9 m) beneath the approximately 10 ft (3 m) of fill that was placed. Of particular interest is the rapid settlement of about 1 ft (0.3 m) which occurred at the center line plate during April and May, 1965, corresponding to the placement of fill at the levee center line and the two or three weeks immediately thereafter. A similar sharp settlement at the 55 ft (17 m) floodwayside (FWS) offset is apparent in October and November, 1964, this corresponding to placement of fill above that settlement plate. Also of interest are the lateral deflections of up to 8 in. (200 mm) recorded by May, 1965, the end of construction, and the continuation of these lateral movements through the following months.

Review of the extensive piezometer data presented in Kaufman and Weaver (10) shows that the excess pore pressures generated by the loading experienced no dissipation immediately after construction. Indeed, in some cases, the pore pressures continued to rise slightly for several weeks after the end of construction, reaching their highest values at approximately the end of June, 1965. Some dissipation did occur subsequently, but more than 80% of the excess pore pressures initially generated remained one year after construction.

It thus appears that the embankment settlements recorded in Fig. 2 contain a large component due to initial settlement and subsequent, largely undrained, creep movements, and further that this component is a very significant design consideration for embankments on these deposits. The writers (8) present comparisons of predicted and measured lateral definitions.

Cross River Embankment.—Between 1975 and 1978 a highway embankment up to 4.7 m high was constructed across the flood plain of the Cross River in Nigeria. The embankment was founded on organic, plastic clay deposits (CH-OH, I_p = 25%–50%) up to 30 m in depth. The lower 10 m approximately of these deposits was medium to stiff and there was a desiccated surface crust of 2 m or more (Fig. 3). However, the intervening clay of up to 18 m thickness was generally soft, particularly for the few meters immediately below the surface crust where strengths of 200 psf (10 kPa) and less were measured in some of the unconfined compression tests. Field vane strengths were typically 275 psf (13 kPa) or higher for these softer deposits.

The design and construction of the Cross River embankment were reported by Foott et al. (6). Present comments are limited to undrained deformation behavior inferred from observed settlement data for the section of embankment built over a buried loose sand lense, which appears to have been the natural levee of a previous river course, as shown in Fig. 3.

The embankment design for this section is illustrated in Fig. 3. It involved an initial construction phase of hydraulically placed sand with three sand drains installed every 10 m along the embankment to ensure that the buried sand lense was free-draining. This first construction phase, considered to have an initial factor of safety in excess of 1.3, was left in place for approximately 1 yr to allow the upper portion of the clay to consolidate, forming a stronger

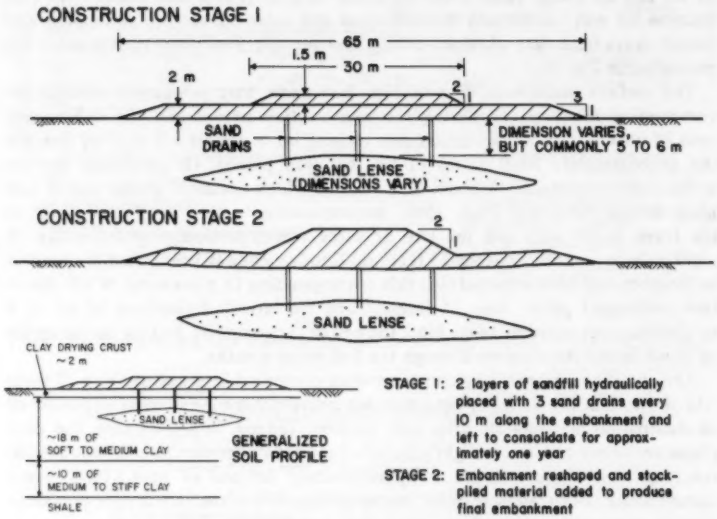

FIG. 3.—Cross River Embankment Design over Buried Sand Lense

layer of clay capable of supporting the final embankment section. The final section was then constructed by reshaping the first embankment stage and adding stockpiled material (construction stage 2 in Fig. 3).

An evaluation of the performance of the first construction phase, undertaken after 1 yr of consolidation, revealed that:

1. The upper levels of the clay, in which consolidation was aided by the buried sand lense and the sand drains, was substantially fully consolidated.
2. Large excess pore pressures still remained in the underlying clay deposits where consolidation was much slower.
3. The total center line settlements measured during the first construction phase were generally in the range 0.75 m–1.25 m, of which 0.50 m–0.75 m typically occurred very quickly during and shortly after load application, with subsequent settlements being much slower and tending to reduce with time in classical consolidation fashion (Fig. 12 of Ref. 6).
4. Based on data obtained during additional field vane testing after the 1-yr consolidation period, it appeared that the thickness of clay overlying the buried sand lense had been reduced on the order of 1 m.

It thus appears that most of the observed settlement probably occurred in the upper clay layer above the sand lense. Since some 2 m of this material is a stiffer surface crust which should not compress significantly under the applied loading, it further appears that much of the observed settlement occurred in the remaining 3 m–4 m of soft clay above the sand lense.

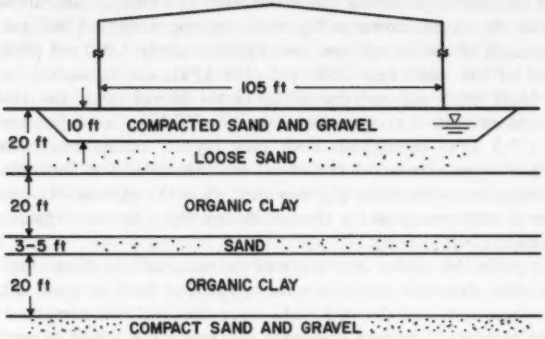

(a) GENERALIZED SOIL PROFILE (1 ft = 0.305 m)

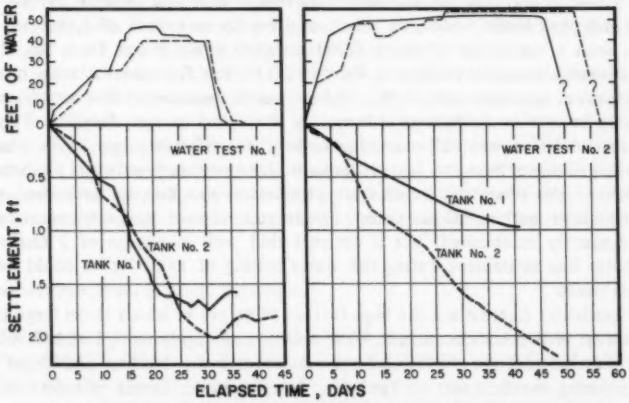

(b) CENTERLINE SETTLEMENTS DURING WATER TESTS (1 ft = 0.305)

FIG. 4.—Storage Tank Soil Profile and Load-Settlement Data

Such movements are far too large to have resulted from consolidation of this thin layer of soft clay. It might thus be concluded that much of the observed settlement was actually an initial undrained settlement caused by lateral movement in the clay above the sand lense.

Storage Tanks on Organic Clay.—The third field study concerns the settlement of two 105 ft (32 m) diameter flexible bottom steel storage tanks constructed in 1970 on a foundation soil profile that included two layers of organic, plastic clay, CH-OH, $I_p = 45\%$, each about 20 ft (6 m) thick, as shown in generalized fashion in Fig. 4(*a*). There were some differences in the soil profiles at each tank, the Tank No. 2 profile having a somewhat greater thickness of clay and including a thin peat layer under part of the tank. The average undrained strength of the upper clay layer shown in Fig. 4(*a*) was approximately 600 psf (30 kPa) and the strength of the lower layer was approximately 1,000 psf (50 kPa). The design load of the tank was 3,300 psf (158 kPa), corresponding to a water height of 53 ft (16.2 m), and the initial factor of safety of the tanks under full load was estimated at approximately 1.5. With an assumed prestress of 1,200 psf (57.5 kPa) throughout both clay layers, center line consolidation settlements of approximately 2 ft (0.6 m) are calculated for Tank No. 2 using the conventional one-dimensional procedure, while the excessively conservative assumption of zero prestress for the foundation clays increases this settlement to approximately 5 ft (1.5 m).

Fig. 5(*b*) plots the center line settlements recorded for these tanks during two water tests. The tank bottoms were mudjacked back to their initial shape after each water test, and the two tanks were then put into service. However, despite relatively low product loadings, the tanks continued to settle, Tank No. 2 experiencing a further approximately 0.75 ft (0.23 m) center line settlement over a 3-yr period. During this time the average load was about 1,200 psf (57.5 kPa) and peak loads were only rarely and briefly in excess of 1,800 psf (86.2 kPa), with a maximum of about 2,100 psf (100 kPa). When Tank No. 2 was subsequently loaded to about 2,400 psf (115 kPa) for two to three months, it underwent approximately 0.25 ft (0.08 m) additional center line settlement.

These in-service settlements are mainly attributed to consolidation. The fact that consolidation was still occurring under these relatively low loads, plus the large magnitude of the water test settlements, demonstrate clearly that a substantial portion of the observed water test settlements was due to undrained shear deformations, both initial and creep. The amount of undrained settlement cannot be accurately established, but it appears that well in excess of 2 ft (0.6 m) of center line settlement during the water testing of Tank No. 2 could be due to this cause.

Of particular interest are the high factors of safety at which these large initial and creep settlements occurred. With a factor of safety of 1.5 at a 3,300 psf (158 kPa) loading, the 40 ft (12.2 m) maximum water loading [2,500 psf (120 kPa)] during the first test of Tank No. 2 represents a factor of safety of 2.0, while the factor of safety for the intermediate loading of approximately 25 ft (7.6 m) of water [1,550 psf (75 kPa)] during this first test increases to slightly over 3.0. Nevertheless, large initial settlements probably occurred at these relatively low loadings, judging from the large settlements shown in Fig. 4(*b*).

Also worthy of note is the fact that the measured long-term settlement behavior of a nearby, heavily loaded tank demonstrated that when consolidation was finally completed, further in-service tank settlements essentially stopped. It, therefore, appears that large settlements due to undrained shear deformations, both initial and creep, would cease being a problem once the foundation clays become fully consolidated, even with repeated loadings to design capacity.

Discussion of Field Studies

These field studies demonstrate the existence of undrained settlements much greater than would be expected based on past experience. Indeed, in the cases of the Atchafalaya Levee test sections and the storage tanks, initial settlements plus continuing settlement due to undrained lateral creep probably were of the same order of magnitude as the consolidation settlement which would occur under the applied loads. Continued shear deformation due to lateral creep is clearly evident for the Atchafalaya Levees from the inclinometer data and can be presumed, but not positively proven, for the storage tanks. It does not appear to have been a major factor with the Cross River embankment, probably because the upper layer of clay, in which the initial settlement movements mainly occurred, consolidated quite rapidly.

Thus, it is apparent that for the three field cases described, the normal situation where ρ_i is small compared to ρ_c does not apply. In all cases, prediction of ρ_c does not apply. In all cases, prediction of ρ_i using even the lower-bound value of $E_u/c_u = 500$, suggested by Bjerrum (1), would greatly underestimate the initial settlements which occurred. Furthermore, unless the soils consolidated fairly rapidly, it appears that continuing creep deformations can lead to substantial additional settlements.

These three soils therefore seem to present a special design problem which requires considerations beyond the conventional design practice discussed previously. Even allowing for the effects of local overstressing using the D'Appolonia et al. (4) approach, it is necessary for the soils to have extremely low values of E_u/c_u in order to explain the large initial settlements.

The foundation soils involved in these three cases exhibiting unusually large undrained shear deformations all had a high plasticity index and, to varying degrees, contained organic matter. A soil combining high plasticity and a large organic content might, therefore, be particularly susceptible to such movements. Accordingly, with designs involving loadings on plastic and organic soils, it is appropriate to carefully consider the possibility that large undrained shear deformations may occur in addition to the conventionally estimated consolidation settlement.

Approximate Prediction of Initial Settlement

The method of predicting initial settlements based on elastic theory presented by D'Appolonia et al. (4) is the most rational approach available, accounting explicitly for the effects of initial stress history and shear stress level in the foundation clay. As noted earlier, their 1971 paper suggested that the required value of E_u be selected based on empirical correlation with E_u/c_c. Since that time, further research at MIT [Ladd et al. (14)] has indicated that an approximate value of E_u can be obtained from K_o consolidated-undrained, CK_oU, direct simple shear (DSS) tests run on samples of the soil reconsolidated using the SHANSEP procedure [Ladd and Foott (13)] to reduce sample disturbance effects (excluding highly sensitive and naturally cemented soils that have very high E_u/c_u values and are not ammenable to the SHANSEP approach). The following design method for the approximate prediction of ρ_i applies these CK_oUDSS data to the D'Appolonia et al. (4) procedure for field situations involving loading

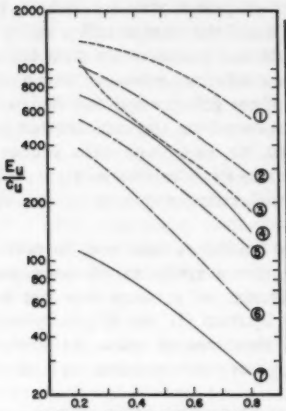

No.	DECRIPTION	c_u/σ'_{vc}
① [1]	PORTSMOUTH SENSITIVE CL CLAY $S_t \geq 10$, LL = 35, I_p = 15	0.20
② [1]	BOSTON CL CLAY LL = 41, I_p = 22	0.20
③ [1]	BANGKOK CH CLAY LL = 65, I_p = 41	0.27
④ [1]	MAINE ORGANIC CH-OH CLAY LL = 65, I_p = 38	0.285
⑤ [2]	AGS CH CLAY LL = 71, I_p = 40	0.255
⑥ [1]	ATCHAFALAYA CH CLAY LL = 95, I_p = 75	0.24
⑦ [3]	TAYLOR RIVER PEAT w_N = 500 %	0.46

(1) FROM LADD & EDGERS (1972)
(2) MIT FOR DAMES & MOORE
(3) MIT FOR HALEY & ALDRICH

(a) NORMALIZED SECANT MODULUS VS. STRESS LEVEL FOR NORMALLY CONSOLIDATED SOILS

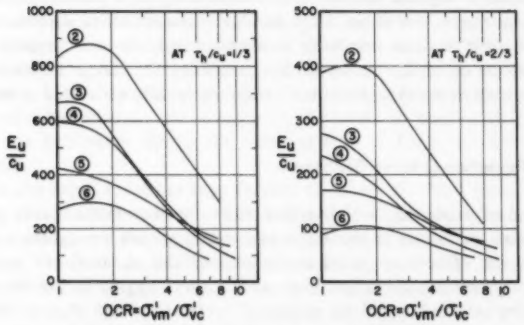

(b) NORMALIZED SECANT MODULUS VS. OVERCONSOLIDATION RATIO

FIG. 5.—Normalized Modulus Data from K_o-Consolidated Undrained Direct Simple Shear Tests [from (14)]

the foundation clay beyond its maximum past pressure.

The prediction involves four steps:

1. *Select a value for* E_u, ideally from DSS tests run using the SHANSEP reconsolidation procedure and selected using an applied shear stress ratio equal to the reciprocal of the stability factor of safety for the loading. Alternatively, Fig. 5 gives guidance for selecting a value based on available data for a wide range of clays. The data in Fig. 5(*a*) are for normally consolidated soils, and Fig. 5(*b*) shows the trends expected with increasing over-consolidation ratio, OCR.

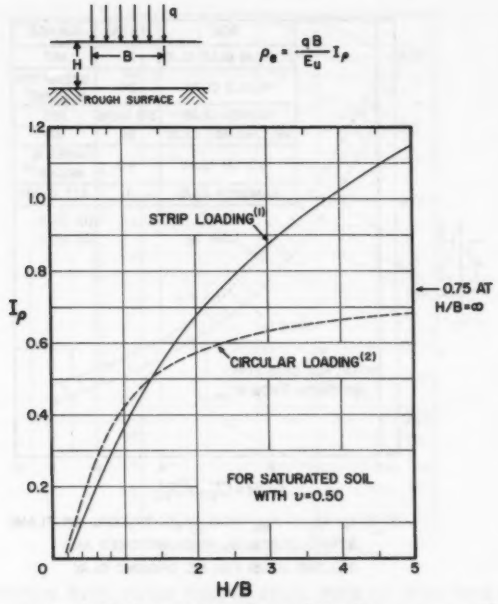

FIG. 6.—Undrained Elastic Settlement Computation for Uniform Loading on Elastic Layer

2. With the value of E_u obtained from Step 1, *compute the elastic settlement,* ρ_e, using the formula and influence factor chart shown in Fig. 6.

3. *Select a value of the initial shear stress ratio* (f) from Fig. 7 as a function of the OCR of the clay.

4. *Select a value of the settlement ratio,* S_R, from Fig. 8 as a function of the applied stress ratio, the geometry of the loading, H/B, and f. The initial settlement, ρ_i, can then be computed as

$$\rho_i = \frac{\rho_e}{S_R} \qquad (2)$$

Note that Fig. 8 applies to strip loadings, but D'Appolonia et al. (4) indicate that it is also reasonably applicable to circular loadings.

It must be emphasized that the above approach is very approximate, particularly when the value of E_u is selected empirically from Fig. 5 without any DSS tests being performed. The effects of partial consolidation that may occur within overconsolidated deposits during construction are also ignored. Nevertheless, the method should indicate the probable order of magnitude of ρ_i and can serve to give some warning of situations wherein ρ_i may be a significant design consideration. In the majority of cases, relatively high values of E_u/c_u should apply and ρ_i will be, at most, a few inches. Whenever low values of E_u/c_u are obtained from DSS tests, however, there is a clear warning that significant ρ_i settlements in relation to ρ_c may occur. This is particularly likely when highly plastic soils containing organic materials are encountered. It should be noted that an E_u/c_u value as low as 40 can be backfigured for the plastic organic clay at the storage tank site.

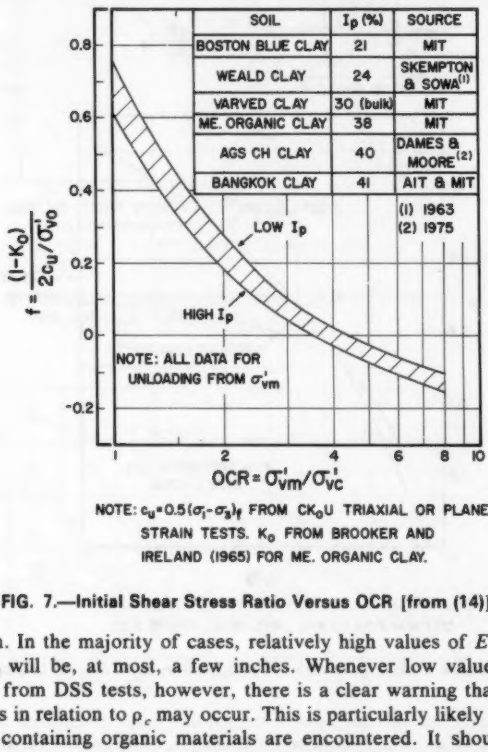

FIG. 7.—Initial Shear Stress Ratio Versus OCR [from (14)]

Accounting for Undrained Settlements in Design

Using the above approach, approximate predictions of initial settlement can

be obtained. Additional, creep-induced, undrained settlements cannot be reliably predicted, but a reasonable and probable general concept is: When initial settlements are small, undrained creep deformation will also be small; when initial settlements are significant but consolidation is rapid, creep settlements will tend to be small; and when initial settlements are significant and consolidation is slow, creep settlements will also tend to be significant. With this concept, the engineer can qualitatively consider the potential effect of these settlements on design.

It should again be recognized that, as discussed previously, most field evidence indicates that ρ_i is usually not an important design consideration and that conventional predictions of ρ_c using the one-dimensional model will generally

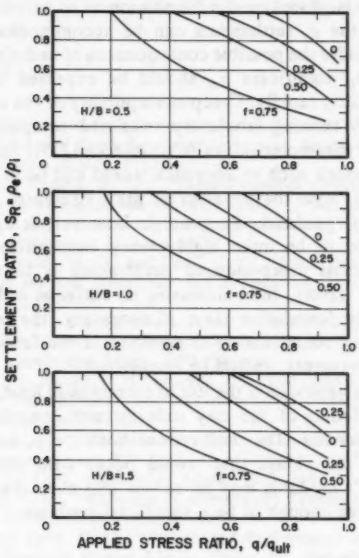

FIG. 8.—Settlement Ratio Versus Applied Stress Ratio for Strip Load on Isotropic Homogeneous Foundation [from (4)]

yield an adequate estimate of the total settlement that will occur. Therefore, design practice does not need to be changed with those situations. The objective is rather to try and detect special cases wherein undrained settlements might become troublesome and to make allowance for potential problems before they occur.

Thus in most cases values of E_u/c_u of 500 or more will apply and ρ_i will be small. Indeed reference to Fig. 5 indicates that even plastic clays nos. 3, 4, and 5 usually have values of E_u/c_u of 200 or higher, for which ρ_i may start to be significant but will rarely be a major design consideration. The low values for E_u/c_u obtained for soils nos. 6 and 7 and backfigured for the storage

tank site, however, are indicative of substantial potential problems and should be considered a distinct warning that large undrained movements may occur and result in major settlements in addition to ρ_c. This possibility should be carefully considered when the soil in question is highly plastic and when it has a significant organic content.

When potentially large ρ_i movements are indicated, the first question must be whether the additional settlement is an important design consideration. With an embankment, wherein additional fill can be added to compensate for ρ_i, it may not be (although this might not be true for continuing undrained creep settlements). With other structures the settlement may not be so easily compensated for, in which case consideration should be given to the use of precompression so that the initial settlement and some consolidation settlement will occur before the final structure is placed on the foundation.

Assuming that the ρ_i settlements can be accommodated in some way, the next step is to consider the possible consequences of undrained creep movements, ρ_{cr}. With large ρ_i, significant ρ_{cr} should be expected unless the foundation soils consolidate fairly rapidly. Creep susceptibility of the soil *might* be estimated to some extent by running laboratory tests and comparing the data obtained to published creep parameter values [e.g., Mitchell (15)] and associated observed soil behavior, although such an approach would still be in the realm of research [Edgers et al. (5)]. Also the behavior of prior structures on the same deposits may give excellent guidance. In general, however, it appears that very low modulus soils tend to be quite highly creep susceptible. The safest way of preventing substantial creep-induced settlements is to ensure that the clay consolidates quite rapidly, thus increasing its stiffness and decreasing the shear stress levels in the foundation clay. If necessary, the installation of vertical drains to accelerate consolidation in portions of the foundation soils, in order to limit lateral movements, should be considered.

Another possible approach is the use of incremental loading via stage construction, allowing stiffening of the clay soils through consolidation before adding the next load increment. This will reduce both the ρ_i and ρ_{cr} components of settlement below the values that would occur with immediate full loading. However, the soil's modulus may be so low that even these reduced undrained settlements are large enough to be a significant problem.

Summary and Conclusions

1. For *soft ground* loading conditions (i.e., clay foundations loaded into the virgin compression range), the conventional practice of computing consolidation settlements using the one-diemsnional model, without explicit computation of initial settlement, will generally yield total settlement estimates of sufficient accuracy for design purposes.

2. Initial settlements due to undrained shear deformations are usually small and for practical purposes can often be assumed to be included in the consolidation settlements computed above. However, the three field studies presented herein show that initial settlements may become very significant with highly plastic or organic foundation soils, or both, especially when loaded to low stability factors of safety, and may even become the predominant design consideration. The occurrence of large initial settlements may also be followed by excessive

undrained creep movements if consolidation occurs very slowly.

3. Approximate predictions of initial settlements can be made using the method of D'Appolonia et al. (4), with modulus values selected from direct simple shear tests or estimated using Fig. 5. These predictions, plus consideration of soil type and consolidation time, should indicate cases where initial and creep-induced settlements could be a significant design problem.

4. In such cases, the effect of the initial settlement on the structure should be evaluated and the possible effects of creep-induced settlements considered.

5. The effect of initial settlement on the structure can be reduced by precompression or, to some extent, by a controlled loading program which allows consolidation to increase the soil stiffness and reduce the shear stress level in the foundation. The adverse effects of creep settlements also can be reduced by installing vertical drains to accelerate the rate of consolidation.

Appendix I.—References

1. Bjerrum, L., "Embankment on Soft Ground," *Proceedings, ASCE Special Conference on Performance of Earth and Earth Supported Structures, Purdue University,* American Society of Civil Engineers, Vol. 2, 1972, pp. 1–54.
2. Brooker, E. W., and Ireland, H. O., "Earth Pressures at Rest Related to Stress History," *Canadian Geotechnical Journal,* Vol. 2, No. 1, 1965, pp. 1–15.
3. Dames and Moore, "Atlantic Generating Station; Engineering Properties of Foundation Soils," *AGS-PSAR Amendment 19,* June, 1975.
4. D'Appolonia, D. J., Poulos, H. G., and Ladd, C. C., "Initial Settlement of Structures on Clay," *Journal of the Soil Mechanics and Foundation Division,* ASCE, Vol. 97, No. SM10, 1971, pp. 1359–1377.
5. Edgers, L., Ladd, C. C., and Christian, J. T., "Undrained Creep of Atchafalaya Levee Foundation Clays," *Research Report R73-16,* Dept. of Civ. Engrg., Massachusetts Inst. of Tech., Cambridge, Mass., 1973, 600 pp.
6. Foott, R., Devecseri, D., Aneke, C. N., Jackson, J. O., and Ladd, C. C., "Embankments Through Cross River Swamp," *Journal of the Geotechnical Engineering Division,* ASCE, Vol. 106, No. GT3, 1980, pp. 219–234.
7. Foott, R., and Ladd, C. C., "The Behavior of Atchafalaya Test Embankments During Construction," *Research Report R73-27, Soils Publication 322,* Dept. of Civ. Engrg., Massachusetts Inst. of Tech., Cambridge, Mass., 1973, 364 p.
8. Foott, R., and Ladd, C. C., "Behavior of Atchafalaya Levees during Construction," *Geotechnique,* Vol. 27, No. 2, 1977, pp. 137–160.
9. Fuleihan, N. F., and Ladd, C. C., "Design and Performance of Atchafalaya Flood Control Levees," *Research Report R76-24, Order No. 543,* Dept. of Civ. Engrg., Massachusetts Inst. of Tech., Cambridge, Mass., 1976, 753 p.
10. Kaufman, R. I., and Weaver, F. J., "Stability of Atchafalaya Levees," *Journal of the Soils Mechanics and Foundation Division,* ASCE, Vol. 93, No. SM4, 1967, pp. 157–176.
11. Ladd, C. C., "Stress-Strain Modulus of Clay from Undrained Triaxial Tests," *Journal of the Soil Mechanics and Foundation Division,* ASCE, Vol. 90, No. SM5, 1964, pp. 103–132.
12. Ladd, C. C., and Edgers, L., "Consolidated-Undrained Direct Simple Shear Tests on Saturated Clays," *Research Report R72-83, No. 284,* Dept. of Civil Engrg., Massachusetts Inst. of Tech., Cambridge, Mass., 1972, 243 p.
13. Ladd, C. C., and Foott, R., "New Design Procedure for Stability of Soft Clays," *Journal of the Geotechnical Engineering Division,* ASCE, Vol. 100, No. GT7, 1974, pp. 763–786.
14. Ladd, C. C., Foott, R., Ishihara, K., Schlosser, F., and Poulos, H. G., "Stress Deformation and Strength Characteristics," *State of the Art Report, Session I, IX ICSMFE,* Tokyo, Vol. 2, 1977, pp. 421–494.

15. Mitchell, J. K., *Fundamentals of Soil Behavior*, John Wiley and Sons, Inc., New York, N.Y., 1976, 422 p.
16. Poulos, H. G., and Davis, E. H., *Elastic Solutions for Soil and Rock Mechanics*, John Wiley and Sons, Inc., New York, N.Y., 1974, 411 p.
17. Seed, H. B., "Settlement Analyses, A Review of No. Theory and Testing Procedures," *Journal of the Soil Mechanics and Foundation Division*, ASCE, Vol. 91, No. SM2, 1965, pp. 39–48.
18. Singh, A., and Mitchell, J. K., "General Stress-Strain-Time Function for Soils," *Journal of the Soil Mechanics and Foundation Division*, ASCE, Vol. 94, No. SM1, 1968, pp. 31–46.
19. Skempton, A. W., and Bjerrum, L., "A Contribution to the Settlement Analysis of Foundations on Clay," *Geotechnique*, Vol. 7, No. 4, 1957, pp. 168–178.
20. Skempton, A. W., and Sowa, V. A., "The Behavior of Saturated Clays During Sampling and Testing," *Geotechnique*, Vol. 13, No. 4, 1963, pp. 269–290.
21. Tavenas, F., and Leroueil, S., "The Behaviour of Embankments on Clay Foundations," *Canadian Geotechnical Journal*, Vol. 17, pp. 236–260.

Appendix II.—Notation

The following symbols are used in this paper:

B = width of loaded area;
c_u = undrained shear strength;
CK_oU = K_o consolidated-undrained shear test;
DSS = direct simple shear;
E_u = undrained Young's modulus;
f = initial shear stress ratio;
H = layer thickness;
I_ρ = influence factor;
I_p = plasticity index;
K_o = coefficient of earth pressure at rest;
LL = liquid limit;
OCR = overconsolidation ratio;
q = applied foundation stress;
q_{ult} = ultimate bearing capacity;
S_R = settlement ratio;
S_t = sensitivity;
w_N = natural water content;
γ = shear strain;
Δu_i = pore pressure increment immediately after loading;
$\Delta\sigma_v$ = vertical stress increment;
ν = Poisson's ratio;
ρ_i = initial settlement (due to undrained shear deformation);
ρ_c = consolidated settlement;
ρ_{cr} = undrained creep settlement;
ρ_e = elastic settlement;
σ'_{vc} = vertical consolidation stress;
σ'_{vm} = maximum past pressure;
σ'_{vo} = in-situ vertical consolidation stress; and
τ_h = horizontal shear stress in DSS test.

PILES SUBJECTED TO TORSION

By M. F. Randolph[1]

INTRODUCTION

The torsional stiffness of a pile embedded in soil is a subject which has received little attention in the past. However, any pile foundation which is loaded laterally is liable to undergo some degree of torsion due to eccentricity of the applied load. Similarly, a rigorous static or dynamic analysis of a structure founded on piles will require knowledge of the torsional stiffness of the foundation, in addition to the axial and lateral stiffnesses. Stoll (8) has pointed out that torsional load tests on piles are often simpler and more economic to perform than axial load tests; the back-analysis of the torsional response of test piles yields values of shear modulus for the soil which are in good agreement with those deduced from axial load tests (Poulos, 4).

Using a numerical method of analysis, based on integral equation techniques, Poulos (4) presented charts of torsional flexibility of piles as a function of pile geometry and relative stiffness. In the present paper, an analysis is developed, based on a simple assumption concerning the stress field around a pile undergoing torsion, which leads to closed-form solutions for the torsional stiffness of a pile. Separate solutions are presented for the case of homogeneous soil (i.e., of constant stiffness) and for the case of soil where the stiffness is proportional to depth. It is shown how these separate solutions may be combined to cover more general variations of the soil stiffness with depth.

The equations leading to the development of the analytical solutions may be used to investigate the effect of slip between pile and soil. In the final section of this paper, this approach is illustrated by a study of the results from torsion tests on full-scale piles.

ANALYSIS FOR RIGID CIRCULAR PILE

In polar co-ordinates (Fig. 1), the equilibrium equation in the circumferential direction may be written

[1]Univ. Asst. Lect., Univ. Engrg. Dept., Trumpington Street, CB2 1PZ, Cambridge Univ., Cambridge, England.

Note.—Discussion open until January 1, 1982. To extend the closing date one month, a written request must be filed with the Manager of Technical and Professional Publications, ASCE. Manuscript was submitted for review for possible publication on May 30, 1980. This paper is part of the Journal of the Geotechnical Division, Proceedings of the American Society of Civil Engineers, ©ASCE, Vol. 107, No. GT8, August, 1981. ISSN 0093-6405/81/0008-1095/$01.00.

$$\frac{1}{r}\frac{\partial \sigma_\theta}{\partial \theta} + \frac{1}{r^2}\frac{\partial}{\partial r}(r^2 \tau_{r\theta}) + \frac{\partial \tau_{z\theta}}{\partial z} = 0 \quad \ldots\ldots\ldots\ldots\ldots\ldots\ldots\ldots\ldots\ldots (1)$$

From symmetry, there can be no variation of stress or displacement in the circumferential direction. Thus, the first term in Eq. 1 must be zero. If the assumption is made that the magnitude of $\tau_{z\theta}$ is negligible compared to $\tau_{r\theta}$ (the shear stress 'imposed' by torsion of the pile) then Eq. 1 may be simplified to

$$\frac{\partial}{\partial r}(r^2 \tau_{r\theta}) = 0 \quad \ldots\ldots\ldots\ldots\ldots\ldots\ldots\ldots\ldots\ldots\ldots\ldots\ldots\ldots (2)$$

On integration, the variation of shear stress away from the pile may be written as

$$\tau_{r\theta} = \frac{(\tau_{r\theta})_0 r_0^2}{r^2} \quad \ldots\ldots\ldots\ldots\ldots\ldots\ldots\ldots\ldots\ldots\ldots\ldots\ldots\ldots (3)$$

in which the subscript, 0, denotes conditions at the pile shaft.

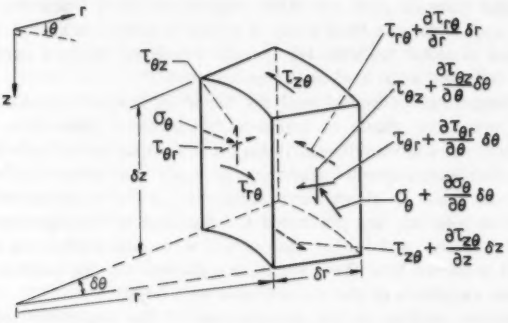

FIG. 1.—Circumferential Equilibrium of Soil Element

Turning to the strain field around the pile, the shear strain, $\gamma_{r\theta}$, may be written

$$\gamma_{r\theta} = \frac{\tau_{r\theta}}{G} = \frac{1}{r}\frac{\partial u}{\partial \theta} + r\frac{\partial}{\partial r}\left(\frac{v}{r}\right) \quad \ldots\ldots\ldots\ldots\ldots\ldots\ldots\ldots\ldots\ldots (4)$$

in which G = the shear modulus of the soil; u = the radial soil movement; and v = the circumferential movement. Since the term, $\partial u/\partial\theta$, will be zero (from symmetry), Eqs. 3 and 4 may be combined to give

$$\frac{\partial}{\partial r}\left(\frac{v}{r}\right) = \frac{(\tau_{r\theta})_0 r_0^2}{G r^3} \quad \ldots\ldots\ldots\ldots\ldots\ldots\ldots\ldots\ldots\ldots\ldots\ldots (5)$$

Integrating Eq. 5 yields

$$\phi = \left(\frac{v}{r}\right)_0 = \frac{\tau_0}{2G} \quad \ldots\ldots\ldots\ldots\ldots\ldots\ldots\ldots\ldots\ldots\ldots\ldots\ldots\ldots\ldots\ldots (6)$$

in which ϕ = the rotation of the pile shaft and the subscript, θr, has been dropped (thus, τ_0 represents the value of $\tau_{r\theta}$ at the pile shaft).

Eq. 6 may be used to deduce the torque per unit length needed to rotate an infinitely long rigid pile by an angle, ϕ. Thus, for a length Δl of pile, the torque ΔT is given by

$$\Delta T = 2\pi r_0^2 \tau_0 \Delta l = 2\pi r_0^2 \cdot 2G\phi\,\Delta l \quad \ldots\ldots\ldots\ldots\ldots\ldots\ldots\ldots\ldots\ldots\ldots\ldots\ldots\ldots (7)$$

whence $\Delta T/\Delta l = 4\pi\, Gr_0^2\phi$—a result previously noted by Booker (see Poulos, 4).

It should be noted that Eq. 6 has been derived solely on the assumption that $\tau_{b\theta}$ (the shear stress in the circumferential direction between horizontal layers of soil) is small compared to the imposed shear stress, $\tau_{r\theta}$. This assumption is strictly true for a long rigid pile and is considered to be reasonable for piles of practical lengths and stiffnesses.

For a pile of finite length, the pile base will contribute to the torsional stiffness of the pile. The contribution of the base may be estimated from the known solution for the torsional stiffness of a rigid punch of radius, a, on the surface of a homogeneous elastic half-space with shear modulus, G. The stiffness of the punch is given by

$$\frac{T}{\phi} = \frac{16}{3} a^3 G \quad \ldots\ldots\ldots\ldots\ldots\ldots\ldots\ldots\ldots\ldots\ldots\ldots\ldots\ldots\ldots\ldots (8)$$

Although the pile base is not at the surface, the soil above the level of the base is already undergoing torsion due to the twisting on the pile shaft. Thus, the torsional stiffness of the pile base may be estimated from Eq. 8 with reasonable accuracy.

For a rigid pile, the overall torsional stiffness may now be estimated by combining Eqs. 7 and 8 to give, for a pile of length, l

$$\frac{T}{Gr_0^3\phi} = \frac{16}{3} + 4\pi\frac{l}{r_0} \quad \ldots\ldots\ldots\ldots\ldots\ldots\ldots\ldots\ldots\ldots\ldots\ldots\ldots\ldots\ldots\ldots (9)$$

It may be seen from this equation that, even for rigid piles, the contribution of the pile base rapidly becomes insignificant as the length of the pile increases. This result will be even more pronounced when the pile flexibility is taken into account.

Effect of Pile Flexibility

In practical situations, the flexibility of the pile will lead to a gradual reduction in the angle of twist, ϕ, down the length of the pile. The variation of ϕ with depth, z, may be deduced by considering the relationship between torque, T, and $d\phi/dz$. For a pile of torsional rigidity $(GJ)_p$, it is possible to write (see O'Neill, 2)

$$\frac{d\phi}{dz} = -\frac{T}{(GJ)_p} \quad \ldots\ldots (10)$$

Also, the torque carried by the pile shaft will reduce with depth as shear stress is transferred to the soil. Thus

$$\frac{dT}{dz} = -2\pi r_0^2 \tau_0 \quad \ldots\ldots (11)$$

Assuming that the variation of ϕ with depth, z, is such that $\partial\tau_{z\theta}/\partial z$ is still small compared with $\partial\tau_{r\theta}/\partial r$, Eq. 6 is still valid and may be combined with Eqs. 10 and 11 to give

$$\frac{d^2\phi}{dz^2} = \frac{2\pi r_0^2}{(GJ)_p}\tau_0 = \frac{4\pi r_0^2 G}{(GJ)_p}\phi \quad \ldots\ldots (12)$$

This equation may be written more simply by introducing an equivalent shear modulus of the pile, G_p (the shear modulus of a solid pile of the same torsional rigidity) defined as

$$G_p = \frac{2}{\pi r_0^4}(GJ)_p = \lambda G \quad \ldots\ldots (13)$$

The quantity, λ, is thus the stiffness ratio of an equivalent solid pile to the soil.

Eq. 12 now reduces to

$$\frac{d^2\phi}{dz^2} = \frac{8}{\lambda r_0^2}\phi \quad \ldots\ldots (14)$$

which has a solution in terms of hyperbolic functions of the form

$$\phi = A\cosh(\mu z) + B\sinh(\mu z) \quad \ldots\ldots (15)$$

in which $\mu^2 = 8/r_0^2\lambda$. The boundary conditions which enable the constants A and B to be found are those at the pile base, in which

$$\phi_{z=l} = \frac{T_{z=l}}{Gr_0^3}\cdot\frac{3}{16} \quad \ldots\ldots (16)$$

$$\left(\frac{d\phi}{dz}\right)_{z=l} = -\frac{2}{\pi r_0^4}\frac{T_{z=l}}{\lambda G} = -\frac{32}{3\pi r_0\lambda}\phi_{z=l} \quad \ldots\ldots (17)$$

Substitution of these boundary conditions into Eq. 16 leads eventually to

$$\frac{T_t}{Gr_0^3\phi_t} = \frac{\left(\frac{16}{3} + 4\pi\frac{l}{r_0}\frac{\tanh(\mu l)}{\mu l}\right)}{\left(1 + \frac{32}{3\pi\lambda}\frac{l}{r_0}\frac{\tanh(\mu l)}{\mu l}\right)} \quad \ldots\ldots (18)$$

in which the subscript, t, denotes conditions at the top of the pile. The quantity, μl, is given by

$$\mu l = \left(\frac{8}{\lambda}\right)^{1/2}\left(\frac{l}{r_0}\right) \quad (19)$$

in which λ = the stiffness ratio, G_p/G.

Fig. 2 shows the torsional stiffness factor, $T_t/(Gr_0^3\phi_t)$, given by Eq. 18, plotted against stiffness ratio, λ. For stiff piles (high λ or low l/r_0), μl tends to zero and the ratio, tanh $(\mu l)/\mu l$, tends to unity. Eq. 18 then reduces to the result obtained previously for a rigid pile [Eq. (9)]. For low values of λ, or high slenderness ratio, l/r_0, tanh (μl) tends to unity and it may be shown that Eq. 18 reduces to

$$\frac{T_t}{Gr_0^3\phi_t} \simeq \sqrt{2}\,\pi\lambda^{1/2} = 4.44\lambda^{1/2} \quad (20)$$

This expression is independent of the length of the pile. Thus, for flexible piles, the torsional stiffness is dependent on the shear modulus of the soil

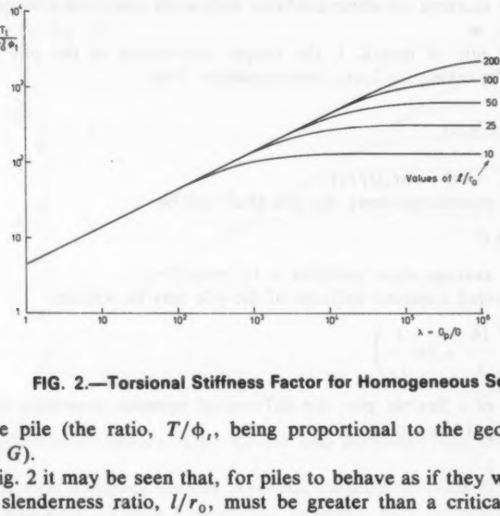

FIG. 2.—Torsional Stiffness Factor for Homogeneous Soil

and of the pile (the ratio, T/ϕ_t, being proportional to the geometric mean of G_p and G).

From Fig. 2 it may be seen that, for piles to behave as if they were infinitely long, the slenderness ratio, l/r_0, must be greater than a critical value given approximately by

$$\left(\frac{l}{r_0}\right)_c \simeq \lambda^{1/2} \quad (21)$$

Similarly, rigid piles must be shorter than one eighth of this critical value in order for Eq. 9 to apply. In practice, most piles (as opposed to piers) will behave as flexible piles under torsion (i.e., as if they were infinitely long). For such piles, Eqs. 10 and 14 imply that the torque (and the angle of twist, ϕ) decay exponentially down the pile according to $T = T_t\, e^{-\mu z}$ (see O'Neill, 2).

Before turning to the case of piles embedded in soil with shear modulus proportional to depth, it is of interest to note the direct analogy between the analytical solution developed here for torsion loading, and that derived by Randolph and Wroth (6) for axial loading. In both cases, the solutions have been developed by considering the load transfer down the pile shaft separately from that at the pile base. The similarity in the form of the final expressions [see Eq. 41 of Randolph and Wroth (6)] is particularly striking.

Soil Shear Modulus Proportional to Depth

Many natural deposits of soil, such as sand or soft clay, have a stiffness profile which increases proportionally with depth. In order to extend the previous solution to such deposits, consider a shear modulus given by

$$G = mz = mr_0\left(\frac{z}{r_0}\right) \quad \ldots\ldots\ldots\ldots\ldots\ldots\ldots\ldots\ldots\ldots\ldots\ldots \quad (22)$$

It is often more satisfactory, analytically, to consider the quantity, mr_0, which is the rate of increase of shear modulus with each pile radius of depth, than the parameter, m.

For a rigid pile of length, l, the torque transferred at the pile base may be estimated by taking the local shear modulus. Thus

$$T_b = \frac{16}{3} r_0^3 \phi_b G_{z=l} \quad \ldots\ldots\ldots\ldots\ldots\ldots\ldots\ldots\ldots\ldots\ldots\ldots \quad (23)$$

in which $G_{z=l} = ml = mr_0(l/r_0)$.

The torque transferred down the pile shaft will be

$$T_s = 4\pi l r_0^2 \phi \bar{G} \quad \ldots\ldots\ldots\ldots\ldots\ldots\ldots\ldots\ldots\ldots\ldots\ldots \quad (24)$$

in which $\bar{G}$ = average shear modulus = $1/2mr_0(l/r_0)$.

Thus the overall torsional stiffness of the pile may be written

$$\frac{T}{mr_0^4\phi} = \frac{l}{r_0}\left(\frac{16}{3} + 2\pi\frac{l}{r_0}\right) \quad \ldots\ldots\ldots\ldots\ldots\ldots\ldots\ldots\ldots\ldots \quad (25)$$

In the case of a flexible pile, the differential equation governing the angular rotation, ϕ, Eq. 14 becomes

$$\frac{d^2\phi}{dz^2} = \frac{8}{\lambda' r_0^2}\frac{z}{r_0}\phi \quad \ldots\ldots\ldots\ldots\ldots\ldots\ldots\ldots\ldots\ldots\ldots\ldots \quad (26)$$

in which $\lambda' = G_p/(mr_0)$.

Solution of this equation is possible in terms of Airy functions (Abramowitz and Stegun, 1), and may be written in the form of an infinite series:

$$\phi = \phi_t\left[1 + \frac{Z}{2.3} + \frac{Z^2}{2.3.5.6} + \frac{Z^2}{2.3.5.6.8.9} \ldots\right] + \left(\frac{d\phi}{dz}\right)_{z=0} z\left[1 + \frac{Z}{3.4} + \frac{Z^2}{3.4.6.7} + \frac{Z^3}{3.4.6.7.9.10} \ldots\right] \quad \ldots\ldots\ldots\ldots \quad (27)$$

in which $Z = 8/\lambda'(z/r_0)^3$.

Applying the boundary condition given by Eq. 23, the term $(d\phi/dz)_{z=0}$ may be found in terms of ϕ_t. This enbales the torsional stiffness, T_t/ϕ_t, to be calculated. The nondimensionalized stiffness, $T_t/(mr_0^4\phi_t)$, is plotted against stiffness ratio, λ', in Fig. 3 for various values of l/r_0. The general pattern is similar to that for piles in homogeneous soil, with a limiting solution, for piles which behave as though they were infinitely long, given by

$$\frac{T_t}{mr_0^4\phi_t} = 2.29(\lambda')^{2/3} \quad \ldots\ldots\ldots\ldots\ldots\ldots\ldots\ldots\ldots\ldots\ldots\ldots \quad (28)$$

in which $\lambda' = G_p/mr_0$.

The critical slenderness ratio at which piles behave as if they were infinitely long may be estimated from Fig. 3 as

$$\left(\frac{l}{r_0}\right)_c \simeq (\lambda')^{1/3} \quad \ldots\ldots\ldots\ldots\ldots\ldots\ldots\ldots\ldots\ldots\ldots\ldots \quad (29)$$

For short, or very stiff piles, the condition for Eq. 25 (the solution for a rigid pile) to apply is that the slenderness ratio is less than a quarter of the critical value given by Eq. 29.

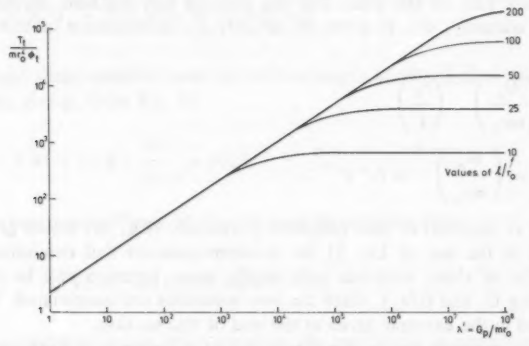

FIG. 3.—Torsional Stiffness Factor for Soil with Stiffness Proportional to Depth

The analytical solutions for the torsional stiffness of piles in homogeneous soil or in soil with stiffness proportional to depth, may be compared with the results obtained using numerical analysis by Poulos (4). In general, excellent agreement is observed over the range of slenderness ratios and stiffness ratios covered. In particular, Poulos (4) points out that most piles in practice behave as infinitely long piles, where the torsional stiffness is a function of the pile and soil stiffness, but independent of the length of the pile. The solutions here corroborate that finding, allowing the torsional stiffness to be calculated simply, from Eqs. 20 and 28.

Extension to More General Soil Conditions

The two preceding sections developed expressions for the torsional stiffness

of piles in either homogeneous soil, or soil where the stiffness is proportional to depth. In many situations, the soil stiffness will vary with depth in a more complex manner than these two idealizations. It is thus necessary to be able to estimate the torsional stiffness of a pile for more general soil conditions.

The problem of a rigid pile is straightforward, since Eqs. 23 and 24 may be combined to give an overall torsional stiffness of

$$\frac{T}{G_{z=l} r_0^3 \phi} = \frac{16}{3} + 4\pi \frac{l}{r_0} \frac{\bar{G}}{G_{z=l}} \quad \ldots \ldots \ldots \ldots \ldots \ldots \ldots \ldots \ldots \ldots \quad (30)$$

in which $\bar{G}$ = the average shear modulus of the soil over the depth of penetration of the pile.

At the other extreme, it would be helpful to be able to estimate the length at which a pile behaves as if it is infinitely long. From Eq. 21, a reasonable estimate of this critical slenderness ratio would seem to be

$$\left(\frac{l}{r_0}\right)_c = \left(\frac{G_p}{G_c}\right)^{1/2} = \lambda_c^{1/2} \quad \ldots \ldots \ldots \ldots \ldots \ldots \ldots \ldots \ldots \ldots \quad (31)$$

in which G_c = the shear modulus at the critical depth (i.e., at the lower end of the active part of the pile). For the case of soil stiffness proportional to depth, the quantity, G_c, is given by $mr_0(l/r_0)_c$. Substitution of this into Eq. 31 yields

$$\left(\frac{l}{r_0}\right)_c = \left(\frac{G_p}{mr_0}\right)^{1/2} \left(\frac{r_0}{l}\right)^{1/2} \quad \ldots \ldots \ldots \ldots \ldots \ldots \ldots \ldots \ldots \ldots \quad (32)$$

or $$\left(\frac{l}{r_0}\right)_c = \left(\frac{G_p}{mr_0}\right)^{1/3} = (\lambda')^{1/3} \quad \ldots \ldots \ldots \ldots \ldots \ldots \ldots \ldots \ldots \ldots \quad (33)$$

This result is identical to that proposed previously (Eq. 29) which gives some confidence in the use of Eq. 31 for nonhomogeneous soil conditions. For a given profile of shear modulus with depth, some iteration will be necessary in calculating G_c and $(l/r_0)_c$ since the two quantities are interrelated. The point is illustrated in the example given at the end of this section.

In order to estimate the torsional stiffness of a long pile in nonhomogeneous soil, it would seem appropriate to use Eq. 20, with G replaced by G_c, and with suitable modification to allow for the variation of G over the active length of pile. Thus, the proposed expression is

$$\frac{T_t}{G_c r_0^3 \phi_t} = 4.44 \left(\frac{G_p}{G_c}\right)^{1/2} \cdot \frac{\bar{G}}{G_c} = 4.44 \lambda_c^{1/2} \frac{\bar{G}}{G_c} \quad \ldots \ldots \ldots \ldots \ldots \quad (34)$$

in which as in Eq. 30, $\bar{G}$ = the average shear modulus over the active length of pile ($0 \le z/r_0 \le \lambda_c^{1/2}$). For the case of soil stiffness proportional to depth, $G_c = mr_0(l/r_0)_c$ and $\bar{G}/G_c = 0.5$. Eq. 34 thus reduces to

$$\frac{T_t}{mr_0^4 \phi_t} = 4.44 \times 0.5 \left(\frac{l}{r_0}\right)_c^2 \cdot = 2.22 (\lambda')^{2/3} \quad \ldots \ldots \ldots \ldots \ldots \quad (35)$$

This expression agrees with that previously obtained (Eq. 28) within 3%. Thus,

for piles which behave as infinitely long, embedded in nonhomogeneous soil, Eq. 34 appears to provide a reasonable estimate of the torsional stiffness, even for the extreme case of soil stiffness proportional to depth.

The application of Eqs. 31 and 34 may be illustrated by an example calculation. Consider a tubular steel pile, 0.355 m (1.16 ft) in diameter, 16 mm (0.63-in.) wall thickness embedded to a depth of 10 m (32.8 ft) in soil with stiffness given approximately by

$$G = 8 + 3z \text{ MN/m}^2 \ (z \text{ in meters}) \ [G = 1{,}160 + 133z \text{ psi} \ (z \text{ in feet})] \quad . \quad . \quad . \quad . \quad (36)$$

The equivalent shear modulus of the pile may be calculated as

$$G_p = G_{\text{steel}} \left[1 - \left(\frac{r_i}{r_0} \right)^4 \right] = 25.4 \times 10^3 \text{ MN/m}^2 \ (3.68 \times 10^6 \text{ psi}) \quad . \quad . \quad . \quad . \quad . \quad (37)$$

in which r_i = the internal radius of the pile. In order to calculate G_c, assume the critical length of pile is 8 m (26.2 ft). This gives $G_c = 32$ MN/m^2 (4,600 psi) and a calculated $(l/r_0)_c$ of 28.2, leading to a revised critical length of 5 m (16.4 ft). Repeating the iteration leads eventually to

$$\left(\frac{l}{r_0} \right)_c = 31.9, \ G_c = 25.0 \text{ MN/m}^2 \ (3{,}620 \text{ psi}) \quad . \quad . \quad . \quad . \quad . \quad . \quad . \quad . \quad . \quad . \quad . \quad . \quad . \quad . \quad . \quad (38)$$

The average shear modulus over the active length of pile is $\bar{G} = 16.5$ MN/m^2 (2,390 psi), giving, from Eq. 34

$$\frac{T_t}{G_c r_0^3 \phi_t} = 4.44 \times 31.9 \times \frac{16.5}{25.0} = 93.5 \quad . \quad . \quad . \quad . \quad . \quad . \quad . \quad . \quad . \quad . \quad . \quad . \quad . \quad . \quad . \quad . \quad . \quad . \quad . \quad (39)$$

Thus, the torsional stiffness of the pile may be estimated as

$$\frac{T_t}{\phi_t} = 13.1 \times 10^3 \text{ kNm/rad} \ (9{,}660 \text{ kips-ft/rad}) \quad . \quad . \quad . \quad . \quad . \quad . \quad . \quad . \quad . \quad . \quad . \quad . \quad . \quad . \quad . \quad (40)$$

While consideration has been given in the preceding to variations of shear modulus, G, with depth z, in certain cases, the effect of radial variation of shear modulus may need to be taken into account. This may be achieved in a manner similar to that proposed for axially loaded piles (Randolph and Wroth, 6) by retaining the shear modulus, G, inside the integration when proceeding from Eq. 5 to Eq. 6. Thereafter, a modified form of Eq. 6 may be used, relating the angle of twist of the pile shaft, ϕ, to the interface shear stress τ_0.

Torsional Failure of Pile

The previous analysis has been concerned with the torsional response of piles assuming the soil to deform in an elastic or pseudo-elastic manner. In practice, as the pile is twisted, the shear stress on the pile-soil interface will reach a limiting value, τ_f, corresponding to the available shaft adhesion. The

angle of twist at which this happens may be estimated with reasonable accuracy from Eq. 6 as

$$\phi_f = \frac{\tau_f}{2G} \quad \text{(41)}$$

(It should be noted that this result is strictly applicable only to an ideal elastic-plastic soil; however, provided a suitable secant shear modulus is taken, such as that at 50% of the failure shear stress, the above expression will give a reasonable estimate of ϕ_f.)

For rigid or stiff piles, failure in torsion will occur fairly suddenly as the applied turque approaches the limiting value of

$$T_f = 2\pi r_0^2 l \bar{\tau}_f \quad \text{(42)}$$

in which $\bar{\tau}_f$ = the average available shaft adhesion (ignoring the contribution from the base of the pile). For more flexible piles, however, the region of pile over which τ_f has been mobilized will propagate gradually down the length of the pile. As has been pointed out by O'Neill and Dutt (2), post-peak reduction in the value of the interfacial shear stress (due to continued twisting of the pile shaft) may lead to a form of progressive failure whereby the failure torque is less than that given by Eq. 42. The mechanism is similar to that proposed by Randolph and Wroth (7) for the case of long compressible piles loaded axially.

If a complete stress-strain relationship in simple shear is available for a particular soil, then Eqs. 10–12 may be used to derive the complete torsional response of a pile right up to failure. The approach will be illustrated here for the case where no strain softening occurs (i.e., in which $\tau_0 = \tau_f$ for all $\phi \geq \phi_f$). Consider a pile in homogeneous soil where the full shaft adhesion has been mobilized down to a depth of z_f. At $z = z_f$, the angle of twist is given by Eq. 41 and the torsional stiffness of the lower portion of the pile (in which $z_f \leq z \leq l$) may be defined as k_f in which

$$\left(\frac{T}{Gr_0^3\phi}\right)_{z=z_f} = k_f \quad \text{(43)}$$

The value of k_f may be estimated from Eq. 18 by considering the unfailed portion of the pile ($z_f \leq z \leq l$) as a new pile, ignoring the effect of soil above the level, $z = z_f$.

Integrating Eq. 12, subject to these boundary conditions, it may be shown that the angle of twist at the pile head is given by

$$\phi_t = \frac{\tau_f}{2G}\left[1 + \frac{2k_f}{\pi\lambda}\left(\frac{z_f}{r_0}\right) + \frac{4}{\lambda}\left(\frac{z_f}{r_0}\right)^2\right] \quad \text{(44)}$$

and that the total torque is

$$T_t = \frac{r_0^3\tau_f}{2}\left[k_f + 4\pi\left(\frac{z_f}{r_0}\right)\right] \quad \text{(45)}$$

The current torsional stiffness of the pile may be obtained from these two equations and written as

$$\frac{T_t}{Gr_0^3\phi_t} = \frac{k_f + 4\pi\left(\frac{z_f}{r_0}\right)}{1 + \frac{2k_f}{\pi\lambda}\left(\frac{z_f}{r_0}\right) + \frac{4}{\lambda}\left(\frac{z_f}{r_0}\right)^2} \quad \ldots\ldots\ldots\ldots\ldots\ldots\ldots\ldots \quad (46)$$

In particular, at the moment when the pile is on the point of failure (i.e., $z_f \rightarrow l$), the stiffness, k_f, becomes negligible and Eq. 46 reduces to

$$\frac{T_t}{Gr_0^3\phi_t} \simeq \frac{\frac{\pi\lambda}{\left(\frac{l}{r_0}\right)}}{1 + \frac{\lambda}{4\left(\frac{l}{r_0}\right)^2}} \quad \ldots\ldots\ldots\ldots\ldots\ldots\ldots\ldots\ldots\ldots \quad (47)$$

Corresponding expressions may be derived for the case of soil where the strength (and the stiffness) are proportional to depth. For a distribution of available shaft adhesion given by

$$\tau_f = nz \quad \ldots\ldots\ldots\ldots\ldots\ldots\ldots\ldots\ldots\ldots\ldots\ldots\ldots\ldots \quad (48)$$

the angle of twist at the pile head, for a depth of yield, z_f, is

$$\phi_t = \frac{n}{2m}\left[1 + \frac{2k_f'}{\pi\lambda'}\left(\frac{z_f}{r_0}\right) + \frac{8}{3\lambda'}\left(\frac{z_f}{r_0}\right)^3\right] \quad \ldots\ldots\ldots\ldots\ldots\ldots \quad (49)$$

in which k_f' = the torsional stiffness, $T/(mr_0^4\phi)$, of the unyielded portion of the pile. The total applied torque is

$$T_t = \frac{nr_0^4}{2}\left[k_f' + 2\pi\left(\frac{z_f}{r_0}\right)^2\right] \quad \ldots\ldots\ldots\ldots\ldots\ldots\ldots\ldots \quad (50)$$

As the pile approaches failure in torsion, the torsional stiffness may be estimated as

$$\frac{T_t}{mr_0^4\phi_t} \simeq \frac{\frac{3}{4}\pi\lambda'}{\left(\frac{l}{r_0}\right)} \Bigg/ \left(1 + \frac{\frac{3}{8}\lambda'}{\left(\frac{l}{r_0}\right)^3}\right) \quad \ldots\ldots\ldots\ldots\ldots\ldots\ldots\ldots \quad (51)$$

In most practical cases, piles will behave in a flexible fashion under torsion (i.e., $l/r_0 > \lambda^{1/2}$ or $\lambda'^{1/3}$) and the second term in the denominator of Eqs. 47 and 51 may be ignored. This enables both equations to be simplified to give the secant torsional stiffness of a pile as it approaches failure as

$$\frac{T_t}{\phi_t} \sim \frac{\pi r_0^4 G_p}{l} = 2\frac{(GJ)_p}{l} \quad \ldots\ldots\ldots\ldots\ldots\ldots\ldots\ldots\ldots\ldots (52)$$

for the case of homogeneous soil conditions and

$$\frac{T_t}{\phi_t} \sim \frac{3}{4}\frac{\pi r_0^4 G_p}{l} = 1.5\frac{(GJ)_p}{l} \quad \ldots\ldots\ldots\ldots\ldots\ldots\ldots\ldots\ldots\ldots (53)$$

for the case of soil where the strength and stiffness are proportional to depth. These results might have been deduced intuitively from consideration of the average torque acting down the length of the pile.

Full Scale Torsional Load Tests

Application of the preceding analysis will be illustrated by the study of full scale load tests reported by Stoll (8). Torsion load tests were conducted on two steel pipe piles of 0.273-m (10.75-in.) external diam and 6.3-mm (0.25-in.) wall thickness. The piles were back-filled with concrete giving a torsional rigidity of (Stoll, 9)

$$(GJ)_p = 12.8 \text{ MN m}^2 \text{ (4.46 kips-in.}^2\text{)} \quad \ldots\ldots\ldots\ldots\ldots\ldots\ldots\ldots (54)$$

The equivalent shear modulus of the pile may be calculated as

$$G_p = 23.5 \times 10^3 \text{ MN/m}^2 \text{ (3.4} \times 10^6 \text{ psi)} \quad \ldots\ldots\ldots\ldots\ldots\ldots\ldots\ldots (55)$$

The piles were driven into deposits consisting of layers of soft organic silt overlying clayey silt, sand, and gravel. Profiles of standard penetration index N, given by Stoll (8), show gradually increasing values of N with depth. Of the two piles, pile A-3 was driven to 17.4 m (57 ft) through soil where the N value increased approximately according to

$$N = 1.38\, z \text{ (} z \text{ in meters) [0.42 } z \text{ (} z \text{ in feet)]} \quad \ldots\ldots\ldots\ldots\ldots\ldots\ldots\ldots (56)$$

The other pile, pile V-4, was installed to a total depth of 20.7 m (68 ft). At this location the measured N values were close to zero over the first 2.4 m (8 ft) and thereafter increased approximately according to

$$N = 2.62\,(z - 2.4) (z \text{ in meters}) [0.8\,(z - 8) (z \text{ in feet})] \quad \ldots\ldots\ldots\ldots\ldots\ldots\ldots\ldots (57)$$

The measured torque-twist behavior of the two piles has been replotted from Stoll (8) in Figs. 4(*a*) and (*b*). The initial torsional stiffness of pile A-3 was $T/(r_0\phi) \simeq 20$ MN/rad (4,500 kips/rad). From Eq. 28, the stiffness is given by

$$\frac{T}{r_0\phi} = 2.29\, G_p^{2/3} (mr_0)^{1/3} r_0^2 \quad \ldots\ldots\ldots\ldots\ldots\ldots\ldots\ldots\ldots\ldots (58)$$

from which a value of mr_0 may be calculated, giving $mr_0 = 0.187$ MN/m^2 (27.1 psi). This corresponds to a variation of the shear modulus of the soil of

$G = 1.37\,z$ MN/m^2 (z in meters)[60.5 z psi (z in feet)] . . . . . (59)

For pile V-4, the measured initial torsional stiffness was $T/(r_0\phi) \simeq 15$ MN/rad (3,400 kips/rad). However, from the profile of N values it may be assumed

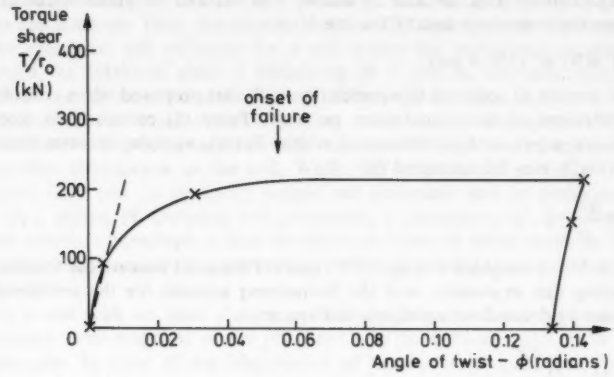

(a) Pile A-3

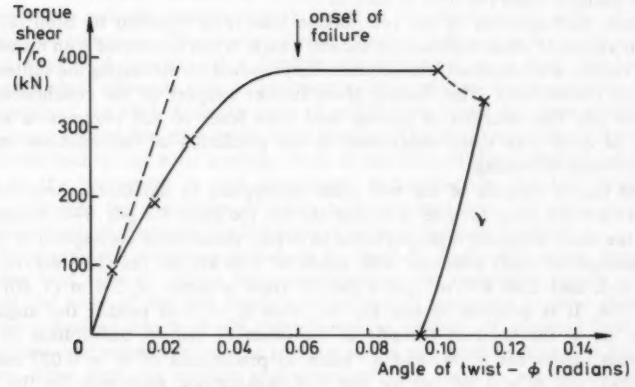

(b) Pile V-4

FIG. 4.—Results from Torsional Load Tests [Replotted from Stoll (8)]: (*a*) Pile A-3; (*b*) Pile V-4

that the top 2.4 m (8 ft) of soil offered negligible resistance. Thus, the torsional stiffness of the pile below 2.4 m (8 ft) would be

$$\left[\frac{T}{(r_0\phi)}\right]_{z=2.4\text{m}} = \left[\frac{1}{15} - \frac{2.4r_0}{(GJ)_p}\right]^{-1} = 24.3 \text{ MN/rad (5,470 kips/rad)} \quad . \quad . \quad . \quad (60)$$

From Eq. 58, a value of mr_0 of 0.334 MN/m^2 (48.5 psi) may be calculated. The corresponding variation of shear modulus with depth is

$$G = 2.45\,(z - 2.4)\ \text{MN/m}^2\ (z \text{ in meters})\,[108\,(z - 8)\ \text{psi}\ (z \text{ in feet})] \quad \ldots\ldots (61)$$

Comparison of Eqs. 59 and 56 and of Eqs. 61 and 57 yields a correlation between shear modulus and SPT value N of

$$G \simeq N\ \text{MN/m}^2\ (150\,N\ \text{psi}) \quad \ldots\ldots (62)$$

It is of interest to compare this correlation with that proposed when considering the settlement of raft foundations on sand. Parry (5) recommends that the settlement, ρ (m), of a foundation of width, B, (m), applying a mean pressure, q (MN/m^2), may be estimated by

$$\rho \simeq 0.3\,\frac{qB}{N} \quad \ldots\ldots (63)$$

in which N = a weighted average SPT value for the sand beneath the foundation. Comparing this expression with the Boussinesq solution for the settlement of a circular rigid punch on an elastic half space:

$$\rho = \frac{\pi}{8}\,(1 - \nu)\,\frac{qB}{G} \quad \ldots\ldots (64)$$

and taking Poisson's ratio, ν, as 0.25, it may be seen that Eq. 63 is consistent with taking a value for G of N MN/m^2.

Thus, back-analysis of the two torsion load tests reported by Stoll (8) has led to values of shear modulus for the soil which, when correlated with measured SPT values, are consistent with correlations proposed for estimating the settlement of raft foundations. This finding gives further support to the conclusions of Poulos (4), that analysis of torsion load tests leads to soil parameters which may be used with some confidence in the prediction of deformations under other forms of loading.

The failure torques of the two piles correspond to mobilized shear forces of 215 kN (48 kips) for pile A-3, and 382 kN (86 kips) for pile V-4. Assuming that the shaft adhesion is proportional to depth, these loads correspond to rates of increase of shaft adhesion with depth of 1.66 kN/m^2/m (10.6 psf/ft) for pile A-3, and 2.66 kN/m^2 [16.9 psf/ft, from a depth of 2.4 m (8 ft)] for pile V-4. It is possible to use Eq. 49, with $z_f = l$, to predict the angle of twist, ϕ, at the head of the pile at the onset of failure. Subsitution of the relevant values for n, m, and λ' leads to predictions of ϕ = 0.027 rad of pile A-3, and ϕ = 0.060 rad for pile V-4 (making due allowance for the top, unresisted, section of the pile). The first of these values is somewhat lower than that suggested in Fig. 4(a); however, both values offer reasonable guidelines for use in design. For example, restricting the twist at the top of a pile to one third of the value calculated from Eqs. 44 or 49 would imply a load factor of approx 2 (see Fig. 4).

Conclusions

Solutions have been presented, in the form of simple algebraic expressions, for the torsional response of cylindrical piles. The solutions have been shown

to be in good agreement with previously published results obtained by numerical analysis (Poulos, 4). In practice, pile geometries and stiffness ratios are such that most piles will behave as infinitely long piles under torsional loading. For this situation, the torsional stiffness, T/ϕ, is proportional to the square root (for homogeneous soil) or cube root (soil with stiffness proportional to depth) of the soil stiffness. Thus, the torsional stiffness of a pile is relatively insensitive to the estimated soil stiffness; for a soil where the stiffness is proportional to depth, an eightfold error in estimating $m = dG/dz$ will only result in a twofold error in the calculated torsional stiffness of the pile.

Analysis of full scale torsional loading tests on piles has given values of soil stiffness which are consistent with values which might have been estimated from other information on the soil. While this supports the usefulness of the torsional load test [a relatively simple and economic test to perform—Stoll (8)] as a means of deducing soil properties, a corollorary of the statements in the previous paragraph is that the deduced value of shear modulus for the soil will be very sensitive to experimental error in measuring the torsional stiffness of the pile.

For a soil with an ideal elastic, perfectly plastic shear stress-strain curve, the torque twist response of the pile head may be deduced right up to failure of the pile. In spite of the idealization of the stress-strain curve, estimates of the angle of twist necessary to fail a pile have shown reasonable agreement with measured values from full scale pile tests.

O'Neill and Dutt (3) have observed that, for many soil types, the shaft adhesion between pile and soil reaches a peak and then decreases as the angle of twist of the pile increases. This strain-softening type of behavior will clearly reduce the overall load capacity of a flexible pile compared to a rigid pile (where the peak shaft adhesion may be assumed to be mobilized simultaneously down the length of the pile). A similar form of progressive failure has been postulated for long compressible piles under axial loading. The obvious similarity between torsional loading and axial loading—both in the form of the analytical solutions and in the agreement in soil parameters deduced from the two types of test—suggests the possibility of using torsional load tests on piles, in order to investigate qualitatively the behavior of piles under axial loading.

The advantages of such an approach are twofold. In the first place, repeated torsion load tests to failure have no effect on the embedded length of pile or on the level of the pile head; with axial load tests, the gradual changing of the embedded length of pile complicates the analysis of repeated load tests to failure, and restrictions on the position of the pile head relative to a reaction frame often limit the number and extent of such tests. A second advantage is in the realm of model tests, where it is often impossible to fabricate piles of suitable dimensions and stiffness in order to model the compressibility of piles currently used in practice (e.g., in the foundations for offshore structures). By contrast, it is relatively simple to make flexible model piles which behave as infinitely long piles under torsional loading. A study of such piles under repeated and cyclic torsional loading may well furnish considerable insight into the behavior of compressible piles under cyclic axial loading.

Appendix I.—References

1. Abramowitz, M., and Stegun, J. A., *Handbook of Mathematical Functions*, Dover

Publications, New York, N.Y., 1968, pp. 446–478.
2. O'Neill, M. W., discussion of "Static and Dynamic Analysis of Pile Foundations," by William E. Saul, *Journal of the Structural Division*, ASCE, Vol. 95, No. ST2, Proc. Paper 6373, Feb., 1969, pp. 289–295.
3. O'Neill, M. W., and Dutt, R. N., discussion of "Torsional Response of Piles," by Harry G. Poulos, *Journal of the Geotechnical Engineering Division*, ASCE, Vol. 102, No. GT6, Proc. Paper 12163, June, 1976, pp. 658–660.
4. Poulos, H. G., "Torsional Response of Piles," *Journal of the Geotechnical Engineering Division*, ASCE, Vol. 101, No. GT10, Proc. Paper 11629, Oct., 1975, pp. 1019–1035.
5. Parry, R. H. G., "Estimating Foundation Settlements in Sand From Plate Bearing Tests," *Geotechnique*, Vol. 28, No. 1, London, England, 1978, pp. 107–118.
6. Randolph, M. F., and Wroth, C. P., "Analysis of the Deformation of Vertically Loaded Piles," *Journal of the Geotechnical Engineering Division*, ASCE, Vol. 104, No. GT12, Proc. Paper 14262, Dec., 1978, pp. 1465–1488.
7. Randolph, M. F., and Wroth, C. P., "Application of the Failure State in Simple Shear to the Shaft Capacity of Driven Piles," *Geotechnique*, Vol. 31, No. 1, London, England, 1981, pp. 143–157.
8. Stoll, U. W., "Torque Shear Test of Cylindrical Friction Piles," *Civil Engineering*, ASCE, Vol. 42, No. 4, Apr., 1972, pp. 63–64.
9. Stoll, U. W., discussion of "Torsional Response of Piles," by Harry G. Poulos, *Journal of the Geotechnical Engineering Division*, ASCE, Vol. 102, No. GT6, Proc. Paper 12163, June, 1976, pp. 660–661.

Appendix II.—Notation

The following symbols are used in this paper:

a = radius of punch;
A = constant of integration;
B = constant of integration and width of loaded area;
G = shear modulus of soil;
G_p = equivalent shear modulus of solid pile;
$(GJ)_p$ = torsional rigidity of pile;
k_f = stiffness factor;
l = length of pile;
m = rate of increase of shear modulus of soil with depth;
n = rate of increase of shaft adhesion with depth;
N = standard penetration test value;
q = bearing pressure;
r = radius;
r_0 = radius of pile;
T = torque;
u = radial movement of soil;
v = circumferential movement of soil;
z = depth;
Z = nondimensional depth factor;
γ = shear strain;
Δ = increment;
θ = polar co-ordinate;
λ = stiffness ratio (homogeneous soil);
λ' = stiffness ratio (soil with stiffness proportional to depth);
μ = constant in analytical solution;

ν = Poisson's ratio;
π = mathematical constant;
ρ = settlement;
σ = normal stress;
τ = shear stress; and
ϕ = angle of twist of pile.

Experimental Study on Footings in Layered Soil

By Adel M. Hanna,[1] M. ASCE

Introduction

Recently, an empirical method was proposed by Satyanarayana and Garg (19) to predict numerically the ultimate bearing capacity of footings on layered soils. The empirical equations, derived to determine the average values of the shear strength parameters, C_a, and ϕ_a, for two-layered soil within the calculated equivalent significant depth, are

$$C_a = \frac{C_1 Z_1 + C_2 Z_2}{Z_1 + Z_2} \quad (1)$$

$$\phi_a = \tan^{-1}\left(\frac{Z_1 \tan\phi_1 + Z_2 \tan\phi_2}{Z_1 + Z_2}\right) \quad (2)$$

in which Z = thickness of the soil layer; C = cohesion of the soil layers; and ϕ = angle of shearing resistance for the soil layer. The subscripts 1 and 2 refer, respectively, to the upper and lower layer.

The equivalent significant depth, D_e, as defined by Satyanarayana and Garg, is the depth to which the net loading intensity due to structural loading can produce a perceptible contribution to settlement or shear stress. This depth for a two-layered soil is given by

$$D_e = Z_1 + (2B - Z_1)\left(\frac{C_1 + \tan\phi_1}{C_2 + \tan\phi_2}\right) \quad (3)$$

in which B = the footing width or diameter.

The ultimate bearing capacity can then be determined by means of the general bearing capacity equation proposed by Terzaghi (21).

The method is attractive to use because of its simplicity; however the predictive accuracy of the method has not been verified for conditions other than those for which the equations were derived.

This paper presents an attempt to examine the validity of the method. An

[1] Assoc. Prof., Concordia Univ., Dept. of Civ. Engrg., 1455 de Maisonneuve Blvd. West, Montreal, Quebec, Canada, H3G 1M8.

Note.—Discussion open until January 1, 1982. To extend the closing date one month, a written request must be filed with the Manager of Technical and Professional Publications, ASCE. Manuscript was submitted for review for possible publication on September 24, 1980. This paper is part of the Journal of the Geotechnical Engineering Division, Proceedings of the American Society of Civil Engineers, ©ASCE, Vol. 107, No. GT8, August, 1981. ISSN 0093-6405/81/0008-1113/$01.00.

experimental investigation on the ultimate bearing capacity of strip and circular model footings on a two-layered soil was conducted, and the data used to check the values predicted by the method for the conditions tested.

Experimental Investigation

Setup.—Plane-strain conditions were simulated for strip footing tests by using a glass-sided soil box, similar to the one used by Ko in his investigation of foundations on sand (13). The length, width, and depth inside the box were 24 in. (610 mm), 8 in. (203 mm), and 20 in. (508 mm), respectively. The glass enabled observations of relative movement along the intermediate principal stress plane during the test and inspection of rupture surfaces after failure.

The horizontal movement of the glass sides was measured at the midspan points. The results showed that, at the maximum stress levels attained, the glass sides were inflexible. The friction between the sand and the glass sides was measured by means of a direct shear box test. In these tests, the bottom half of the shear box was packed with dense sand, while the upper half consisted of a piece of glass attached to a block of wood, both having the same inner dimensions of the shear box. The results indicated that the angle of friction between the glass and the dense sand varied from 4.91°–7.84° for normal pressures of 9.58 psi (66 kPa) and 3.26 psi (22.46 kPa), respectively. Since the stress on the intermediate principle plane varies through the failure plane both in the vertical and horizontal directions, an accurate assessment of its frictional contribution to the ultimate bearing capacity is difficult. However, if it is assumed that the stress on the intermediate principal plane is about halfway between the major and minor principal stresses (20), then an estimate of the stress component due to friction contribution would be small and negligible.

A steel drum 19 in. (483 mm) in height and 20 in. (508 mm) in diameter was used for circular footing tests.

The strip and circular model footings used in this investigation were machined from aluminum sections. The width/diameter of these footings was 2 in. (50 mm), and they had a thickness of 1.5 in. (38 mm) in order to simulate rigid footing conditions. A threaded hole in the center of the footing allowed rigid connection to a loading ram through which the loads were applied. The bases of the footings were roughened by cementing fine grain sandpaper onto them, using epoxy resin glue. The strip footing was 8 in. (203 mm) long (the same as the inside width of the test box) to ensure plane-strain conditions.

To minimize friction at the interface between the strip footing and the glass sides of the testing box, a cut was made in the footing material at both ends, and the cutaway metal was replaced with flexible foam. One side of the foam was glued to the footing, while the other side was covered with polyethylene.

In order to enhance the confidence in the experimental results of the strip footing tests, an instrumented model strip footing was also used in this investigation. This instrumented footing was also fabricated from an aluminum section with the shape and dimensions given in Fig. 1. The main concept used in the design of this footing was to avoid increasing the observed load due to friction between the footing edges and the box sides. For this purpose, the footing base was divided into three sections where the loads were only measured from the middle section. The other two sections were to ensure plane-strain loading

conditions. A comparison between test results of the two-strip footings used in this investigation under the maximum expected loads showed very good agreement. Thus, strip footing tests were continued using the one-piece model footing for simplicity and time-saving purposes.

A loading frame of a compression machine was used. In order to maintain the load in a vertical direction during the footing tests, the loading ram was passed through a lubricated ball-bearing guide. Proving rings, each having a different sensitivity and maximum capacity, were used to measure the applied loads. In the case of the three-piece footing tests, the total load was measured using a proving ring and the load per cell was recorded by connecting the load cells to a Solartron Data Acquisition System, where the electronic signals were displayed and recorded by a printer. The proving rings and the load cells

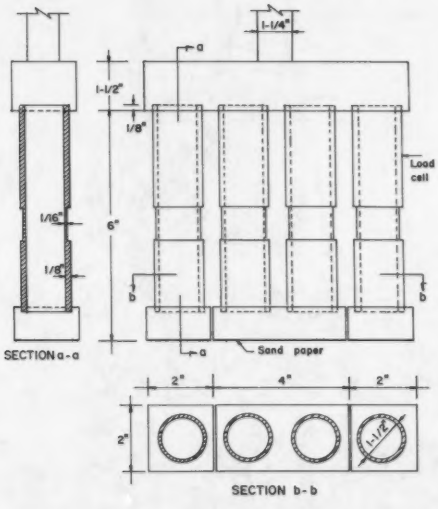

FIG. 1.—Instrumented Strip Footing Model (1 in. = 25.4 mm)

(individually and as a group) were calibrated prior to testing using an Instron Universal Testing Machine. Dial gages, having at least count of 0.001 in. (0.025 mm), were used to measure the vertical displacement.

All tests were conducted at a nominal rate of feed of 0.01 in./min (0.25 mm/min). The load readings were recorded at predetermined strain values defined as the ratio of settlement to the footing width or diameter (S/B) (usually the load readings were recorded at intervals equal to 0.5%). Fig. 2 shows a photograph of the test setup.

Test Materials.—The sand used in this investigation was an air-dried, medium-to-coarse angular silica. The predominant minerals of this sand were quartz and feldspar. The grain size distribution showed a uniformity coefficient equal to 2.76. The specific gravity of the particles was found to be 2.64. Laboratory

tests on this sand indicated maximum and minimum void ratios of 1.01 and 0.395, corresponding, respectively, to maximum and minimum porosities of 0.502 and 0.283.

In order to assure reproducibility of the sand density throughout the testing program, a sand-placing technique was employed consistently. A procedure was developed by raining the sand from a certain height to give uniform and desired density. For the purpose of this investigation, the relationship between the height

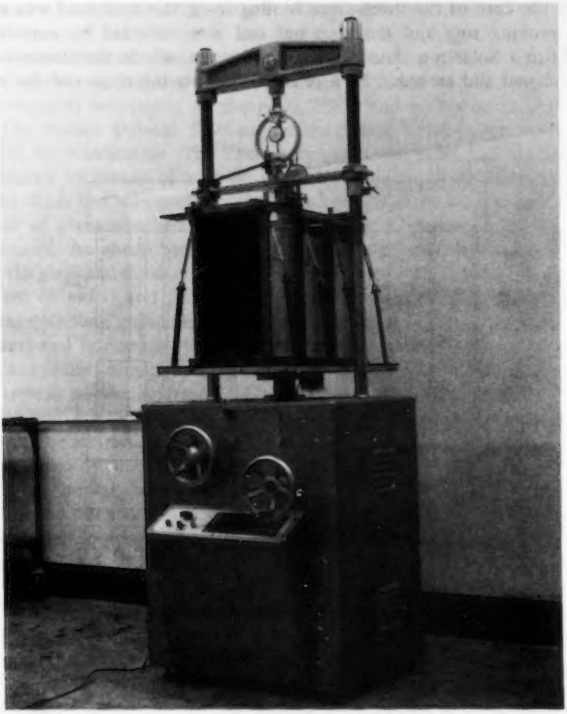

FIG. 2.—Setup for Strip Footing Tests

of fall and sand density was established in the laboratory for the sand used (see Fig. 3). Dense packing was achieved by raining the sand from a height of 36 in. (914 mm) for each 3-in. (76-mm) layer by means of a metallic sieve, 18 in. (457 mm) in diameter. Compact packing was achieved by raining the sand from a height of 6 in. (152 mm) for each 1-in. (25-mm) layer, through a funnel with a rubber tube and end sieve. Loose packing was obtained by pouring the sand slowly from a very low height, using the same funnel used for obtaining compact sand.

The sand box was kept at the same level of the platform of the testing machine during the sand-pouring process, and with caution, the box was pushed on rollers to the loading system; this proved to be a relatively satisfactory technique to prevent any disturbances to the sand density.

Plane-strain tests were conducted on samples 2.63 in. (67 mm) long, 1.5 in. (38 mm) wide, and 2.95 in. (75 mm) deep (see Fig. 4). Deformation in the longitudinal direction was restricted by means of two rigid steel plates, where the intermediate principal stress, σ_2, was measured. The minor principal stress was applied to the sample through two cells filled with water as the case of triaxial test. The apparatus was put on a compression machine where the major principal stress was applied up to failure. Typical results of the plane-strain tests on dense, compact, and loose sands are given in Table 1.

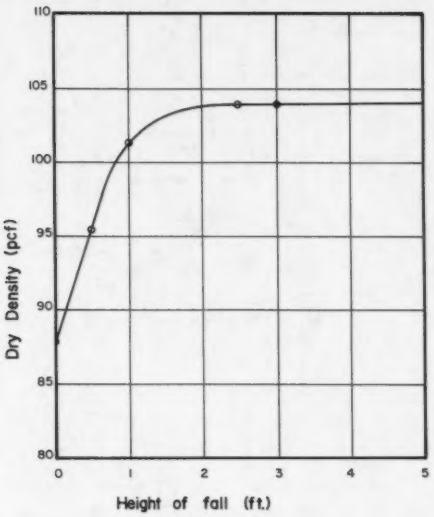

FIG. 3.—Relationship between Sand Density and Height of Fall (1 pcf = 0.157 kN/m^3; 1 ft = 305 mm)

The clay used in this investigation was classified as an inorganic clay of medium plasticity, brown in color, and the dominant clay mineral was illite with quartz and feldspar making up the nonclay minerals. The specific gravity was 2.74 and the water content varied from 25%–30%. The liquid limit, plastic limit, and plasticity index were 43%, 23%, and 20%, respectively. The clay, silt, and sand fractions were 35%, and 1%, respectively.

The clay was mixed with hydrated lime to reduce the plasticity index and decrease the deformation and volume change (14). Also, the shear strength was increased with increasing lime content. In the present investigation, 3% lime of the dry weight of the clay was added, and a period of 3 days–5 days

was allowed for curing. The mixed clay was placed in the testing box by tamping molded balls in layers of about 2-in. (50-mm) thickness. Each layer was compacted (2 cycles/layer) by means of a tamper with rectangular base of 1.5 in. (38 mm) width and 8 in. (203 mm) length. The tamper was 10 lb (3.73 kg) in weight, and the height of fall was 12 in. (305 mm). The testing box was placed on a rigid surface during the compaction process. The inside and seams of the

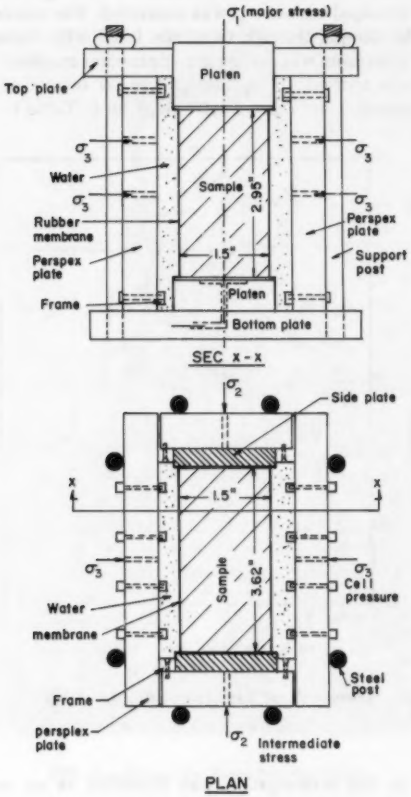

FIG. 4.—Plane-Strain Apparatus (1 in. = 25.4 mm)

footing test box were sealed with petroleum jelly to prevent the loss of water and adhesion of the clay in contact with the box. After packing, the surface was covered with a double layer of Saran Wrap and the box was stored for curing. The procedure was determined in advance in order to maintain the clay strength within a limited range for all footing tests. The specific gravity of the mixed clay was 2.76, the bulk density as obtained in all tests varied

between 104.7 lb/cu ft and 108.4 lb/cu ft (1,677 kg/m^3 and 1,736 kg/m^3), with a water content of 48.9% and 56%, respectively. The degree of saturation varied between 97.9% and 98.9%. Since 98% saturation was achieved, the clay might have been treated as fully saturated (1), which meant that the shear strength was independent of the confining pressure, and the $\phi = 0$ concept could be applied in the analysis of the results. Therefore, the shear strength was measured by conducting unconfined compression tests on a sample 3 in. (76 mm) long and 1.5 in. (38 mm) in diameter, trimmed from a block of clay

TABLE 1.—Plane-Strain Test Results

Packing state (1)	Dry density, in pounds per cubic foot (kilonewtons per cubic meter) (2)	Porosity, η, as a percentage (3)	Relative density, D_r, as a percentage (4)	Cell pressure, σ_3, in pounds per square inch (kilopascals) (5)	Intermediate stress, σ_2, in pounds per square inch (kilopascals) (6)	Major stress σ_1, in pounds per square inch (kilopascals) (7)	Angle of shearing resistance, ϕ, in degrees (8)
Dense	104 (16.3)	0.369	0.691	5 (34.45)	13.90 (95.77)	59.20 (407.89)	48.8
		0.369	0.691	5 (172.25)	51.00 (351.39)	200.00 (1,378.00)	47.7
		0.369	0.691	50 (344.50)	98.10 (675.91)	353.80 (2,437.68)	45.8
Compact	95 (15.0)	0.420	0.465	5 (34.45)	11.40 (78.55)	38.50 (265.26)	43.6
		0.420	0.465	25 (172.25)	51.03 (351.60)	159.80 (1,101.02)	42.0
Loose	86 (13.8)	0.467	0.218	5 (34.45)	8.18 (56.36)	18.80 (129.53)	34.0

cut from the box, immediately after each footing test. At least two, vertically-trimmed test samples were obtained for each footing test.

Test Results

Test results of strip and circular footings are presented in Figs. 5–10 except for the case of strip footing on dense sand overlying clay which is presented in Table 2. These figures show the variation of the ultimate bearing capacity, q_u, with the ratio of the upper layer thickness below the footing base to the footing width or diameter, H/B. The observed ultimate bearing capacity showed an increase with increased thickness of the upper layer below the footing base in the case of a strong layer overlying a weak layer, and a rapid decrease

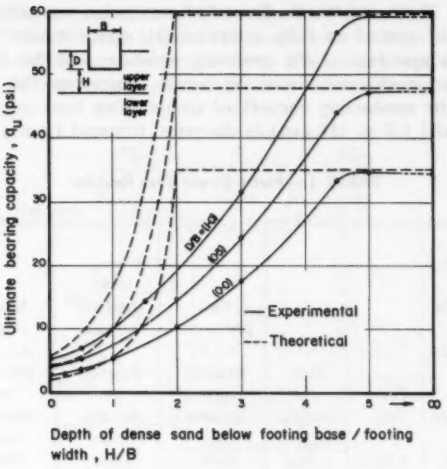

FIG. 5.—Summary of Results: Strip Footing in Dense Sand Overlying Loose Sand (1 lb/sq in. = 6.90 KPa)

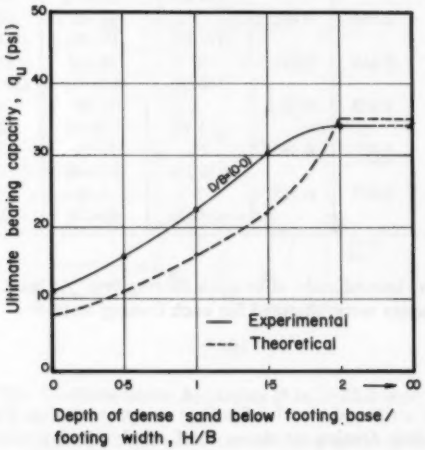

FIG. 6.—Summary of Results: Strip Footing on Dense Sand Overlying Compact Sand (1 lb/sq in. = 6.90 KPa)

in the case of a weak layer overlying a strong layer. As would be expected, the observed ultimate bearing capacity increased with increasing ratio of the buried depth of the footing to the footing base D/B. The ultimate bearing capacity of layered system varies between the two limits of footings on homogeneous lower and upper layer soils for H/B ratios of zero and infinity, respectively.

The failure loads were determined from load-settlement curves. The shape of the load-settlement curve and consequently, the mode of failure generally depends on the size and shape of the footing, the composition of the supporting

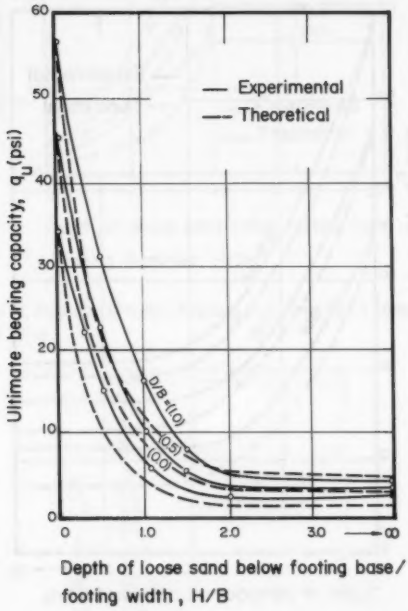

FIG. 7.—Summary of Results: Strip Footing in Loose Sand Overlying Dense Sand (1 lb/sq in. = 6.90 KPa)

soils, and rate of the loading (23). In addition, in the case of footings on two-layered soils, the mode of failure is influenced by the shear strength of the upper and lower layers, location of the weaker layer, and upper layer thickness below the footing base. The three principal modes of shear failure under foundations have been described in the literature as general, local, and punching shear failures (6,21–23).

In the case of general shear failure, which is characterized by the existence of a well-defined failure pattern, there was no difficulty in determining the failure point. Under strain-controlled conditions (testing conditions), a visible

decrease of load necessary to produce footing movement after failure was observed. In this case, the load settlement curve exhibits a peak load which defines the ultimate bearing capacity. This is less clearly defined and is often difficult to establish for local and punching shear failures, and different methods for selecting the ultimate load have been published. Terzaghi, in Ref. 21, defined the ultimate load in these modes of failure as the point where the load settlement curve becomes relatively steep and straight. Brinch Hansen, in Ref. 12, has defined the failure point as the stress, for which the strain is twice the strain at a 10% smaller stress. Vesic, in Ref. 22, defined the failure point as the

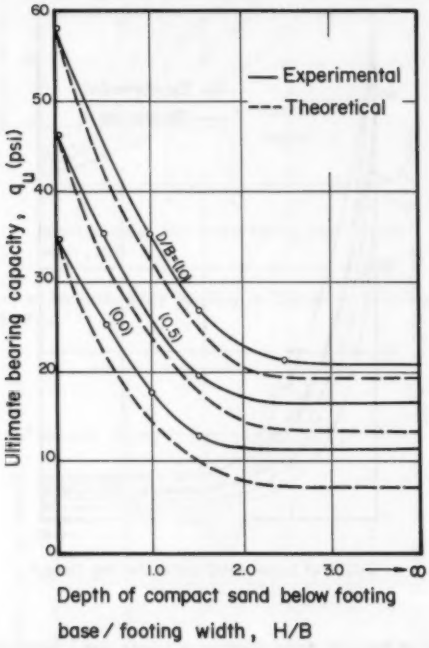

FIG. 8.—Summary of Results: Strip Footing in Compact Sand Overlying Dense Sand (1 lb/sq in. = 6.90 KPa)

point where the slope of the load-settlement curve first reaches zero or a steady, minimum value. Christiaens (in Ref. 4), found, by plotting the settlement against the load on a log-log scale, that the diagram consisted of an upper curved part and a lower part, which is a straight line. The intersection of these two lines is considered as the rupture point. DeBeer, in Ref. 5, reported that Christiaens' method was in close agreement with the criterion defined by Hansen, in Ref. 12. In the present investigation, both Terzaghi's and Christiaens' criteria were

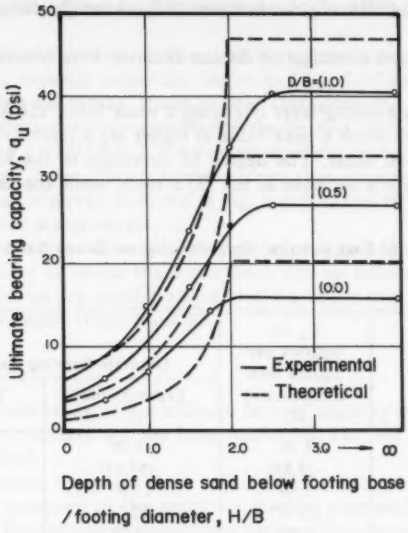

FIG. 9.—Summary of Results: Circular Footing in Dense Sand Overlying Loose Sand (1 lb/sq in. = 6.90 KPa)

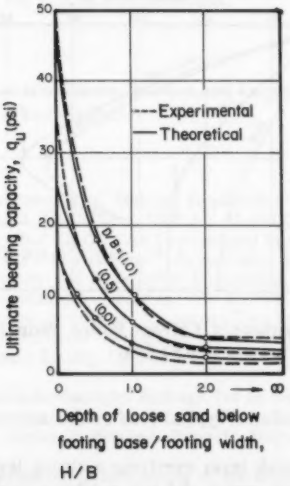

FIG. 10.—Summary of Results: Circular Footing in Loose Sand Overlying Dense Sand (1 lb/sq in. = 6.90 KPa)

used to determine the failure point in cases of local and punching shear failure of footings.

Based on the present investigation distinct features were observed:

1. For footings in a strong layer overlying a weak layer, the load settlement curves were found to reach a peak value at higher H/B ratios where the mode of failure was general shear. The degree of curvature of the load settlement curves decreased with a decrease in the H/B ratio, while the mode of failure

TABLE 2.—Summary of Test Results: Strip Footing on Dense Sand Overlying Clay ($\phi_1 = 47.7°$)

D/B ratio (1)	H/B ratio (2)	C_2, in pounds per square inch (kilopascals) (3)	Ultimate Bearing Capacity, q_u	
			Experimental (4)	Theoretical (5)
0.0	1	1.28 (8.83)	8.28 (57.13)	19.08 (131.65)
0.0	1	1.80 (12.42)	11.90 (82.11)	39.73 (274.14)
0.0	2	3.09 (21.32)	29.01 (200.17)	34.20 (235.98)

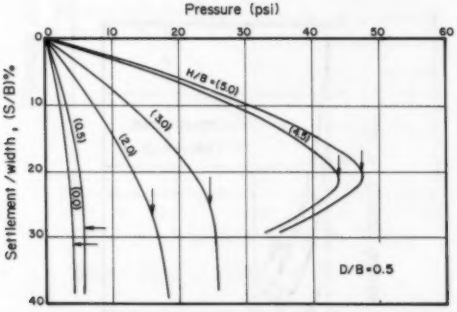

FIG. 11.—Typical Load-Settlement Curves: Buried Strip Footing in Dense Sand Overlying Loose Sand (1 lb/sq in. = 6.90 KPa)

changed to local shear failure. Typical load-settlement curves are given in Fig. 11.

2. For footings in a weak layer overlying a strong layer, and for high H/B ratios, the load-settlement curves did not exhibit a peak load, and the mode of failure was local shear. The degree of curvature of the load-settlement curve increased with decreasing H/B ratio, where a peak load could be found.

Evaluation of Empirical Method of Satyanarayana and Garg (19)

This method was applied under the conditions utilized in the tests; the calculated ultimate bearing capacity values are shown in Figs. 5–10 and Table 2 together with the experimental values. It can be seen that, generally, the Satyanarayana and Garg method tends to underestimate the bearing capacity up to the ratio of H/B less than 2; at $H/B \geq 2$, the method treats the system as a homogeneous soil of the upper layer. The predicted values thus obtained are considerably higher than those observed as shown in Fig. 5; it is in fact this case that displays the most dramatic disagreement.

It is of interest to note that the present test results indicate that the depth of the upper layer at which the lower layer has no influence on the bearing capacity depends on the relative strength of the two layers (Figs. 5–7), as well as the type of footings (Figs. 5 and 9).

Conclusion

An experimental study of the ultimate bearing capacity of strip and circular footings on a two-layered soil has been conducted. The test setup and materials used are described.

The experimental data have been utilized to furnish a basis for evaluating the predictive accuracy of the empirical method proposed by Satyanarayana and Garg (19). The extensive comparisons between the observed ultimate bearing capacity values and those predicted by the method reveal discrepancies ranging between 70% and 85%. Thus, it is the writer's opinion that the method needs more refinement and further experimental, and possibly field verifications before it can be recommended for practical applications.

Acknowledgment

The financial support of the Natural Science and Engineering Research Council of Canada is gratefully acknowledged.

Appendix I.—References

1. Bishop, A. W., "The Strength of Soils as Engineering Materials," *Geotechnique*, London, England, Vol. 16, No. 2, June, 1966, pp. 91–130.
2. Brown, J. D., and Meyerhof, G. G., "An Experimental Study of the Ultimate Bearing Capacity of Layered Clay Foundations," *Proceedings*, Seventh International Conference on Soil Mechanics and Foundation Engineering, International Society for Soil Mechanics and Foundation Engineering, Vol. 2, 1969, pp. 45–51.
3. Button, S. J., "The Bearing Capacity of Footings on a Two-Layered Cohesive Sub-Soil," *Proceedings*, Third International Conference on Soil Mechanics and Foundation Engineering, International Society for Soil Mechanics and Foundation Engineering, Vol. 1, 1953, p. 356.
4. DeBeer, E. E., "Proefondervindelijke Bijdrage Tot de Studie Van Het Gransdraagvermogen Van Zand Onder Funderingen op Staal; Bepaling Van der Vormfactor S_b, *Annales des Travaux Publics de Belgique*, Brussels, Belguim, Vol. 68, No. 6, Dec., 1967, pp. 481–506.
5. DeBeer, E. E., "Experimental Determination of the Shape Factors and the Bearing Capacity Factors of Sand," *Geotechnique*, London, England, Vol. 20, No. 4, Dec., 1970, pp. 387–411.
6. DeBeer, E. E., and Vesic, A. B., "Etudé Expérimentale de la Capacite Portate du

Sable sous des Fondations Directes Établies en Surface," *Annales des Travaux Publics de Belgique*, Brussels, Belguim, Vol. 59, No. 3, June, 1958, pp. 5–53.
7. Desai, C. S., and Reese, L. C., "Ultimate Capacity of Circular Footings on Layered Soils," *Journal of Indian Natural Society Soil Mechanics and Foundation Engineering*, Vol. 96, No. 1, Jan., 1970, p. 41.
8. Hanna, A. M., "Bearing Capacity of Footings Under Vertical and Inclined Loads on Layered Soils," thesis presented to the Nova Scotia Technical College, at Halifax, Nova Scotia, in 1978, in partial fulfillment of the requirements for the degree of Doctor of Philosophy.
9. Hanna, A. M., "Bearing Capacity of Foundations on a Weak Sand Layer Overlying a Strong Deposit," *Canadian Geotechnical Journal*, Toronto, Ontario, Canada, 1980.
10. Hanna, A. M., and Meyerhof, G. G., "Ultimate Bearing Capacity of Foundations on a Three-Layer Soil, With Special Reference to Layered Sand," *Canadian Geotechnical Journal*, Toronto, Ontario, Canada, Vol. 16, No. 2, May, 1979, pp. 412–414.
11. Hanna, A. M., and Meyerhof, G. G., "Design Charts for Ultimate Bearing Capacity of Foundations on Sand Overlying Soft Clay," *Canadian Geotechnical Journal*, Toronto, Ontario, Canada, Vol. 17, No. 2, May, 1980, pp. 300–303.
12. Hansen, J. B., "A Revised and Extended Formula for Bearing Capacity," *Bulletin No. 28*, Danish Geotechnical Institute, Copenhagen, Denmark, 1970.
13. Ko, H. Y., and Davidson, L. W., "Bearing Capacity of Footings in Plane-Strain," *Journal of the Soil Mechanics and Foundations Division*, ASCE, Vol. 99, No. SM1, Proc. Paper 9496, Jan., 1973, pp. 1–23.
14. Kwaku, S. F., "Laboratory Study of Lime Stabilized Clay Sub-Grade Under Static and Repeated Loads," thesis, presented to Nova Scotia Technical College, at Halifax, Nova Scotia, in 1964, in partial fulfillment of the requirements for the degree of Master of Engineering.
15. Meyerhof, G. G., "Ultimate Bearing Capacity of Footings on Sand Layer Overlying Clay," *Canadian Geotechnical Journal*, Toronto, Ontario, Canada, Vol. 11, No. 2, May, 1974, pp. 223–229.
16. Meyerhof, G. G., and Hanna, A. M., "Ultimate Bearing Capacity of Foundations on Layered Soils Under Inclined Load," *Canadian Geotechnical Journal*, Toronto, Ontario, Canada, Vol. 15, No. 4, Nov., 1978, pp. 565–572.
17. Myslivec, A., "Bearing Capacity of Layered Subsoil," *Proceedings*, Fourth Budapest Conference on Soil Mechanics and Foundation Engineering, Hungarian Academy of Science and International Society for Soil Mechanics and Foundation Engineering, 1971, p. 677.
18. Purushothamraj, P., et al., "Bearing Capacity of Strip Footings in Two-Layered Cohesive Friction Soils," *Canadian Geotechnical Journal*, Toronto, Ontario, Canada, Vol. II, No. 1, Feb., 1974, p. 32.
19. Stayanarayana, B., and Garg, R. K., "Bearing Capacity of Footings on Layered C-ϕ Soils," *Journal of the Geotechnical Engineering Division*, ASCE, Vol. 106, No. GT7, Proc. Paper 15578, July, 1980, pp. 819–824.
20. Shibata, T., and Karube, D., "Influence of the Variation of the Intermediate Principal Stress on the Mechanical Properties of Normally Consolidated Clays," *Proceedings*, Sixth International Conference on Soil Mechanics, International Society for Soil Mechanics and Foundation Engineering, 1965.
21. Terzaghi, K., *Theoretical Soil Mechanics*, John Wiley and Sons, Inc., New York, N.Y., 1943.
22. Vesic, A. S., "Bearing Capacity of Deep Foundations in Sand," *Record No. 39*, Highway Research Board, pp. 112–153.
23. Vesic, A. S., "Analysis of Ultimate Loads of Shallow Foundations," *Journal of the Soil Mechanics and Foundations Division*, ASCE, Vol. 99, No. SM1, Proc. Paper 9480, Jan., 1973, pp. 45–73.
24. Yamaguchi, H., "Practical Formula for Bearing Value of Two-Layer Ground," *Proceedings*, Second Asian Regional Conference on Soil Mechanics, International Society for Soil Mechanics and Foundation Engineering, 1965, p. 176.

Appendix II.—Notation

The following symbols are used in this paper:

B = width or diameter of footing;
C = cohesion parameter for soil layer;
C_a = average value of cohesion parameter of layered soil;
C_1 = cohesion parameter of upper layer;
C_2 = cohesion parameter of lower layer;
D = buried depth of footing;
D_e = equivalent significant depth;
D_r = relative density of sand;
H = thickness of upper layer below footing base;
N_c, N_q, N_γ = bearing capacity factors;
q_u = ultimate bearing capacity;
S = foundation settlement;
Z = thickness of soil layer;
Z_1 = thickness of upper layer;
Z_2 = thickness of the lower layer;
γ = bulk density of soil;
η = porosity of sand;
σ_1 = major principal stress;
σ_2 = intermediate principal stress;
σ_3 = minor principal stress;
ϕ = angle of shearing resistance of soil layer;
ϕ_a = average value of angle of shearing resistance of layered soil;
ϕ_1 = angle of shearing resistance of upper soil layer; and
ϕ_2 = angle of shearing resistance of lower soil layer.

PERMANENT DISPLACEMENTS DUE TO CYCLIC WAVE LOADING[a]

By W. Allen Marr, Jr.,[1] M. ASCE and John T. Christian,[2] F. ASCE

INTRODUCTION

When a soil is subjected to a sequence of cyclic loads, both cyclic strains and residual or permanent strains develop. The latter are the strains that remain at the end of each cycle of load and represent a cumulative effect that must be added to the effects of previous storms. To date, most attention has been directed toward evaluating the peak cyclic displacement that occurs during a storm rather than the permanent displacement, even though the permanent displacement is an important consideration for structures that must resist many storms, such as breakwaters and some offshore platforms.

One could predict permanent displacements in two ways. First, one could develop a hysteretic stress-strain relation for the soil and use the resulting nonlinear relations with a finite element program to solve each cycle of the loading history (5). Although this procedure has several advantages, it suffers from disadvantages. No generally recognized hysteretic stress-strain relation exists for soils that includes effects of load reversal for two- or three-dimensional conditions, despite the great deal of important and useful work in progress in this area. Even with such a relation, the solution would have to proceed by small steps through each cycle of a storm that might contain several hundreds or thousands of cycles. The computer runs could be quite long, and the results would apply to one time-history of wave loading.

This paper describes a second approach that develops relations among the initial soil properties and conditions, the stress changes in a cycle, the number of cycles, and the permanent strains. Thus, the distribution of permanent strains at the end of cyclic loading can be computed. To use this information in a finite element program requires the capability to generate strains and deformations for no net change in load.

[a]Presented at the April 2–6, 1979, ASCE Convention and Exposition, held at Boston Mass.

[1]Research Assoc., Mass. Inst. of Tech., Cambridge, Mass.

[2]Consulting Engr., Stone & Webster Engrg. Corp., P.O. Box 2325, Boston, Mass. 02107.

Note.—Discussion open until January 1, 1982. To extend the closing date one month, a written request must be filed with the Manager of Technical and Professional Publications, ASCE. Manuscript was submitted for review for possible publication on September 24, 1979. This paper is part of the Journal of the Geotechnical Engineering Division, Proceedings of the American Society of Civil Engineers, ©ASCE, Vol. 107, No. GT8, August, 1981. ISSN 0093-6405/81/0008-1129/$01.00.

The relations among soil properties, cyclic loading, and residual strains must also consider another factor not usually dealt with in current practice—cycling about a nonzero, constant shear stress. Most cyclic tests on soils use triaxial testing equipment with isotropic initial stresses, which rarely exist in nature. Vertical and horizontal stresses usually differ in the geostatic case. Stresses from the weight of the facility alter the shear stresses in the foundation. Additionally, in many practical cases, such as dikes, barriers, and breakwaters, a constant horizontal load develops from static, tidal head differences across the structure so that the horizontal wave loads cycle about some constant value. The effects of cycling about a nonzero, constant shear stress must be addressed to develop the relations for permanent strains.

This paper describes the results of an experimental investigation into the permanent deformations caused by cyclic loading about states of stress that include initial shear stress. The physical model is then converted into a finite element formulation. The program computes permanent displacements for the design storm for the Oosterschelde closure barrier. Because previous consolidation analyses for the practical case that motivated this work indicated that most residual excess pore pressures dissipate before the end of the storm, the experimental and analytical procedures involve completely drained behavior.

The experimental and analytical work on the project were reported using tonnes instead of newtons. In the figures, t/m^2 (tonne/m^2) should be multiplied by 9.81 to obtain kPa.

Experimental Program

Fig. 1 shows typical stress paths beneath the Oosterschelde barrier, calculated by finite element methods using elastic soil properties and plane strain conditions.

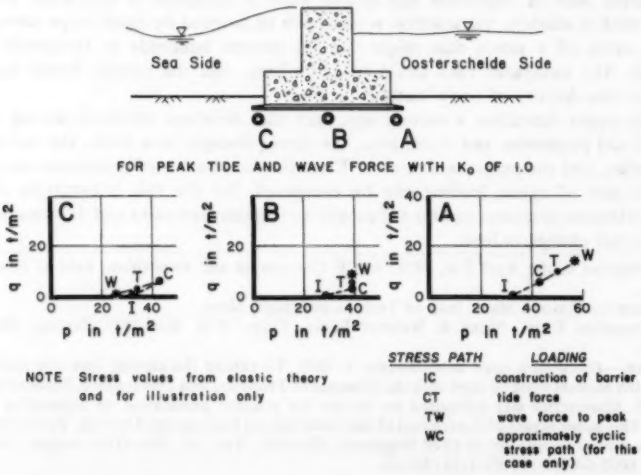

FIG. 1.—Typical Stress Paths for Offshore Foundation

Depending on the initial stress, the effects of the interaction of structure and soil, the nonlinear properties of the soils, and the magnitude of the waves, the stress paths vary considerably. Triaxial tests with isotropic initial stresses and cyclic shear stresses that are equal in extension and compression do not represent these loading conditions adequately.

Cyclic loading on an element of soil leads to permanent deformations from two causes: volume change and shear distortion. Fig. 2 shows results from two cyclic triaxial tests with drained conditions. The "isotropic" test has the shear stress cycled about an average value of zero; the "anisotropic" test has

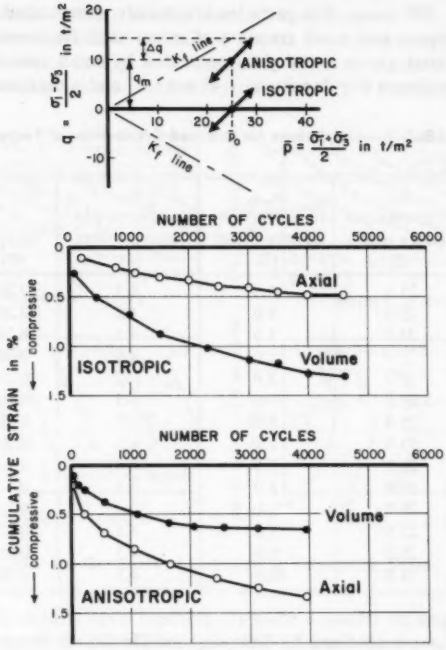

FIG. 2.—Drained Cyclic Triaxial Test Results

a positive average shear stress. Permanent strains accumulate with each additional cycle, the increment of strain decreases with each added cycle, and values of strains vary with the value of the average shear stress. Clearly, the average shear stress has an important effect on the residual strains developed in an element of soil.

Because the permanent strain depends on many factors, including porosity, stress history, mean confining stress, mean cyclic shear stress, amplitude of cyclic shear stress, and orientation of the stress path, and because soil behavior is very nonlinear, a comprehensive constitutive model of soil behavior for cyclic

loads cannot be achieved at this time. However, Hedberg (3) describes an approach for predicting cumulative strains in undrained, triaxial tests for different stress paths by using empirical constants to account for the effects of porosity, mean stress level, and cyclic stress amplitude. The techniques described here use Hedberg's procedure to develop similar relations to define cumulative strains for drained cyclic loading.

Test Equipment and Procedures.—The soil for this investigation comes from the Neeltje Jans Harbor in the Oosterschelde inlet of the North Sea on the coast of the Netherlands. It is an alluvial sand with nearly uniform gradation and a mean grain size of 0.17 mm. Less than 5% of the sample by weight passes the No. 200 sieve. The particles are mainly subrounded, quartz grains with some feldspars and small amounts of mica, shell fragments, and calcite. Some of the quartz grains are slightly cemented by small amounts of calcium carbonate. A minimum dry density of 1.43 ton/m^3 and a maximum dry density

TABLE 1.—Conditions for Drained Cyclic Triaxial Tests

Porosity, in percent (1)	$\bar{p}_0$, in tonnes per square meter (2)	q_m, in tonnes per square meter (3)	Δq, in tonnes per square meter (4)	$q_m/\bar{p}_0$ (5)	$\Delta q/\bar{p}_0$ (6)
40.0	25.0	5.0	4.5	0.20	0.18
43.2	25.0	5.0	4.5	0.20	0.18
44.2	25.0	5.0	4.5	0.20	0.18
46.1	25.0	5.0	4.5	0.20	0.18
42.9	15.0	3.0	2.7	0.20	0.18
43.5	35.0	7.0	6.3	0.20	0.18
43.2	25.0	5.0	1.5	0.20	0.06
43.2	25.0	5.0	6.3	0.20	0.25
43.0	25.0	5.0	10.0	0.20	0.40
43.0	30.0	5.0	4.5	0.17	0.15
43.1	20.0	5.0	4.5	0.25	0.23
43.0	27.5	7.5	4.5	0.27	0.16
43.1	25.0	9.0	4.5	0.36	0.18
42.6	25.0	10.0	4.5	0.40	0.18

of 1.73 ton/m^3 were obtained by following ASTM D2049-69 procedures. The solid particles have a specific gravity of 2.64.

Triaxial samples 1.4 in. (36 mm) in diameter and 3 in. (76 mm) high were prepared in a mold by tamping moist sand in layers according to the method of undercompaction recommended by Ladd (4). Compaction was followed by assembly of the equipment, saturation by flushing with carbon dioxide followed by water, back pressuring to 50 tons/m^2 or more, and consolidation.

After consolidation, a nearly sinusoidal cyclic axial load was applied through a hanger connected to a horizontal lever arm with a translating weight that was made to oscillate by a rotating, motor-driven disk. A loading period of 8 sec was used to allow sufficient time for digitizing and storing data as well as to model typical wave periods. Axial strains were monitored by a DCDT with an accuracy of ±0.017% strain at 1% accumulated strain and sensitivity

of ±0.003% strain. Volumetric strains were monitored by a DCDT mounted on a diaphragm accumulator connected to the sample. Sensitivity was ±0.003% strain. Loads were monitored by a load cell with an accuracy of ±0.59 N at a load of 490 N and a sensitivity of ±0.13 N. Hedberg (3) describes further details of the apparatus.

Data were collected with a data logger and stored on magnetic tape for computer processing. The data were reduced by a computer program, which applied corrections for changes in area of the sample and for resistance of the membrane.

Test Results.—Several series of tests were conducted to determine the influence of porosity, stress level, average shear stress, and cyclic shear stress on the accumulated strains. Table 1 summarizes test conditions.

The results for cumulative volumetric strains are summarized in Fig. 3 and those for axial strains in Fig. 4. Examination of these results shows a nearly log-linear relationship among cumulative strain, number of cycles, porosity, stress

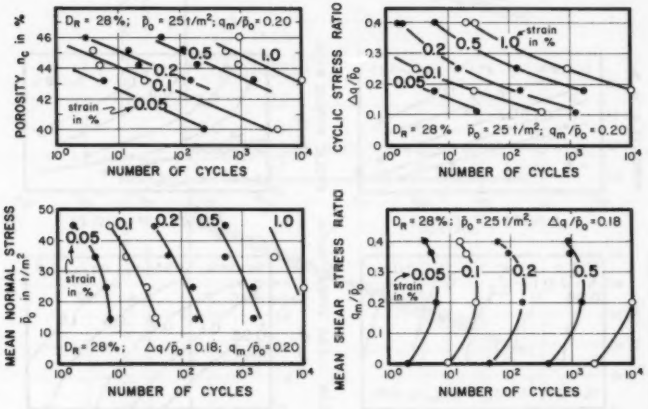

FIG. 3.—Contours of Cumulative Volumetric Strain

level, and cyclic shear stress. Hedberg (3) made a similar finding for undrained tests. These suggest an extension of the well-known Miner procedure that has been used for years in fatigue analysis and more recently in liquefaction studies.

Assuming that a log-linear relationship applies and that the slope of strain contours is constant for all values of strain, one can develop equations that describe the influence of number of cycles (N), porosity (n_c), cyclic shear stress ratio ($\Delta q/\bar{p}_o$), and mean normal stress ($\bar{p}_o$) on permanent strain. The influence of porosity on axial strain as shown in Fig. 4 allows the following observation: a test at 42% porosity with 38 cycles of stress produces 0.05% axial strain, which is equivalent to a test at 40% porosity with 2,150 cycles of stress. Using this equivalence, one can incorporate the influence of porosity on strain as an equivalent change in the number of stress cycles. Data for different porosities can be expressed with the use of an equivalent number of cycles as

$$N_e = N \cdot 10^{**}\left(\frac{n - n_{ref}}{d}\right) = NC_n \quad \ldots\ldots\ldots\ldots\ldots\ldots\ldots\ldots\ldots\ldots (1)$$

in which d = the slope of the strain contours in the plot of porosity versus $\log N$; n_{ref} = an arbitrarily chosen reference; and ** indicates exponentiation. Similar relations exist for cyclic shear stress ratio and mean shear stress:

$$N_e = N \cdot 10^{**}\left[\frac{\frac{\Delta q}{\bar{p}_0} - \left(\frac{\Delta q}{\bar{p}_0}\right)_{ref}}{a}\right] = NC_{\Delta q} \quad \ldots\ldots\ldots\ldots\ldots\ldots\ldots\ldots\ldots\ldots (2)$$

$$N_e = N \cdot 10^{**}\frac{\bar{p}_0 - \bar{p}_{0_{ref}}}{b} = NC_p \quad \ldots\ldots\ldots\ldots\ldots\ldots\ldots\ldots\ldots\ldots (3)$$

in which a, b = average slopes of strain contours in Figs. 3 and 4.

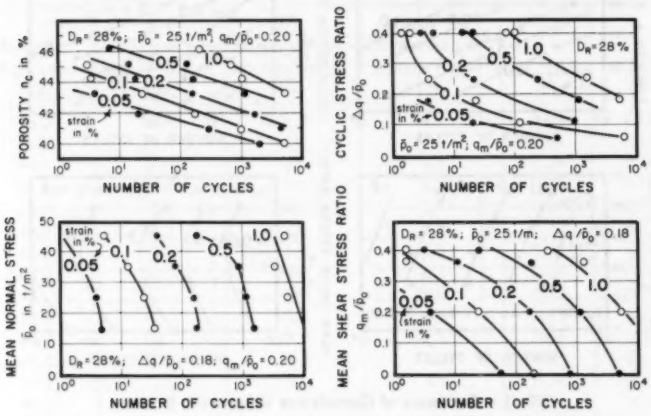

FIG. 4.—Contours of Cumulative Axial Strain

With these relations, the data in Figs. 3 and 4 for different values of porosity, cyclic shear stress ratio, and mean normal stress can be altered to one value of each parameter to obtain a plot of cumulative strain versus N_e as shown in Fig. 5.

Fig. 5 gives the data for tests listed in Table 1 with $q_m/p_0 = 0.20$ transformed by the above procedure to one set of parameters, $n = 43.2\%$, $\Delta q/\bar{p}_0 = 0.18$, and $\bar{p}_0 = 25$ tonne/m^2 (245 kPa). Points in Fig. 5 are data points with the number of cycles multiplied by a constant that depends on the conditions of each test. Fig. 5 shows a linear relation exists between the logarithms of N_e and of cumulative strain. From the nine tests at various n, $\Delta q/\bar{p}_0$, and $\bar{p}_0$, an average line is shown for $q_m/\bar{p}_0 = 0.20$. This is the first point where an approximate relation replaces actual data. Departures of data from the average

line in Fig. 5 represent the differences between measured data and strains obtained from this procedure.

Fig. 6 shows the relations between cumulative strain and N_e for other values of $q_m/\bar{p}_0$ established from limited data. Fig. 6 reproduces the behavior shown in Figs. 3 and 4 in that $q_m/\bar{p}_0$ has a smaller effect on cumulative volumetric strain than on cumulative axial strain.

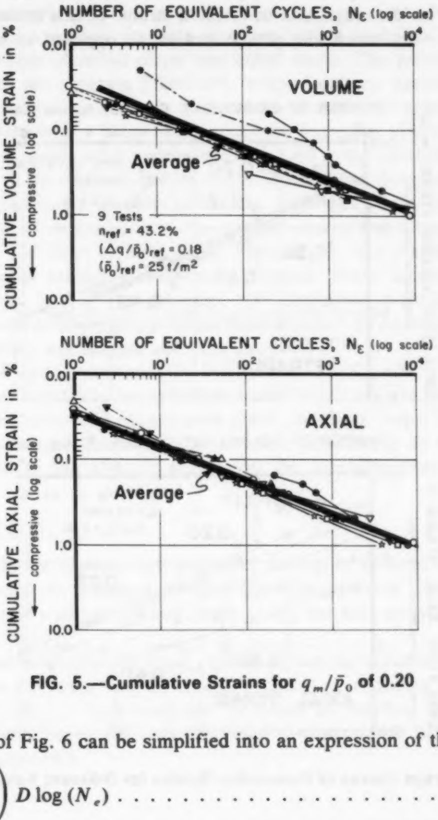

FIG. 5.—Cumulative Strains for $q_m/\bar{p}_0$ of 0.20

The curves of Fig. 6 can be simplified into an expression of the form

$$\log \epsilon = f\left(\frac{q_m}{\bar{p}_0}\right) D \log (N_e) \quad (4)$$

in which ϵ = axial or volumetric cumulative strain; D = a constant; N_e = number of equivalent cycles = $NC_nC_{\Delta q}C_p$; and C_n, $C_{\Delta q}$, and C_p = constants from Eqs. 1–3.

A simple, approximate fit of the data in Fig. 6 is

$$\epsilon = \frac{q_m}{\bar{p}_0} C N_e^D \quad (5)$$

in which C and D = constants. The constants for the above equations differ for axial and volumetric strain.

Limited laboratory data suggest that soil type has a primary influence on the constants C and D of Eq. 5 and a secondary influence on the constants in Eqs. 1–3. A soil that has a high resistance to cyclic loading has a small value of C, and a soil with low resistance has a large value of C.

One important consequence of Eq. 5 is that the mean shear stress, q_m, has a direct effect on the magnitude of residual strain. In this manner, the residual strains behave very much like plastic strains, as opposed to nonlinear elastic strains.

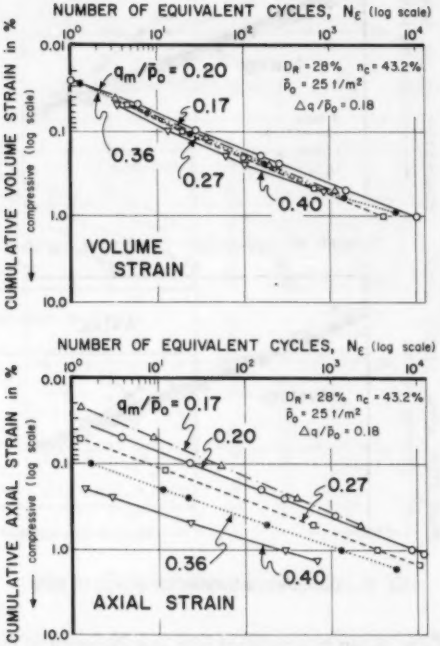

FIG. 6.—Average Curves of Cumulative Strains for Different Values of $q_m/\bar{p}_o$

The effect of the inclination of the stress path has not been considered. This is actually part of a larger problem for more general, 3-dimensional states of stress in which the definition of Δq and rotation of principal planes can be significant. Limited triaxial tests indicate that the inclination of the stress path is not important so long as the stress paths remain well inside the failure envelope. The effects of rotation of principal planes are worthy of further investigation using more versatile apparatus. It should also be noted that inertial effects are ignored in this approach.

Finite Element Implementation

Algorithms based on Miner's procedure have been combined with finite element procedures to calculate movement of dams (6) and offshore structures without static horizontal loads (2). The latter example performs the analysis by modifying the modulus of the soil, which can create some problems when the in-situ stresses are not computed directly from applied loads.

The relations developed from the experimental program can be implemented more generally into a finite element program used a technique similar to the well-known methods of initial stress and initial strain. The procedure has been programmed into the program FEECON, which has been described by Simon et al. (7). The application is one in plane strain. Some error arises from mixing triaxial parameters with a plane strain analysis, but these effects are probably less than those of many other approximations used in the solution.

The stresses in an element before cyclic loading are designated $\{\sigma\}_0$. The cyclic loading consists of N cycles of loading, each with an amplitude of $\{\Delta\sigma\}_c$. The notation "{ }" indicates that the components are arranged in a vector, as is customary for finite element work. From Eq. 5, it is possible to compute the residual strains caused by the cyclic stresses. These increments of strain are designated by $\{\Delta\epsilon\}_R$, the subscript "R" indicating residual effects. The principal analytical problem is to produce these strains with no change in boundary loads and to satisfy equilibrium and continuity.

The matrix of elastic constants for the element is $[G]$, which for a nonlinear material can be instantaneous stiffness terms based on the current state of stress $\{\sigma\}_0$. The strains have not yet taken place; they have simply been calculated. Since no displacements have yet occurred, the situation is as though stresses had been added to the element to prevent the displacements. Such stresses would be

$$\{\Delta\sigma\}_R = -[G]\{\Delta\epsilon\}_R \quad (6)$$

In other words, an element that wishes to deform so as to have strain $\{\Delta\epsilon\}_R$, but is prevented from doing so because the displacements have not changed, is the same as one wishing to have strain $\{\Delta\epsilon\}_R$ but also carrying an additional imposed stress $\{\Delta\sigma\}_R$.

To remove the dummy stress $\{\Delta\sigma\}_R$ and to induce the necessary deformations, the nodes of the elements must be loaded with self-equilibrating forces statically equivalent to $-\{\Delta\sigma\}_R$. Such loads can be found by recalling first that for any element the nodal forces $\{P\}$ and the nodal displacements $\{u\}$ are related by the nodal stiffness $[K]$

$$\{P\} = [K]\{u\} \quad (7)$$

and that the strains $\{\epsilon\}$ are computed from the nodal displacements by means of a matrix $[B]$:

$$\{\epsilon\} = [B]\{u\} \quad (8)$$

also $$[K] = \int_V [B]^T[G][B]\,dV \quad (9)$$

in which V = the volume (or area) of the element. Therefore,

$$\{P\} = \int_V [B]^T [G] \{\epsilon\}_R dV \quad \ldots\ldots\ldots\ldots\ldots\ldots\ldots\ldots\ldots\ldots (10)$$

and it follows that the equivalent nodal forces are

$$\{\Delta P\}_R = -\int_V [B]^T \{\Delta\sigma\}_R dV \quad \ldots\ldots\ldots\ldots\ldots\ldots\ldots\ldots\ldots\ldots (11)$$

Sufficient accuracy can usually be obtained by using only one point in the numerical integration of Eq. 10 and evaluating it at the centroid of the element. This gives

$$\{\Delta P\}_R = -V [B]^T \{\Delta\sigma\}_R \quad \ldots\ldots\ldots\ldots\ldots\ldots\ldots\ldots\ldots\ldots (12)$$

The computation proceeds as follows:

1. Initial stress $\{\sigma\}_0$ is computed from geostatic stresses, weight of structure, static horizontal loads, etc.
2. The cyclic stresses $\{\Delta\sigma\}_c$ are evaluated for each element by applying the cyclic loads to the finite element array with a static stress-strain law and solving for the stresses.
3. The residual strains $\{\Delta\epsilon\}_R$ are computed from Eq. 5.
4. $\{\Delta\sigma\}_R$ is computed.
5. Nodal forces $\{\Delta P\}_R$ are computed from Eq. 12.
6. After nodal forces have been computed for all elements, the forces are applied to the entire array of elements and the system solved for displacements $\{\Delta u\}$ and strains $\{\Delta\epsilon\}$. This may cause changes in stress that are sufficiently large to warrant modifying $\{\sigma\}_0$ and repeating the analysis.
7. If iterations are necessary, $\{\sigma\}_0$ is modified to account for redistribution of stresses under the combined effects of $\{\Delta\sigma\}_R$ and $\{\Delta P\}_R$ and step 2 is repeated.

Some Details of the Finite Element Application

The vector of residual strains $\{\Delta\epsilon\}_R$ is expressed in terms of the components of strain in the finite element coordinate system. The residual strains in Eq. 5 are composed of a volumetric and a major principal strain, and these must be rotated to the local finite element coordinate system. This is done by considering the principal strains of $\{\Delta\epsilon\}_R$ to be oriented in the same directions as the principal stresses of $\{\sigma\}_0$ and then computing the required strain components from the results of Eq. 5.

A typical storm consists of many waves with varying amplitudes. Calculations are greatly simplified by dividing the storm into a number of different parcels of waves with each parcel containing an equivalent number of cycles of a wave with fixed amplitude. If the subscript "i" indicates the parcel number, Eqs. 1–5 can be extended:

$$\Delta\epsilon_R = \frac{q_m}{\bar{p}_0} C \left[C_n C_p \sum_i (N_i C_{\Delta qi}) \right]^D \quad \ldots\ldots\ldots\ldots\ldots\ldots\ldots\ldots (13)$$

Thus, an entire storm containing waves of various amplitudes can be replaced

with an equivalent load. This approach does assume that the constants in Eqs. 1–5 are not affected by changes in conditions during the cyclic loading. In some cases, it is desirable to examine the effect of each parcel separately. Examples are cases in which the effects of the order of loading are to be investigated and those in which there is some change in average stress from parcel to parcel. Because the model requires the residual strains generated in earlier parcels, it is necessary to store these strains, which are identified by $\Delta\epsilon_R^*$. Then, a new parcel of load starts from this strain, which has an equivalent number of cycles N^*:

$$N^* = \left(\Delta\epsilon_R^* \frac{\bar{p}_0}{q_m C} \right)^{1/D} \quad \ldots \ldots \ldots \ldots \ldots \ldots \ldots \ldots \ldots \ldots \ldots \ldots \quad (14)$$

In Eq. 14, the terms $\bar{p}_0$ and q_m are those applying to the new parcels of load, not the old. The total residual strain from old and new cyclic loads is

$$\Delta\epsilon_R = \frac{q_m}{\bar{p}_0} C \left[N^* + C_n C_p \sum_i (N_i C_{\Delta qi}) \right]^D \quad \ldots \ldots \ldots \ldots \ldots \ldots \quad (15)$$

in which all load parameters are those of the new cyclic load and "i" indicates subparcels of the new load. The residual strain from the new load alone is simply $\Delta\epsilon_R - \Delta\epsilon_R^*$.

Test runs of the computer program showed that $q/\bar{p}_0$ could become unreasonably large, particularly at the toe and heel of the structure. Since this ratio appears as an exponent of 10, the resulting residual strains immediately dominate the solution. The problem occurred because Δq was determined from an elastic analysis that assumed linear properties during one application of the wave. To correct this difficulty, each element must be examined to determine whether Δq is sufficient to exceed the shear strength of the element in either direction of wave loading. If so, Δq is reduced to the value just sufficient to reach the shear strength. This is realistic in that once Δq exceeds the shear strength, the stress path must move along the Mohr-Coulomb line, which gives a nearly constant $\Delta q/\bar{p}_0$. It does ignore the redistribution of stress caused by yielding, but including that nonlinearity in the computation of Δq would complicate the model beyond what is a reasonable extrapolation from laboratory results. In all cases, Δq is computed as the difference between the total q for the static state plus the wave loading effect in each direction and the q that existed in the static state.

It should be noted that the effect of the cyclic load is to make the soil behave as essentially a nonlinear visco-elastic material, with N taking the place of time. When there is substantial redistribution of stress, the nonlinearity may cause the iterations to diverge for the full load history, and the cyclic load must be treated in smaller parcels.

The Oosterschelde Barrier

The governmental organization, Rijkswaterstaat Deltadienst, has the responsibility of designing a barrier dam across the Oosterschelde inlet located southwest of Rotterdam, the Netherlands. The barrier dam, which links with dikes placed along the coast, must allow tidal flow during normal sea states but resist storm

tides and waves. Dutch engineers chose large gates resting on reinforced concrete piers to effect the 3.5 km long closure. Fig. 7 illustrates a section of one of the massive piers with base plane dimensions of 25 m wide and 50 m long. Each pier will be fabricated in a dry dock, floated into position, sunk into a dredged trench, and ballasted. A protective cover or sill will be placed over the foundation and around each pier to prevent erosion of the foundation.

A key design question is how much permanent displacement will occur over the design life of these structures.

The foundation consists of fine-to-medium sand of uniform gradation over most of the closure. The upper part has been deposited in the Holocene epoch and is loose-to-medium dense. The underlying sand, deposited in the Pleistocene epoch, is medium dense to very dense. Holocene sand directly under each

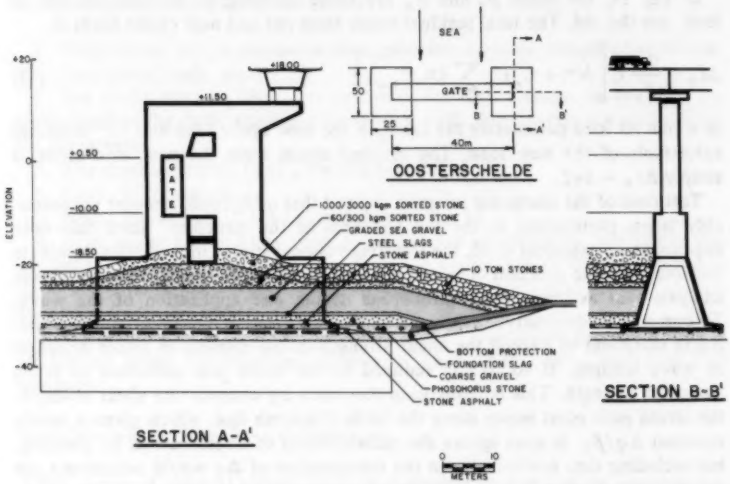

FIG. 7.—Oosterschelde Pier

pier will be densified and a protective layer of foundation slag placed and densified prior to placing the pier.

The wave loads and the corresponding moments were converted to equivalent forces on a 1 m thick section for plane strain analyses. The horizontal wave forces are assumed to act at the same point on the structure for all wave heights; this is an assumption that is very close to the prescribed design case.

Finite Element Programs and Models

Finite element analyses of pore pressure dissipation show drained conditions prevail in this foundation. Christian and Audibert (1) describe the computer program, CLIP, which considers consolidation of a linearly elastic material with

internal pore pressure generation. Fig. 8 illustrates typical results of these analyses for three points in the foundation soil. Excess pore pressures from undrained cyclic triaxial tests were used to establish contours of excess pore pressure for a complete storm of several hours' duration. These contours were used to establish pore pressure/generation coefficients in the consolidation program, assuming linear buildup of excess pore pressure in a conservative time of 30 min. The dashed lines in Fig. 8 show the resulting excess pore pressure generation with no dissipation or redistribution of excess pore pressure allowed. The solid lines show excess pore pressures with the same rate of generation but with

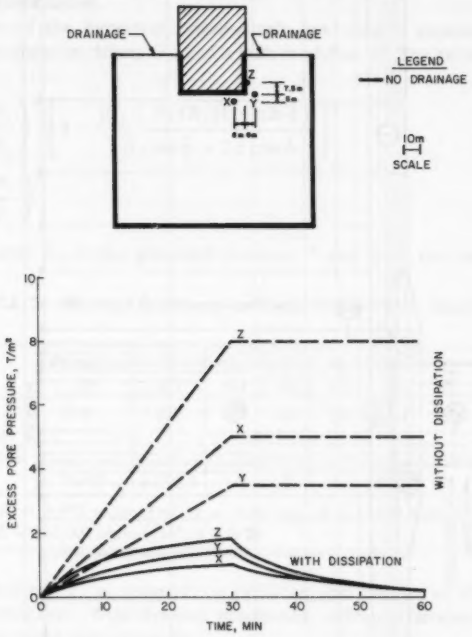

FIG. 8.—Dissipation of Excess Pore Pressure during Storm

dissipation and redistribution of excess pore pressure during and after the 30-min storm. These calculations used conservative assumptions, including reasonable values of the lowest permeability and highest compressibility for the soils, no change in the pore pressure generation coefficient determined from undrained cyclic tests, no drainage around the pier, and a storm compressed from several hours to 30 min. Even with these extreme conditions, only small values of excess pore pressure develop, so in the actual case drained conditions should prevail.

Fig. 9 shows the finite element array for the displacement and permanent

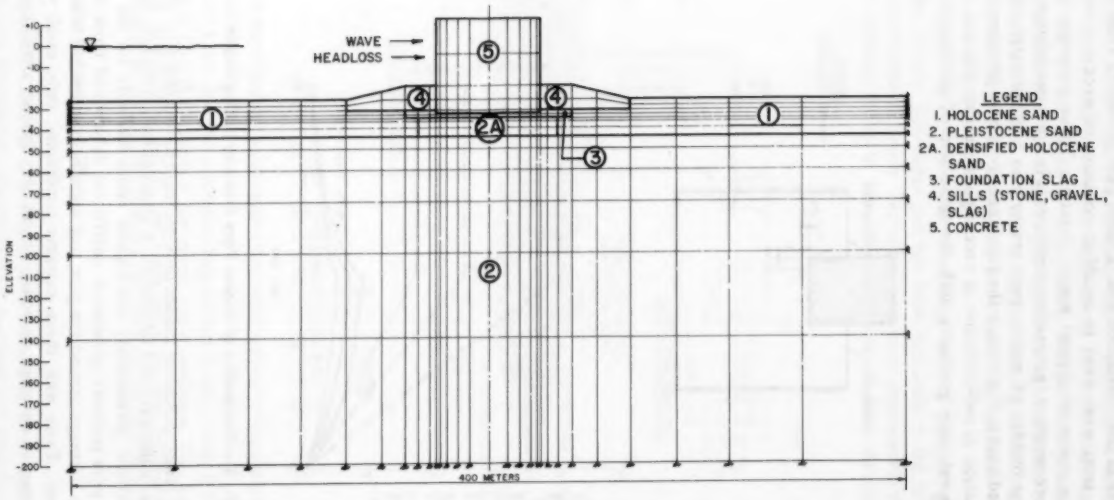

FIG. 9.—Finite Element Geometry and Mesh

strain calculations, and indicates material types and locations. Boundaries of the finite element mesh were established at sufficient distances to avoid influence on displacement of the pier.

Material Properties for Stress-Strain Calculation

Determination of residual strains requires that one first determine stresses from geostatic forces, the weight of the structure, and the horizontal force from the tidal difference and the increment of stress for the wave. This calculation requires a stress-strain relation for static loading, for which FEECON uses a hyperbolic formulation.

The version of the hyperbolic stress-strain law used is expressed in terms of a tangential shear modulus, G_t, and a bulk modulus, K. The general equations are

$$G_t = \Gamma P_a \left(\frac{\bar{\sigma}_3}{P_a}\right)^n \left[1 - \frac{(\bar{\sigma}_1 - \bar{\sigma}_3) R_f (1 - \sin\bar{\phi})}{2\,\bar{\sigma}_3 \sin\bar{\phi} + 2c\cos\bar{\phi}}\right]^2 \quad \ldots\ldots\ldots\ldots (16)$$

$$K = \beta_0 P_a \left(\frac{\sigma_3}{P_a}\right)^{\alpha} \quad \ldots\ldots\ldots\ldots\ldots\ldots\ldots\ldots\ldots\ldots (17)$$

in which $\bar{\sigma}_1$ and $\bar{\sigma}_3$ = the principal stresses; $\bar{c}$ and $\bar{\phi}$ = the Mohr-Coulomb

TABLE 2.—Material Constants for Static Stress-Strain Relations

Soil (1)	Porosity (2)	Γ (3)	K_0 (4)	$\bar{c}$ (5)	$\bar{\phi}$ (6)	R_f (7)	n (8)	β_0 (9)	α (10)
Holocene	41%	657	0.5	0	36	0.88	0.5	876	0.5
Pleistocene and densified Holocene	39.4%	1,070.4	1.0	0	42	0.88	0.5	1,427	0.5

Note: Slag: E = 9,950 tonnes/m^2; ν = 0.45; sill: E = 1,990 tonnes/m^2; ν = 0.20; and concrete: E = 300,000 tonnes/m^2; ν = 0.20.

strength parameters; P_a = atmospheric pressure; and the rest of the parameters = material constants. With drained conditions, effective stresses equal total stresses minus static pore pressure.

Table 2 summarizes stress-strain parameters for the materials illustrated in Fig. 8. Loose Holocene sand, densified Holocene sand, and dense Pleistocene sand use the nonlinear hyperbolic relation. The foundation slag, the sill, and the concrete pier were assigned values of Young's modulus, E, and Poisson's ratio, ν, shown in Table 2, appropriate for the average stress and strain levels developed by loading. The modulus for concrete was adjusted to reflect the difference in moment of inertia between the actual pier section and that of the solid concrete section used in the analysis.

Material Properties for Residual Strain Calculation

Only Holocene and Pleistocene sands were assumed to develop residual strain

from cyclic loading. The other materials were considered to be elastic to allow assessment of effects of the properties of the foundation sand on permanent displacement. Two equations and sets of material parameters are needed, one to compute the cumulative volumetric strain $\Delta\epsilon_{vol}$ and one to compute the cumulative major principal strain $\Delta\epsilon_1$.

Two different samples of Holocene sand were tested. Cyclic tests on the first indicated a sand with relatively high resistance to cyclic deformations, and most of the results described here were obtained using the properties of this sand. The second set indicated a much softer material that required an average of 300 times fewer cycles to achieve the same strain. This was true even though there is no significant difference between the two sands as regards grain size distribution, mineral content, shape of particles, and static stress-strain behavior.

Calculations were made for both "stiff" and "soft" sand, and the results are reported below. The same static properties were used for both sands. Table

TABLE 3.—Soil Parameters for Residual Strains in Stiff Soil

Residual Strain Parameters—Eqs. 2 and 4		
Parameters (1)	Volumetric strain (2)	Major principal strain (3)
C	0.001037	0.001680
D	0.4307	0.3700
n_{ref}	43.2%	43.2%
d	1.7%	1.4%
$(\Delta q/\bar{p}_0)_{ref}$	0.2	0.2
a	0.09	0.09
$\bar{p}_{ref}$	20 tonnes/m^2	20 tonnes/m^2
b	50 tonnes/m^2	45 tonnes/m^2

Note: parameters applicable for: $38\% \le n \le 45\%$; $0.05 \le \Delta q/\bar{p}_0$; $0.15 \le q_m/\bar{p}_0 \le 0.45$; 5 tonnes/m$^2 \le \bar{p}_0 \le 50$ tonnes/m^2.

3 gives residual strain parameters for the "stiff" Holocene sand. Residual strain parameters for the soft Holocene sand were identical to those in Table 3 except for values of C which increased from 0.001037 to 0.311 and from 0.00168 to 0.504.

Because elements with very low cyclic stresses are not expected to undergo permanent strain, a lower limit of $\Delta q/\bar{p}_0$ was established at 0.05, based on laboratory results. Elements with less than this level of $\Delta q/\bar{p}_0$ could not undergo permanent strain.

The excavation, densification, and construction processes were simulated by the computer program FEECON to obtain the initial stress condition before application of the static head loss and repeated wave loading. These stresses were then used as the starting conditions to study the effects of different combinations of head loss and wave loads and the effects of the degree of densification on residual strain. Simulation of the construction and the application of the head loss and wave loads caused displacement of the caisson, but these

TABLE 4.—Static Head Loss and Cyclic Wave Load Combinations

Case (1)	Maximum loads, in meganewtons (2)		Cyclic Wave Load	
			Magnitude, in meganewtons (3)	Number of waves (4)
A. Design	Max head loss	76.8	15.9	284
			25.3	187
	Max wave load	70.2	36.5	90
			48.7	31
			61.8	9
			70.2	2
B. Large tide	Max head loss + 1/2 Max wave load	111.9	8.0	284
			12.7	187
			18.3	90
	1/2 Max wave	35.1	24.5	31
			30.9	9
			35.1	2
C. Large wave	1/2 Max head loss	38.4	24.6	284
			39.1	187
	Max wave + 1/2 Max head loss	108.6	56.5	90
			75.3	31
			95.6	9
			108.6	2
D. No tide	No head loss	0.0	15.9	284
			25.3	187
	Max wave load	70.2	36.5	90
			48.7	31
			61.8	9
			70.2	2

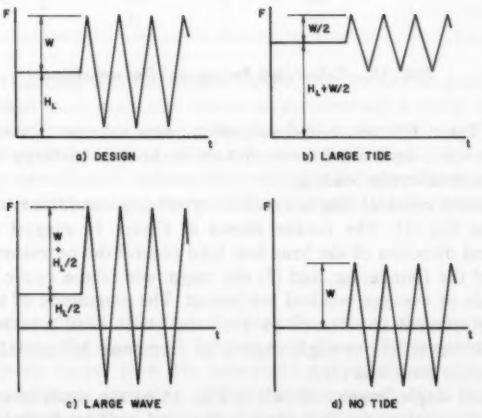

FIG. 10.—Combinations of Static and Cyclic Loads

are not reported here because the main interest is in the permanent displacements.

The analyses considered four different combinations of static head loss and cyclic wave load at two different densities of the Holocene sand. Table 4 gives the loads for the four combinations. All combinations use the same statistical characteristics and relative magnitudes of waves. The sum of the static head loss and wave load is equal for all the combinations except Case D, which has no head loss load. Fig. 10 illustrates these load combinations. Case A is the combination of head loss and wave loading for design predicted from hydraulic studies. In Case B, the static load consists of the design static load plus one-half of the design cyclic load; the cyclic wave load is one-half of the design cyclic load. In Case C, the static load is one-half of the design static load; the cyclic load consists of the remaining half of the design static load plus the design cyclic load. Thus, Case B has the total load heavily biased toward the static component, and Case C has the total load heavily biased toward the cyclic

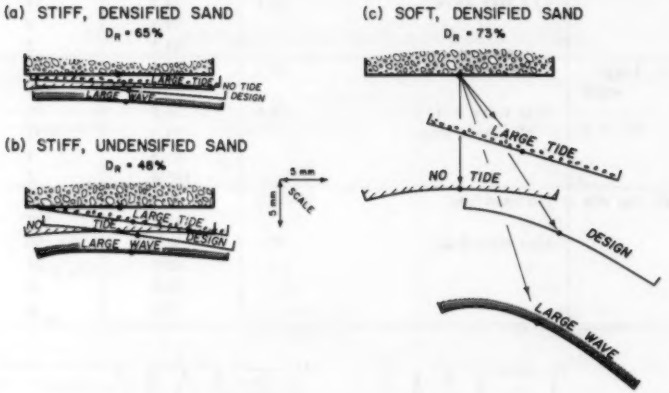

FIG. 11.—Calculated Permanent Deformations

component. These different load combinations were selected to study the relative influence of static horizontal force and cyclic horizontal force on permanent displacement from cyclic loading.

The computed residual displacements for several conditions under the pier are shown in Fig. 11. The results shown in Figure 11 suggest that: (1) The magnitude and direction of the head loss load control the permanent differential settlement of the foundation; and (2) the magnitude of the cyclic load controls the magnitude of average residual settlement. The magnitude of the horizontal residual displacement is affected by both the static head loss and the cyclic wave load. However, as one might expect, no permanent horizontal displacement occurs with zero head loss load.

The residual displacements shown in Fig. 11(*a*) are small in comparison to the elastic deformations for first time loading and residual displacements determined from other approaches such as physical models. These small residual

displacements occur in large part because the parameters for the calculations come from laboratory tests on one Oosterschelde sand with a relatively high resistance to cyclic loading. Predicted permanent displacements increase if the foundation is not densified, as shown for the "stiff" sand by comparing Figs. 11(*a*) and 11(*b*).

The other Oosterschelde sand, similar in grain size to the stiff sand, gave less resistance to cyclic loading. With parameters for this "soft" sand and a porosity of 39.4%, residual deformations increase substantially [Fig. 11(*c*)].

Other explanations for the small computed deformations are:

1. The slag layer was assumed elastic with no residual deformation, but it may have a significant contribution.
2. The calculations were for one defined storm, and other patterns of loading may give different effects.
3. Reconstituted samples may not give results comparable to field conditions.

From the results of the finite element calculations, it is possible to determine how the strains contributing to the settlement of the center line are distributed

TABLE 5.—Sources of Center Line Settlement and Effects of Densification

Case (1)	Source of Residual Settlement for $n = 39.4\%$, Stiff Holocene Sand, as a percentage		Ratio of settlement at $n = 41\%$ to settlement at $n = 39.4\%$, as a percentage (4)
	Holocene sand (2)	Pleistocene sand (3)	
Design	65	35	2.0
Large tide	92	8	2.4
Large wave	56	44	1.8
No tide	51	49	1.9

between the Holocene and Pleistocene sands. The effects of densification can also be evaluated more explicitly. These are summarized in Table 5. The results show that the relative magnitude of the residual settlement contributed by the densified Holocene sand increases with the increase in the head loss load. They also show that densification reduces the residual settlement. The beneficial effect of densification increases as more of the horizontal load derives from head loss.

Conclusions

Experimental and theoretical investigations have been directed at three questions important in the design of barriers and dikes: What permanent strains result from cyclic loads? How are permanent strains related to soil conditions and stress conditions, including initial shear stresses? How can permanent displacements resulting from cyclic loading be predicted with current analyses?

From the results of laboratory triaxial tests, a relationship has been developed

among the initial state of the soil, the cyclic loading history, and the residual or permanent strain. These results show a strong effect of the presence of initial shear stresses, in addition to the cyclic shear stresses. Ignoring the initial shear stresses leads to drastic distortion of the effects of cyclic loading.

The new relationships for residual strain have been incorporated into a finite element program. This requires that the program develop strains and deformations under conditions of no change in applied external load. The technique developed permits an arbitrary load sequence.

The results of initial application of the model to the Oosterschelde barrier show that the magnitude and pattern of motions are sensitive to the distribution of load between static and cyclic components. The magnitude and direction of the head loss force control the residual differential settlement of the foundation. The magnitude of the cyclic wave load controls the magnitude of the average residual settlement. The magnitude of horizontal residual displacement is affected by both the head loss force and the cyclic wave load. As would be expected, displacements are larger for loose than for dense soil, and they can change considerably with only slight apparent changes in the soil.

Field measurements of performance of the barrier for storm loads will not be available for at least 6 yr. The results described do not constitute a prediction of performance, since many important details of the foundation were simplified in the analyses to allow concentration on the mechanism of permanent deformation from cyclic loading. Further, considerable laboratory and analytical work is required to answer some detailed questions that occur with this general approach. The approach should be applied to several cases such as model tests, before high confidence is placed in its predictive capability. Nevertheless, results do point out the great importance of the in-situ state of stress on behavior of foundations stressed with a cyclic load and do allow one to assess the relative importance of various parameters on the magnitude and pattern of permanent foundation deformations.

Acknowledgments

This work is part of the studies associated with design and construction of the Oosterschelde Closure. The support of the Rijkswaterstaat Deltadienst is gratefully acknowledged. J. Hedberg of M.I.T. and T. Y. Chang of Stone and Webster Engineering Corp. made major contributions to the work. We appreciate the valuable assistance and cooperation of J. W. Boehmer, Scientific Advisor for the Deltadienst, and T. W. Lambe of M.I.T.

Appendix.—References

1. Christian, J. T., and Audibert, J. M. E., "Analysis of Offshore Concrete Caisson Dikes Under Cyclic Loading," *Proceedings*, Second International Conference on Numerical Methods in Geomechanics, Vol. II, June, 1976, pp. 979–990.
2. Dumas, F., and Lee, K. L., "Cyclic Movements of Offshore Structures on Clay," *Journal of the Geotechnical Engineering Division*, ASCE, Vol. 106, No. GT8, Proc. Paper 15655, Aug., 1980, pp. 877–897.
3. Hedberg, J., "Cyclic Stress Strain Behavior of Sand in Offshore Environment," thesis presented to the Massachusetts Institute of Technology, at Cambridge, Mass., in 1977, in partial fulfillment of the requirements for the degree of Doctor of Philosophy.

4. Ladd, R. S., "Specimen Preparation and Liquefaction of Sands," *Journal of the Geotechnical Engineering Division*, ASCE, Vol. 100, No. GT10, Proc. Paper 10857, Oct., 1974, pp. 1180–1184.
5. Prevest, J. H., and Hughes, T., Jr., "Mathematical Modeling of Cyclic Soil Behavior," *Earthquake Engineering and Soil Dynamics*, Vol. II, ASCE, June, 1978, pp. 746–761.
6. Serff, N., and Seed, H. B., "Earthquake Induced Deformations of Earth Dams," *Report EERC 76-4*, Univ. of California, Berkeley, Calif., Sept., 1976.
7. Simon, R. M., Christian, J. T., and Ladd, C. C., "Analysis of Undrained Behavior of Loads on Clay," *Analysis and Design in Geotechnical Engineering*, Vol. I, ASCE, June, 1974, pp. 51–84.
8. "Soil Behavior Under Earthquake Conditions, State-of-the-Art Evaluation of Soil Characteristics for Seismic Response Analyses," Shannon and Wilson—Agbabian—Jacobsen Associates (SW-AJA), Report to U.S. Atomic Energy Commission, 1972, Chap. 5, pp. 129–159.

DISCUSSION

Note.—This paper is part of the Journal of the Geotechnical Engineering Division, Proceedings of the American Society of Civil Engineers, ©ASCE, Vol. 107, No. GT8, August, 1981. ISSN 0093-6405/81/0008-1153/$01.00.

Discussions

Discussions may be submitted on any Proceedings paper or technical note published in any *Journal* or on any paper presented at any Specialty Conference or other meeting, the *Proceedings* of which have been published by ASCE. Discussion of a paper/technical note is open to anyone who has significant comments or questions regarding the content of the paper/technical note. Discussions are accepted for a period of 4 months following the date of publication of a paper/technical note and they should be sent to the Manager of Technical and Professional Publications, ASCE, 345 East 47th Street, New York, N.Y. 10017. The discussion period may be extended by a written request from a discusser.

The original and three copies of the Discussion should be submitted on 8-1/2-in. (220-mm) by 11-in. (280-mm) white bond paper, typed double-spaced with wide margins. The length of a Discussion is restricted to two *Journal* pages (about four typewritten double-spaced pages of manuscript including figures and tables); the editors will delete matter extraneous to the subject under discussion. If a Discussion is over two pages long it will be returned for shortening. All Discussions will be reviewed by the editors and the Division's or Council's Publications Committees. In some cases, Discussions will be returned to discussers for rewriting, or they may be encouraged to submit a paper or technical note rather than a Discussion.

Standards for Discussions are the same as those for Proceedings Papers. A Discussion is subject to rejection if it contains matter readily found elsewhere, advocates special interests, is carelessly prepared, controverts established fact, is purely speculative, introduces personalities, or is foreign to the purposes of the Society. All Discussions should be written in the third person, and the discusser should use the term "the writer" when referring to himself. The author of the original paper/technical note is referred to as "the author."

Discussions have a specific format. The title of the original paper/technical note appears at the top of the first page with a superscript that corresponds to a footnote indicating the month, year, author(s), and number of the original paper/technical note. The discusser's full name should be indicated below the title (see Discussions herein as an example) together with his ASCE membership grade (if applicable).

The discusser's title, company affiliation, and business address should appear on the first page of the manuscript, along with the *Proceedings* paper number of the original paper/technical note, the date and name of the *Journal* in which it appeared, and the original author's name.

Note that the discusser's identification footnote should follow consecutively from the original paper/technical note. If the paper/technical note under discussion contained footnote numbers 1 and 2, the first Discussion would begin with footnote 3, and subsequent Discussions would continue in sequence.

Figures supplied by the discusser should be designated by letters, starting with A. This also applies separately to tables and references. In referring to a figure, table, or reference that appeared in the original paper/technical note use the same number used in the original.

It is suggested that potential discussers request a copy of the *ASCE Authors' Guide to the Publications of ASCE* for more detailed information on preparation and submission of manuscripts.

Laboratory Tests on Model Piled Raft Foundations[a]

Discussion by Joe O. Akinmusuru,[3] A. M. ASCE

The authors' paper on the bending and settlement behaviors of piled footings in overconsolidated clay has thrown more light on the problem of soil-footing interaction. Some years ago, the writer carried out similar laboratory-scale experiments on the interaction of piles and footings in normally consolidated dry sand (13). A simplified mode of cap-group-soil interaction has been proposed (14) and it is suggested that the lateral pressures due to cap push and the attendant soil reaction induce bending moments in the piles and also cause an increase in skin friction on the pile shafts. The writer takes the view that the effect of bending is likely to be more significant on the piles than on the footing. For this reason, in the writer's experiments, the model piles, and not the footing, were instrumented.

The piles used were perspex tubes each 3/4 in. (19 mm) OD, 1/2 in. (13 mm) bore, 14 in. (350 mm) long, and sealed at the lower end. The model footing was a 6-in. × 12-in. × 5/8-in. (150-mm × 300-mm × 16-mm) steel plate. The piles were symmetrically positioned in a 2 × 3 rectangular array under the footing with the center-to-center distances between piles being 120 mm along the longer direction and 90 mm along the shorter direction. The middle pair of piles were instrumented on the inside with strain gages at six sections along the pile length. On each section in each pile, the gages were installed at two diametrically opposite positions such that all the gages were in the vertical plane containing the pile centers and parallel to the shorter edge of the footing. The details concerning soil properties, methods of strain gage installation, and cap-pile connection and installatin have been described elsewhere (13). The cap was initially kept clear of the soil surface to obtain freestanding group failure. The group was then pushed into the soil until the cap rested on the soil. Loading on the combination piled footing was continued but stopped well short of ultimate footing failure because of the risk of damaging the model piles. At each load application, the strain gage readings on the piles were monitored. The average bending moment, M, on each instrumented pile was obtained from the expression

$$M = \frac{1}{2} E_p Z_p (e_1 - e_2) \qquad (7)$$

in which E_p and Z_p = respectively, the elastic and section moduli of the pile; and e_1, e_2 = the strains measured on the pile section in question.

The variation of bending moment with pile length is shown in Fig. 16 for

[a] July, 1980, by Terence J. Wiesner and Peter T. Brown (Proc. Paper 15576).

[3] Lect., Faculty of Tech., Univ. of Ife, Ile-Ife, Nigeria.

varying λ—values, where λ is the ratio of the axial load on the pile top at any instant to that at freestanding pile failure. Also, in Fig. 17, the effect of

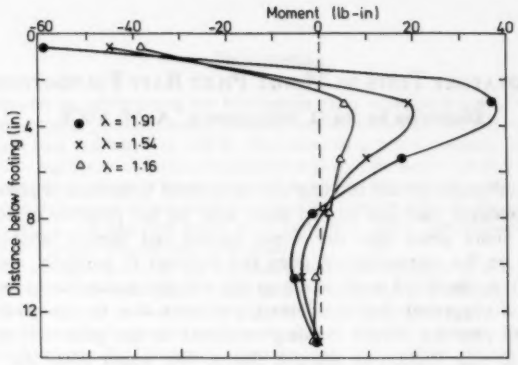

FIG. 16.—Bending Moments on Pile Shaft (1 in. = 25.4 mm, 1 lb-in. = 113.0 Nmm)

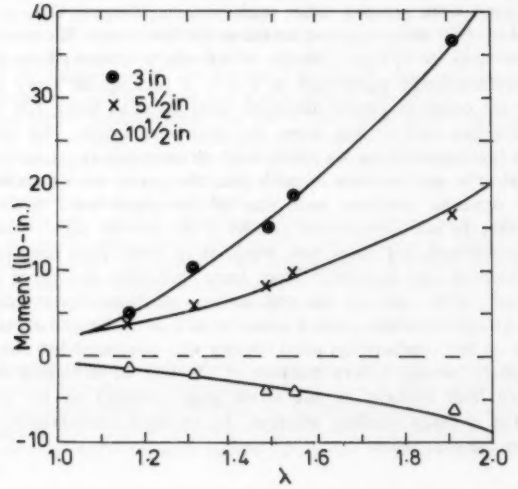

FIG. 17.—Bending Moment Variations with Load Levels (1 in. = 25.4 mm, 1 lb-in. = 113.0 Nmm)

bending at each section of the pile is shown for varying load levels. The graphs show that bending moments are greatest near the footing and that, at any section, the rate of increase of bending moment increases with applied load.

APPENDIX.—REFERENCES

13. Akinmusuru, J. O., "The Influence of a Pile Cap on the Bearing Capacity of Piles in Sand," thesis presented to Ahmadu Bello University, at Zaria, Nigeria, in 1973, in partial fulfillment of the requirements for the degree of Master of Engineering.
14. Akinmusuru, J. O., "Interaction of Piles and Cap in Piled Footings," *Journal of the Geotechnical Engineering Division*, ASCE, Vol. 106, No. GT11, Proc. Paper 15790, Nov., 1980, pp. 1263–1268.

Discussion by Eldon Burley,[4] Roger C. Harvey,[5] Bhas kar Nath,[6] and Lawrence A. Wood[7]

The authors are to be congratulated on their well documented series of tests which raise a number of interesting points.

The writers have been carrying out a series of tests (15,17,18) on uplift resisting anchors at both model and field level, and a number of loading tests were conducted on model anchors driven into reconstituted clay. The samples were prepared in a large circular cell of 19.7-in. (500-mm) internal diam by 17.7 in. (450 mm) high using air dried London clay mixed into a slurry at a moisture content of approx 100%; the liquid limit of the clay being approx 65%. The apparatus for carrying out the consolidation process consisted of a rubber membrane pressurized by water by means of an air/water cylinder in much the same way as the method described by the authors. During consolidation at a pressure of between 40-lb/in.^{2} (275-kPa) and 100-lb/in.^{2} (689-kPa) drainage in both the vertical and radial directions was encouraged by the positioning of a porous medium [0.08-in. (2-mm) thick porous plastic] at the top and bottom, and around the outside of the clay sample; a number of drainage holes being located in the sides and top and bottom of the consolidation cell. As consolidation proceeded, more clay slurry was introduced into the cell in order to prepare a sample of the required height, i.e., 15.7 in. (400 mm), in approx 3 weeks.

In order to determine the strength characteristics of the sample, vane tests were conducted at various locations and, in addition, to confirm the accuracy of the vane results, specimens were cut from the clay sample and tested in unconfined and triaxial compression machines. Fig. 18 shows some typical strength profiles and indicates that a variation of strength occurred across the sample.

The writers would be interested to know if the authors found similar strength profile variations particularly bearing in mind the relatively fewer drainage holes in their consolidation cell. If this is the case, could these variations have substantially affected the authors' test results?

In order to reduce the influence of the cell boundaries on the model tests, the maximum lateral dimension of the model anchors used was restricted to 3.0 in. (75 mm). It is noted that the authors used models with a lateral dimension greater than twice this value. Were the authors satisfied that the influence of

[4]Sr. Lect. in Civ. Engrg., Queen Mary College, Univ. of London, London, England.
[5]Lect. in Civ. Engrg., Queen Mary College, Univ. of London, London, England.
[6]Sr. Lect. in Civ. Engrg., Queen Mary College, Univ. of London, London, England.
[7]Lect. in Civ. Engrg., Queen Mary College, Univ. of London, London, England.

the boundaries on their tests was relatively unimportant?

Finally, the writers also considered other methods of sample formation. For example, an alternative method briefly reported by Bemben and Kupferman (16), in which powdered clay was placed in a container and water allowed to seep into the specimen, was tried, and even though fairly high water pressures were eventually used to speed up percolation, achieved little success in forming a suitable sample in a reasonable time. Success was only achieved when the resulting mixture was then compacted and excess water drained off. As this

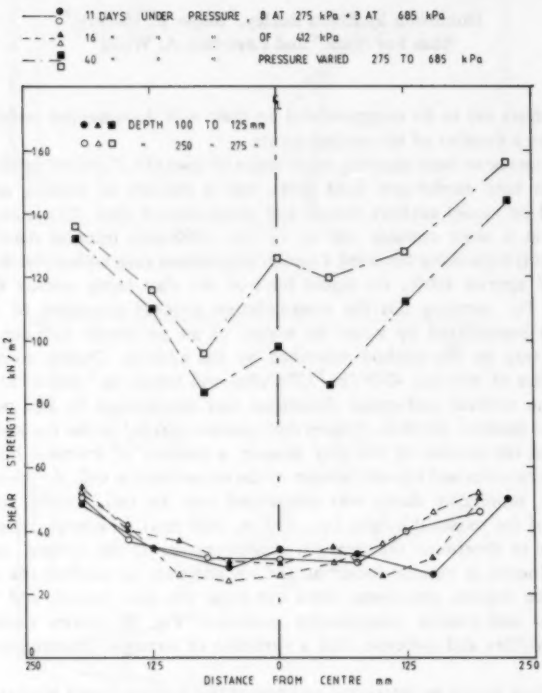

FIG. 18.—Vane Test Results

operation required the equivalent of a consolidation cell, there seemed little point in pursuing these trials further. Did the authors also consider other methods of sample preparation and, if so, why were these rejected in favor of the method used?

APPENDIX.—REFERENCES

15. Andreadis, A., Harvey, R. C., and Burley, E., "Embedded Sea Bed Anchors Subjected

to Repeated Loading," *Transactions of the Royal Institution of Naval Architects*, Vol. 121, London, England, July, 1979.
16. Bemben, J. M., and Kupferman, M., "The Vertical Holding Capacity of Marine Anchor Flukes Subjected to Static and Cyclic Loading," presented at the May, 1975, Offshore Technology Conference, held at Houston, Tex. (Paper No. OTC 2185).
17. Burley, E., Harvey, R. C., Martin, R., and Nath, B., "Recent Developments in Embedded Anchors," *Symposium on the Anchoring of Offshore Structures*, Sept., 1980.
18. Harvey, R. C., Burley, E., and Nath, B., "The Development of an Embedded Anchor to Provide Multi-Directional Restraint," presented at the March, 1978, International Offshore Conference, held at Brighton, England.

Closure by Terence J. Wiesner[8] and Peter T. Brown[9]

The writers would like to thank Akinmusuru for bringing to their attention his interesting results regarding the bending of piles beneath piled raft foundations.

The writers would also like to thank Burley, Harvey, Nath, and Wood for their interest in the paper and the queries they raised. The writers and discussers used cells to contain the clay which were almost identical in size. Apart from side friction, the stress and drainage conditions in the writers' cell were uniform since several layers of filter paper were used at the top and bottom of the clay to allow drainage from the whole of the top and bottom clay surfaces. The final increment of consolidation pressure was applied for 4 days and the coefficient of one-dimensional consolidation was approx 0.2 $in.^2/min.$, and the writers considered that essentially all excess pore pressures had dissipated by this time. The uniformity of the sample was checked by determination of moisture content at a number of points throughout the sample, and by back-figuring the Young's modulus of the soil from settlement measurements made on pile and raft foundations located at various distances from the center of the cell. No systematic variation of moisture content or Young's modulus with radial location was observed.

On the basis of finite element analyses by Small and Booker (19) it appeared that undrained settlements would be reduced by 10% due to the lateral boundaries of the consolidation cell, but that drained settlements would be reduced by only 3%.

The writers are unaware of a method of sample preparation which appears likely to give as low an occurrence of air pockets as the method adopted. Since that form of inhomogeneity appeared to be the most important source of error arising from sample preparation, the method described was used in preference to other commonly used methods of sample preparation.

Appendix.—Reference

19. Small, J. C., and Booker, J. R., "Geotechnical Analysis and Computer Applications," Post Graduate Course notes of the School of Civil Engineering, Chapter 11, The University of Sydney, Sidney, Australia, May–June, 1977.

[8]Soils Engr., Ground Test Pty Ltd, Sydney, Australia.
[9]Sr. Lect., Dept. of Civ. Engrg., Univ. of Sydney, Sidney, 2006 New South Wales, Australia.

Errata.—The following correction should be made to the original paper:

Page 772, paragraph 2, line 1: Should read "with liquid limit 41" instead of "with liquid limit 4 L"